UNIVERSIDAD DEL NORTE

COMBINED MISALIGNMENTS IN SPUR GEAR TRANSMISSION SYSTEMS: A SEMI-EMPIRICAL APPROACH

PhD THESIS

RAFAEL EDUARDO TUIRÁN VILLALBA

UNIVERSIDAD DEL NORTE

MECHANICAL ENGINEERING

COMBINED MISALIGNMENTS IN SPUR GEAR TRANSMISSION SYSTEMS: A SEMI-EMPIRICAL APPROACH

RAFAEL EDUARDO TUIRÁN VILLALBA

Submitted to fulfil the requirements for the degree of Doctor in Mechanical Engineering

DIRECTORS:
HERIBERTO ENRIQUE MAURY RAMÍREZ, PhD
HECTOR ÁGUILA ESTRADA, PhD

ENGINEERING DIVISION
MECHANICAL ENGINEERING DEPARTMENT
BARRANQUILLA
2023

Acknowledgments

To God, who is the one who sustains and puts the interest in knowing and understanding His creation.

To my wife Alejandra, for listening to me, supporting me and giving me ideas in difficult moments.

To Professor Heriberto, for making me part of this project and for helping him along this path.

To Professor Héctor, for his excellent reception in Punta Arenas and for his constant support in the development of this project.

To my family, because if I have come this far it is thanks to them.

To my friends, José, Hugo, Iván, who supported this project from their areas.

To the Universidad del Norte for facilitating the development of this work. To the University of Magallanes: to Sergio, César, José, Ricardo and Iván.

This document comprises confidential information considered intellectual property of the Materials, Process and Design Research Group of the Universidad del Norte. This document can be released to whom it concerns for exclusive confidential review and evaluation regarding its content. Further distribution or disclosure without authorization is not allowed.

_____

Thesis Director
HERIBERTO MAURY RAMÍREZ, PhD.
Mechanical Engineering Department – Universidad del Norte
Barranquilla, Colombia 2023

_____

Thesis Co-Director
HÉCTOR ÁGUILA ESTRADA, PhD.
Mechanical Engineering Department – Universidad de Magallanes
Punta Arenas, Chile 2023

This document has been approved by the Engineering Division to fulfil the requirements to obtain the degree of PhD in Mechanical Engineering

_____

Thesis Director
Heriberto Maury, PhD

_____

Thesis Co-Director
Héctor Águila Estrada, PhD

_____

Comitee Member 1

_____

Comitee Member 2

_____

Comitee Member 3

_____

Comitee Member 4

Table of contents

List of figures 6
List of tables 8
Design and vibrations in mechanical transmission systems 9
Introduction 9
Science mapping method 10
Analysis of reviews 10
Design and vibration 13
Gears 15
Bearings 22
Conclusions 26
Research problem 28
Objectives 30
Experimental approach 33
Testing workbench 33
Operation of the testing workbench 35
Shafts alignment 36
Experimental runs 37
Chapter conclusions 56
Dynamic model 58
Stress analysis 72
Guidelines for spur gear power transmission considering shaft misalignments 78
Conclusions 85
Future works 87
References 89

List of figures

Figure 1. Cumulative production of papers and citations per year. 13
Figure 2. Thematic map, according to the papers found. 14
Figure 3. Design processes of spur gears which consider the minimization of vibration as a design goal. (a) Design procedure of a two-stage spur gear system through a Min-Max method combined with a direct search technique [89]. (b) Design process of parallel-axis gear by changing gear parameters [102]; (c) Design of gear body based on topology optimization [98]; (d) General design process of pair gears for minimum vibrations found in the literature. 18
Figure 4. Design processes of helical gears that consider the minimization of vibration as a design goal. (a) Design process of cylindrical gear pairs for the reduction of gear size and meshing vibration [103] (b) Modified optimization of double helical gears [108] (c) Algorithm for generating CMSG (Constant Mesh Stiffness Gears) [109]..... 21
Figure 5. Sides view of misalignments investigated. (a) Radial (b) Axial (c) Positive yaw (d) Negative yaw 33
Figure 6. Testing workbench for misalignments. (a) Reactive side (b) Motor side (c) Gear pump (d) Lower base plate (motor) (e) Machine bed (f) L plates (g) Upper base plate (motor) (h) Flexible coupling (motor) (i) Vertical screws (motor) (j) Base plate (reactive side) (k) Support hubs (j) Top plate (reactive side) (k) Flexible coupling (reactive side) (l) Motor power (m) System for axial movement of the reactive side. 36
Figure 7. Accelerometers on the motor side. (a) Horizontal position (b) Vertical position. 36
Figure 8. Alignment of the motor axis in the horizontal and vertical plane. 37
Figure 9. Measurement distances for the aligned condition (left), d1 and d2 and a positive angular misaligned condition (right), d3 and d4. Side view. 41
Figure 10. Signal time for one of the runs in the alignment condition for the horizontal accelerometer in the motor side. 42
Figure 11. Histogram for the alignment condition for the horizontal accelerometer in the motor side. 42
Figure 12. Frequency spectrums for the six runs of the point (Axial = 0, Radial = 0, Yaw = -2,69°). Values on the x-axis are in Hz and on the y-axis in g. 46
Figure 13. Contact area on a pair of aligned and individual misaligned teeth. (a) aligned condition (b) axial misalignment (c) radial misalignment (d) positive yaw misalignment. 48
Figure 14. Contact area on a pair of combined misaligned teeth. (a) Axial-Radial (b)Axial-Angular (+) (c) Axial-Angular (-) (d) Radial-Angular (+) (e) Radial-Angular (-) (f) Radial-Axial-Angular (+) (g) Radial-Axial-Angular (-) 50
Figure 15. Zoom for contact area on axial-positive yaw misalignment..... 50
Figure 16. Zoom for contact area on radial-positive yaw misalignment..... 51
Figure 17. Zoom for contact area on axial-radial-positive yaw misalignment. 52

Figure 18. %CA vs %Change for positive yaw misalignments y(+) and negative yaw misalignments. y(+). 55
Figure 19. %CA vs average contact ratio for positive yaw misalignments y(+) and negative yaw misalignments y(-). 55
Figure 20. Finite element model for the analyzed spur gear pair. 61
Figure 21. Pair of spur gears with 1,5 mm, 4 mm and 2,69° of radial, axial and yaw misalignment respectively (left) and 1,5 mm, 2 mm and -2,69° of radial, axial and yaw misalignment respectively (right). 62
Figure 22. Vertical force (Fy) in the center of the pinion gear (RP-2) in a period of meshing for the aligned condition (black) and an angular misalignment condition with 2,69° (red). 63
Figure 23. Simplified dynamic model to predict the vibratory behavior in bearings 1 and 2 of the shaft that supports the pinion gear in a single stage spur gear transmission system. 63
Figure 24. Values of M/m according to the work of H. R. El-Sayed [140] 66
Figure 25. Radial stiffness of the UCP 205 ball bearing 66
Figure 26. Schematic diagram in Simulink Matlab® for the solution of the system of non-homogeneous second-degree differential equations (42) and (45). The green block gives the solution for $x1$ and the blue block gives the solution for θ. 67

List of tables

Table 1. Analysis of reviews in the last 20 years of principal elements of power transmission related to vibrations..... 12
Table 2. Results of the design methods for reducing vibration in principal mechanical transmission elements. 23
Table 3. Workbench displacement ranges. 34
Table 4. Final alignment values for the motor..... 37
Table 5. Parameters of the gears used in the misalignment bench..... 38
Table 6. Extreme values for each type of misalignment for the experimental analysis. 39
Table 7. Experimental points considering all possible combinations. 39
Table 8. Order of experimentation. 41
Table 9. Kurtosis and skewness values for time signals. 44
Table 10. Percentage of change of spectrum for different experimental point for the horizontal accelerometer in the motor side. 46
Table 11. Standardized effect and percentage of contribution for axial, radial and yaw misalignment on vibration measurements. 47

Design and vibrations in mechanical transmission systems

Introduction

Vibrations in power transmission elements are of extreme care since their occurrence outside specific ranges can generate problems in the operations of the element or the system to which it belongs. They can even cause mechanical failure. In this way, vibration measurements in specific points of a power transmission system let monitor and diagnose faults [1].

The main elements of a power transmission system are gears, shafts, bearings, and the gearbox housing. Gears and bearings are the central elements where more damage occurs in a gearbox. The National Renewable Energy Laboratory recorded 257 gearboxes damaged, in which 70% of failures were by bearings, 26% by gears, and 4% by other elements [2]. These elements are mostly associated with mechanical vibrations, and therefore they are the most investigated. The inadequate interaction of these elements can generate vibrations and noise, reflected in an inefficient transmission of power and less availability.

Historically, vibrations have been studied mainly as a fault early detection technique. Vibration analysis has been used to support machinery maintenance decisions [3]. Therefore, many of the research work focus on maintenance, but only a little number of works consider the gear vibrations from the design stage.

In recent years, the design methodologies tend to maintain an integrating view that considers the largest number of variables associated with the different stages in the product's development. Principles and tools as Robust Design (RD), Quality Function Deployment (QFD), Design for Manufacturing and Assembly (DFMA), Computer-aided technologies (CAx), Design for Service (DFS), Design for reliability (DFR), and Design for Six Sigma (DFSS) have been developed since the middle of the last century to develop robust, high-value products at all stages of their life cycle [4]. This document presents a review of the different studies carried out in the last 20 years in which vibrations were taken into account as a tool for design and research in which design is made to minimize vibrations in gears and bearings. This research aims to show the benefits of considering the vibrations from the design stage for those interested in developing formal design methodologies that consider the mechanical vibrations in a system. This approach is very useful to the mechanical system and machinery design.

Science mapping method

The standard 5-step method for science mapping was followed [5]. The first step in Research Design is to propose the research question. In this review, the principal question is: "Which are the studies that take into account the vibrations for the design of the principal elements of mechanical transmission as gears and bearings in the last 20 years?". The second step is the compilation. The databases used were Web of Science and ScienceDirect; the search formula was different for each transmission's element and explained in the following sections. The analysis, which is the third step, was made through a recent open-source tool called Bibliometrix, which is developed in the statistical computing and graphic R language. In the next sections, Visualization and Interpretation, which are the fourth and fifth step, were developed.

Analysis of reviews

Since the interest is know the design methods used that take into account vibrations in mechanical transmission elements, the search problem was divided into three main topics: Vibrations, Mechanical transmission elements, and Design methodologies. These are the main topics of search. This review considers these topics with subdivisions according to the particular interest of each subtopic. The simple topic search, including the above mentioned as search words, yields results that may exclude relevant papers or that may include those that are not closely related to the topic of interest. For this reason, the search must be refined without losing focus that one or more topics classified as significant are implied.

The first step was to determine the elements or systems involved in the mechanical transmissions that had more relevance in the vibrations, and these were bearings, gears, shafts, and gearboxes. The study begins with the search of reviews in which these elements are related to vibrations. A first review search was performed in Web of Science through the search formula: TOPIC (gear or shaft or bearing or transmission or drive train) and TOPIC (vibration). The results were filtered by "review" and the works related to biology, medicine, civil structures, among others, were excluded. Five main topics were distinguished in the works found: fault diagnosis, dynamic characterization, math tools or signal processing methods, vibration control or noise control, and design. Table 1 shows the 84 reviews found, each article's main topic, and the corresponding application. 56% of the works are related to the use of vibrations for faults diagnosis in different elements of gear transmission systems. 31% of them studied the dynamic characterization of bearings, gears, and other more complex systems as gearboxes, carbodies, mechanical structures, among others. 27% of the reviews are about signal processing methods in vibration measurement and mathematical

tools for vibration measurement or vibration analysis. The main topics in this area are enhanced fast Fourier transform [6], free and forced vibration analysis of structures with cyclic symmetry [7], wavelet for fault diagnosis [8], finite element analyses [9] and statistical energy analysis in high-intermediate frequency acoustics vibration problems [10]. 13% of works are about vibration control or noise control, and 10% of reviews consider the design as one of their topics.

Most of the design's reviews focus on gears. F. Li et al. [11] present essential conclusions for planetary gear design to solve vibration noise by considering mesh phase, tooth profile errors, bearing clearance, bearing contact, tooth profile modification, and gear contact ratio. K. Mohan et al. [12] studied the works related to the gearbox dynamics and the methodologies of analysis for various types of gearboxes. They give some design guidelines for machine tool structures, gearboxes, and associated rotors, take into account dynamics characteristics as chatter, vibration, and noise radiation. L. Prášil et al. [9] made a list of published papers on the design, analysis, and simulation of gears and gear drives. The design of bearings was studied too: Q. Gao et al. [13] reviewed the design and optimization of aerostatics bearings; they studied the design from the dynamic performance perspective and considered micro-vibration and pneumatic hammer vibration (large amplitude) for suppression of pneumatic hammer vibration. They found two strategies through structural optimization and considering external damping. In a previous review, F. Al-Bender [14] also studied aerostatic bearing films; in his work, he considered the dynamic behaviour to complement the determination of static characteristics, which is considered the first step in the bearing design process. S Hong et al. [15] studied the research related to rolling-element bearing modelling due to the high variant loads and high vibration levels that bearings experience in many applications. H. Mahdisoozani et al. [16] focused on vibration reduction and engine modifications for the performance enhancement of internal combustion engines through vibration control, which was classified in Table 1 as design. However, in strict terms, it is redesign. S. Sharma et al. [17] include vibration as an essential variable in the dynamic behaviour for the design of aircrafts. Although some works include vibration in the design process, there are no reviews where vibrations are analyzed for purposes of systematic design of gear drives. Although there are no reviews whose main topic is the topic of interest, it is important to show the reviews in Table 1.

Good management of mathematical tools is required for the acquisition and analysis of vibrations; also, the dynamic characterization of the element to design and the fault diagnosis through vibrations; these are inputs for a fair design process. The applications shown in Table 1 are of interest. Although there are typical applications such as bearings, gears, shafts, and plates, specific ones such as helicopter transmissions and wind turbines

are also found. The study of vibrations on wind turbines is because the wind power industry experiences a high failure rate and operation and maintenance cost. The transmission failures contribute considerably to that rate [18].

In the following section are analysed the papers found in which gears and bearings are designed, taking into account some aspects related to the associated vibrations of these elements.

Table 1. Analysis of reviews in the last 20 years of principal elements of power transmission related to vibrations.

Principal topic	Applications	Works
Fault Diagnosis	Bearings, motor bearings, wind turbine planetary gearboxes, solar photovoltaic, rolling element bearings, gears, rotors, rotating machinery, active magnetic bearings, high-speed railway bridges, internal combustion engines, rotating shafts, squirrel-cage induction motors, low-speed bearings, heavy-load slewing bearings, fixed axis gearboxes, power equipment, gerotor pumps, micro-vibration detection, rolling/sliding bearings, hybrid electric vehicles, engines, turbines and motors, gear transmission systems, wind turbine bearings, wind turbines, offshore wind turbines, machinery, planetary gearboxes, induction machines and drive trains in offshore applications, rotating electrical machinery and helicopter transmissions.	[1], [3], [8], [18]–[61]
Dynamic characterization	Mechanical structures, landing gear shock absorbers, gearbox, carbody vibrations, rolling element bearings, rolling bearing rotor systems, rotating machinery, gearboxes, rotating laminated shafts, spur gear pairs, transmission lines, beams, shafts, plates, aircrafts, gears, journal bearings, drive train systems in wind turbines, journal bearings, flexible rotor-bearing systems, planetary gears, epicyclic gears, mounting elements of rotating machinery, tilting-pad journal bearings, aerostatic bearing films, magnetic bearings, and out-of-round wheels.	[11], [12], [14], [15], [17], [32], [49], [55], [57], [60], [62]–[77]
Math tools or signal processing methods	Bearings, vehicles, ships, aviation, and other transportation engineering fields, complex elastic multibodies, low-speed slew bearings, magnetic bearing systems, joined structures, wind turbine drive trains, marine power transmission systems, rotating machines, mechanical structures with cyclic symmetry, rotary machines, structures coupled with elastic media, gears, and gear drives.	[6]–[10], [20], [24], [26], [28], [33]–[36], [39], [40], [48], [56], [57], [69], [78]–[81]
Vibration control or noise control	Long shafts, flexible rotors, hybrid magnetic bearings, sliding bearings, dampers, wind turbines, rotors, ergonomic, magnetic bearings, plate-like structures, air bearing systems and shafts of highspeed tooling spindles, automotive components, machine tool transmission housings, nonlinear vibration isolations, aerospace vehicles, and ultralight structures.	[12], [41], [42], [52], [65], [82]–[87]
Design	Aerostatic bearings, internal combustion engines, vehicles, and dynamic vibration neutralizers.	[11]–[17], [88]

Design and vibration

The two principal search formulas were: TITTLE (gear*) AND TITTLE (optimization* OR modification* OR dynamic* OR kinematic* OR mesh* OR transmission error OR analysis* OR design* OR vibration*) AND TOPIC (design*) AND TOPIC (vibration*) for gears and TITTLE (bearing*) AND TOPIC (design*) AND (VIBRATION*) for bearings. After checking the results, papers with no significant contribution were found and therefore they were excluded. Seventy-seven papers were processed in Bibliometrix; an increasing interest in the topic in the last 20 years is shown in Figure 1. The growth was approximately linear in the first years, with an inflection point in 2017 where, through a standardized plot, a slope of 1 begins, increasing considerably in 2018 and 2019. That behavior evidences a recent interest in the thematic. Although the production articles has increased in the last two years, the most cited papers are produced at the beginning of the century, as shown in Figure 1.

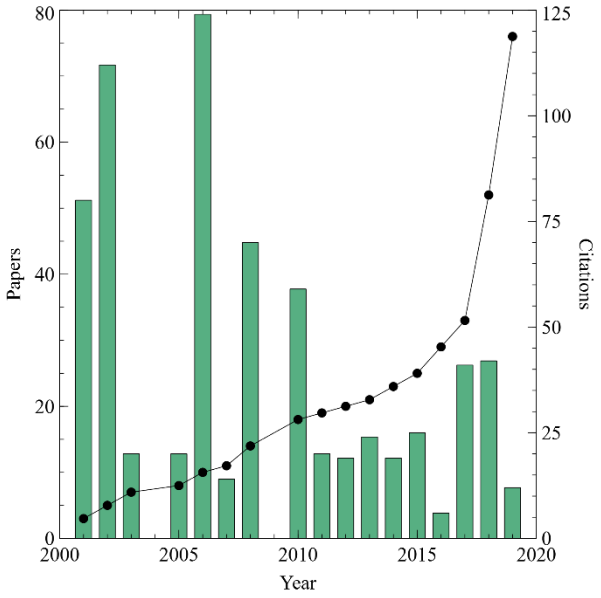

Figure 1. Cumulative production of papers and citations per year.

A thematic map shows the state of the topic found in the papers analyzed in terms of their grade of importance and development. A thematic map is divided into two axes: the x-axis shows the centrality: a measure of the theme's importance in the entire research field. The y-axis shows the density: a measure of the topic's development.

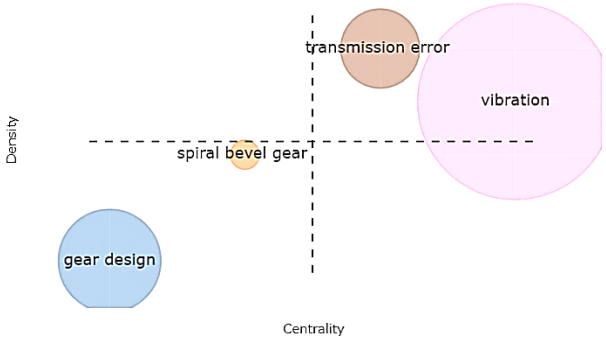

Figure 2. Thematic map, according to the papers found.

Figure 2 shows the thematic map of the search made. The analysis was made with the keywords; the word shown in the bubble is the word with the highest occurrence in that cluster, and bubble size is proportional to the cluster word occurrence. The first quadrant contains the highly developed and most important topic according to the citations. The vibration cluster is the most developed and the cluster with the highest importance, followed by the transmission error cluster. The transmission error (TE) has been identified as one of the principal causes of vibration in geared systems; because of their location, these two topics are the motor themes; great numbers of studies consider reducing the TE in order to reduce the vibrations in geared systems.

In the third quadrant of Figure 2, it is observed that gear design is an emerging topic, which is corroborated with the increasing slope in the last two years of Figure 1. Gear design in itself is not a recent theme, however in the context of the search for this review, considering the vibrations, it could be considered an emerging theme. In the gear design cluster, mesh stiffness is the second word in occurrence order that suggests the importance of considering the mesh stiffness in gear design.

The Spiral bevel gear appears as an emerging theme too. That is because of the complexity in the geometry of that type of gear. The most significant research efforts have been in spur and helical gears, as shown in the following sections.

According to the results found, the information has been divided into four main topics: spur gears, helical gears, spiral bevel gears, and bearings. The main findings of design methodologies that consider vibrations for each of the elements mentioned are shown in the following sections.

Gears

To find the appropriate research papers related to gears, the optimized search formula in Web of Science was: *TITTLE (gear* NOT gearbox*) AND TITTLE (optimization* OR modification* OR dynamic* OR kinematic* OR mesh* OR transmission error OR analysis* OR design* OR vibration*) AND TOPIC (design*) AND TOPIC (vibration*).* Although there are considerable studies in which the phenomenon of vibration is researched on gears, the ones that show a clear and explicit methodology for the design of gears taking into account vibrations to reduce it, is much smaller. The main studies are related to spur gears, helical gears, and spiral bevel gears.

Spur gears

Spur gears have been one of the most studied gears. Vibrations on gears have been of interest since the last century, and many papers consider vibrations as a variable to reduce. However, there are a few of them which show an explicit design methodology for reducing vibrations. Abuid Ba and Ameen YM [89] developed a methodology for the optimum design of a two-stage spur gear system. Although the authors did not measure, directly, vibrations on the system, the proposed procedure got to reduce dynamic factors. The volume of gears and the center distance of the system were also reduced. The dynamic factors were studied in the input shaft, first –teeth meshing, intermediate shaft, second meshing, and the output shaft. The principal goal was to design a compact gear system with quiet running compared with classical design. The design variables were numbers of teeth of pinions, stiffness of shafts and teeth, and gears' inertia. Refined min-max technique as the optimization technique was used and a direct min-max search method in a second stage for refinement. The methodology was compared with classical design, and the dynamic factor was reduced by 22% and 53% in the first and second teeth meshing zone, respectively. Two years later, Fonseca D et al. [90] developed a genetic algorithm for reducing the TE of automotive spur gear sets. The model minimizes the magnitudes of gear mesh frequency components' weight sum through a formal methodology proposed by Tavakoli, M.S [91] consisting of involute profile generation, profile modification curve-fit, mesh compliance analysis, TE, and load sharing computations. Jiang, J, and Fang, Z [92] also work on TE; their method works on the design of tooth surface modifications; authors used particle swarm optimization for the design of loaded TE. Wang, Y [93] proposed a method to identify a gear system's dynamic model to make a profile modification for reducing gear noise and vibration. A significant contribution is the relationship between the rotational movement and the acoustical noise from the identified model. Yildirim N et al. [94] proposed a helicopter transmission design

by changing the standard low contact ratio spur gears by high contact ratio (HCR) spur gear and applying a profile modification type of "double relief." The redesign achieved two to four times casing vibration reduction at tooth meshing frequency. Karpat, F [95] developed a computer program for the dynamic analysis of spur gears with symmetric and asymmetric teeth in order to minimize dynamic loads. Authors obtained important conclusions for the design of spur gears with asymmetric teeth; design rules were achieved considering gear contact ratio, pressure angle and addendum.

Tribo-dynamic performance of spur gear has been analyzed too for guiding gear design. Ouyang T et al. [96] developed a gear dynamic model taking into account the lubricant properties. Gear parameters and lubricant properties are the inputs of the computation program created. The next step is the load distribution model and the gear elastohydrodynamic lubrication model by using a multigrid method. The final step is the gear dynamic model obtained by applying a Runge-Kutta method. In a recent work [97] a method for predicting dynamic characteristics and lubricating property in spur gear of ink vibrator was developed. This was achieved by applying a Runge-Kutta and a multigrid method for solving the governing equations as the previous work reported [96].

Recently, techniques such as topological optimization have been used for gear design. Ramadani, R et al. [98] designed a gear body as a cellular lattice structure to benefit from weight reduction and vibration behavior. Topology optimization was employed to remove stress concentration and stress levels as much as possible. They found that a lattice structure gear body might notably reduce vibrations and even offer the opportunity to be filled with an adequate polymer, which may further reduce the vibrations.

As future work, it would be important to manufacture these geometries and gear structures through additive manufacturing to experimentally verify, contrast, and complement works like this. Studying different types of materials in terms of their damping coefficient and stiffness in different modes of vibration could be a relevant topic for future research, the results of which would serve to generate highly useful design guidelines to improve the vibratory behavior of gearboxes.

Xu L. et al. worked on reducing a power turret gear train's vibrations by modifying design parameters [99]. The gear transmission system of power turret consisted of a three-stage gear train with four spur gears. Since gear vibration and noise can be reduced by a HCR [100], and this can be changed by modifying such parameters as the outer diameter of gear, the pressure angle, or the number of gear tooth [101], authors chose the smallest module and pressure angle to enlarge the contact ratio. They found that the improvement of gear modulus and pressure angle yields better dynamic behavior with a lower vibration than before by comparison in the time domain, and the modification of turret generally decreases

the vibration amplitude and nonlinear behavior effectively by the comparison in frequency domain.

Figure 3. shows different gear design processes in which the vibration minimization methodology is varied. Studies shown in Figure 3. are those with the most precise design methodology according to its approach. The first one describes a flow chart for the process of the design of a two-stage spur gear system. In the second one [102], design parameters as the module, pressure angle, face width, and helix angle (for helical gears) are modified. The third one [98] shows a design process for minimum vibration through topological optimization. All of the found methodologies begin with input gear specifications, which are processed according to the approach proposed in each work, and finally, the gear parameters are obtained.

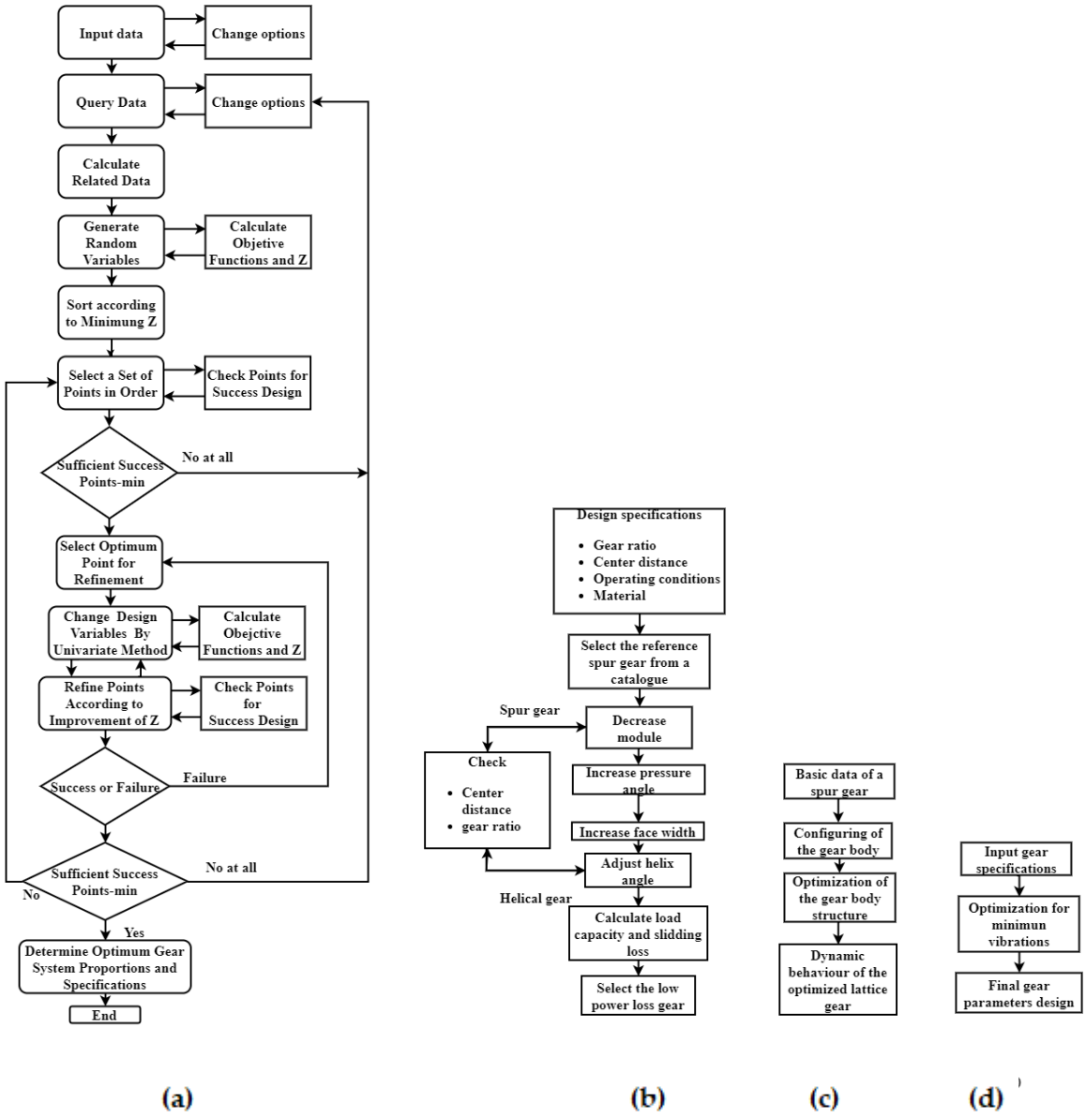

Figure 3. Design processes of spur gears which consider the minimization of vibration as a design goal. (a) Design procedure of a two-stage spur gear system through a Min-Max method combined with a direct search technique [89]. (b) Design process of parallel-axis gear by changing gear parameters [102]; (c) Design of gear body based on topology optimization [98]; (d) General design process of pair gears for minimum vibrations found in the literature.

Helical gears

Helical gears have been the second most researched type, and the main studies focus on tooth modifications for reducing vibrations. One of the first papers, dated 2000, was written by Chong TH et al. [103]. The authors faced the problem of minimizing gear sizes and reducing vibrations in them; they proved that there is a conflicting tendency between the vibrational excitation force by the tooth meshing and the gear size or the geometrical volume of a gear pair. Gear pairs with lightweight may have noise or vibration problems. Therefore, a single objective function is not suitable for the purpose since minimizing one design variable can adversely affect another. The authors used the goal programming method as a multi-objective optimization technique (Figure 4). Since the vibrations in gears are reduced with the decrease in vibrational excitation forces, which were established as an objective function as well as the size of the gear. The design variables used were normal module, number of teeth in pinion, face width, pressure angle, helix angle, and addendum modifications coefficients. The technique was applied to the redesign of a helical gear pair used in an elevator reduction drive. The volume (mm^3) was reduced by 38%, and the vibrational excitation force (N/mm) by 60%.

Komori M et al. [104] worked on optimizing the tooth flank form to perform low vibration and high load-carrying capacity; the author proposed a design algorithm under different misaligned conditions. Hedlund J & Lehtovaara [105] faced the problem of evaluating the mesh stiffness between all meshing teeth, which is one of the principal sources of vibration. The proposed model shows the best combination of gear parameters to minimize parametric excitation in a specific application. Fuentes A et al. [106] studied helical gears finished by plunge shaving. They proposed a computerized method for modifying the geometry of helical gear drives. The optimal design is a partial crowning of the pinion tooth surface, yielding the lower contact stresses and TEs when errors of alignment occur. Wu J et al. [107] also work on tooth profile modification (TPM) in helical gears for vibration reduction. The authors proposed a dynamic simulation method to evaluate the effect of TPM on vibration reduction in the designing stage; simulations were validated by experimental works. Wang C [108] developed a method for reducing vibration in double-helical gear by tooth modification through tooth contact analysis (TCA) and loaded tooth contact analysis (LCTA); the algorithm gets the tooth design parameter when the amplitude of TE is minimum (Figure 4).

Theerarangsarit K & Ratanasumawong C et al. [102] developed a series of steps to design parallel-axis gear to minimize power loss and its effect on vibration characteristics 6]. The

authors establish that load, operating speed, center distance, gear ratio, and gear material are defined. The steps are: 1) Decrease module, 2) Increase pressure angle, 3) Increase face width, 4) Adjust helix angle. Once these steps are done, gear tooth strength is calculated by the AGMA method, and if it is not met in the first iteration, the necessary number of times is carried out until it meets the minimum strength. Authors verified the design methodology experimentally with a reference gear pair and two gear pairs designed; they proved that the sliding losses of both designed gear pairs are significantly lower than the reference gear pair. Lower vibration amplitude is achieved from this design methodology.

Marafona J et al. [109] developed an algorithm methodology for generating constant mesh stiffness gears (CMSGears) considering the gears' safety factors and mesh efficiency. The methodology (Figure 4) needs a starting point of gear geometry to initiate the iterations and continues until no further minimization is possible. The CMSGears developed were compared with C14, H501, and H951 gears, and it was concluded that CMS Gears promote a more stable and smooth dynamic performance than conventional gears.

Tanaka. E et al. developed a design of a low-noise gearbox [110]. The design process starts from a phase of determination of the vibrational behavior to add ribs near the gearbox vibration mode antinodes. The first stage consists of three steps: gear-vibration analysis, gearbox vibration analysis, and sound-radiation analysis. The authors validated their method experimentally in an apparatus consisting of second-stage helical reduction gears; they measured the displacement of a gear shaft, the acceleration of points on the gearbox's surface, and the sound-pressure levels around the gearbox, and the values of the measurements coincided with the calculations made.

Other authors who have worked on decreasing vibrations by improving gear meshing quality are Wang F et al. [111]. They proposed a methodology to determine a tooth surface modification with a sixth-order TE that minimizes vibration noise, which considers the vibration model of a herringbone gear coupling. The methodology consists of the next steps: 1) Input gear pair basic parameters, 2) initial design parameters, 3) Solving the curve coefficients of a higher order polynomial function of TE (H-TE), 4) TCA and LTCA 5) Solving the herringbone gear dynamics model, 6) Genetic algorithms optimizing solving, 7) Return to the second step if the optimal solution was not found. They concluded that vibration reduction under meshing vibration acceleration optimization is much better than optimizing the loaded TE amplitude. They also found that in the range of design conditions, the herringbone gear with 6H-TE has the best vibration stability.

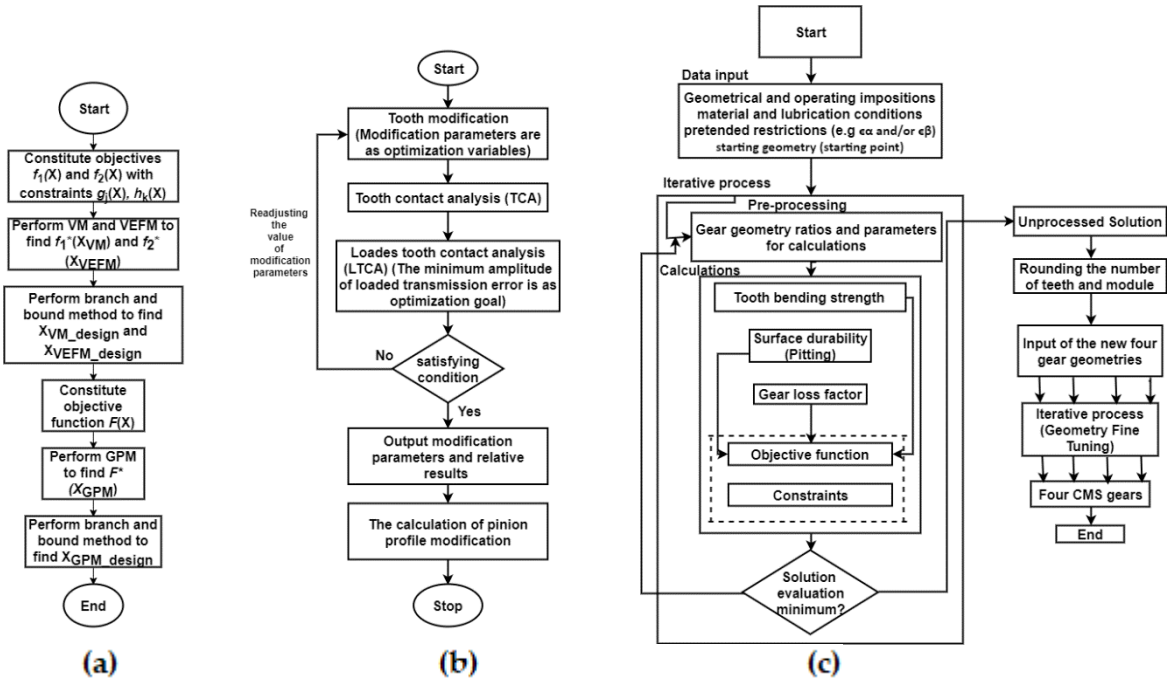

Figure 4. Design processes of helical gears that consider the minimization of vibration as a design goal. (a) Design process of cylindrical gear pairs for the reduction of gear size and meshing vibration [103] (b) Modified optimization of double helical gears [108] (c) Algorithm for generating CMSG (Constant Mesh Stiffness Gears) [109]

Spiral bevel gears

The complex geometry of gear tooth surfaces in spiral bevel gears makes the design problem more complicated, and most of the papers focus on reducing TE. Litvin F et al. [112] developed a method for design spiral bevel gear to reduce TE, which reduces noise and vibration through the application of local synthesis algorithm, TCA, and stress analysis by application of finite element method. Su J et al. [113] proposed an approach to design and implement a seventh-order polynomial function of TE to reduce the running vibration and noise of gear drive and improve the tooth's loaded distribution through a reverse TCA process. Astoul J et al. [114] also worked to reduce the TE, specifically the quasi-static TE; the developed approach is based on an optimization process including loaded meshing simulations. The optimization strategy consists of minimizing the maximal contact pressure and reducing the quasi-static TE. Mu Y and Fang Z [115] developed a method to design a seventh-order TE for HCR spiral bevel gears for reducing gear vibration and noise.

Mu Y et al. [116] developed a method for designing HCR spiral bevel gears. The authors proposed a tooth surface correction method for modifying HCR spiral bevel gears.

Argyris J et al. [117] proposed an integrated approach for the design and stress analysis of spiral bevel gears. Their method lets the determination of machine-tool settings for the generation of low-noise stable bearing contact spiral bevel gear drives. This method analyses the manufacturing process, and through finite element analysis, it allows the formation of bearing contact during the meshing cycle; the method reduces vibration and noise. Fuentes-Aznar et al. [118] proposed an integrated computerized approach of design, generation, and stress analysis of low noise, high endurance face milled spiral bevel gear drives machined using a five cut process.

Bearings

The relationship between the design of bearings and vibrations is less systematic than the relationship between the design of gears and vibrations. Yang B et al. worked on the optimum vibration design for the low-pressure steam-turbine rotor of a 1007-MW nuclear power plant [119]. They assumed small vibrations in the bearing elements in order to linearize the nonlinear characteristics of the bearings. A hybrid genetic algorithm (HGA) was used for the optimization. HGA consist of two main processes: global search and local search. Bearing length, bearing clearance, and shaft diameter were optimized through HGA. These variables were chosen because it is considered that bearing length and diameter have a significant influence on the vibration characteristics; they showed that Q-factor and unbalance response can be improved by the optimization of selected variables.

Ohta H et al. [120] designed crowning to reduce ball passage vibrations of a linear guideway; this is because of the increase in noise and vibration of machines that use linear bearings due to the increase in the speed of these machines. The design conditions were: length of carriage body, oversize of the balls, the distance between adjacent balls, contact angle, and crowning length. The crowning procedure design was developed in six steps; the calculated ball passage vibration amplitude for the designed power function crowning is lower than those of the commercial linear bearing. The designed linear bearing was manufactured, and the vibrations were measured. The ball passage vibrations' measured amplitude for the designed power function crowning was lower than that of the commercial linear bearing.

Kirk R et al. [121] studied the dynamic characteristics of three custom, fixed bore, bearing designs in a turbocharger of a 3,9 liter 130 HP diesel engine. They obtained the two-mode frequency for the different bearings, and they compare it with the initial stock floating bush bearing. A significant contribution is the work of Chasalevris A et al. [122]; they designed and manufactured a variable geometry journal bearing (VGJB) and showed a decrease in the vibration amplitude at resonance by up to 70% compared to a conventional journal bearing.

Cao J et al. [123] considered several bearing designs for a large turbocharger for an industrial reciprocating engine. They showed that a fixed pad bearing design resulted in a highly unstable rotor and tilting pad journal bearings have greatly reduced cross-coupled forces compared to fixed-geometry bearings. Table 2 shows the principal results of the design methods found related with vibration reduction and the element or system which were applied. Another classification, not by the application but by the methodological approach used, is shown in Figure 5.

Since the design of geared systems, taking into account vibrations, is a dynamic problem, all approaches will have a dynamic component in their methodology; therefore, the dynamic models approach covers all of them. Transmission error is one of the principal variables considered since its reduction is reflected in a better vibratory behavior of the system, and this approach has been applied mostly in spiral bevel gears.

Other researchers are focused on developing or implementing an optimization algorithm to improve the transmission's vibratory behavior. The rest of the papers modify design parameters as module, pressure angle, and tooth geometry to obtain a better vibratory response.

Table 2. Results of the design methods for reducing vibration in main mechanical transmission elements.

Transmission element	Method	Application	Results
Spur gear	Refined min-max technique and direct min/max search method [89]	Two-stage spur gear system	Reduction of dynamic factor by 22% and 53% in the first and second teeth meshing zone, respectively
	Genetic algorithm [90]	Two mating gears	22,1 microns of TE
	Higher-order functions of transmission error [92]	Gear pair	High effective contact ratio with the higher-order TE
	HCR and profile modification [94]	Two-stage helicopter transmission	Vibration decrease of three to four times compared with regular design
	Dynamic behavior of spur gears with asymmetric teeth[95]	Involute spur gear pairs	Design rules for spur gears with asymmetric teeth

Transmission element	Method	Application	Results
Spur gear	Tribo-dynamic model [96]	Spur gear pair	Conclusions about dynamic mesh force and load ratio
	Unified tribo-dynamic model [97]	Spur gear of ink vibrator	Optimal range of the crown radius and round corner radius for reducing maximum pressure
	Topology optimization [98]	Titanium alloy's gear	Lower frequency ranges in some dominating frequency components in the lattice structure proposed
	Optimization of the dynamic response of the turret gear system by improving the modulus and the pressure angle [99]	Three-stage gear train	Reduction of vibration of 28% - 60%
Helical gear	Multiobjective optimization technique through goal programming method [103]	Gear pair used in an elevator reduction drive	Reduction of the vibrational excitation force (N/mm) by 60%
	Optimization of tooth flank form [104]	Gear pair	Reduction of the vibrational excitation force (N/mm) in the range of 16% - 50%
	Model for excitation calculation [105]	Gear pair	Mesh stiffness variation in the frequency domain and reasonable computational time
	Computerized method for geometry modification [106]	Gear pair	Reduction on the transmission error
	Tooth profile modification [107]	Gear pair	Vibration reduction for the studied load conditions
	Modification of different gear parameters [102]	Gear pair	Maximum vibration reduction of 85% for the studied load condition
	Constant mesh stiffness [109]	Gear pair	Lowest RMS of the Dynamic Transmission Error for the evaluated gears
	Analysis of dynamic behavior to add ribs in helical gearbox [110]	Second-stage helical reduction gears	Concordance with experimental measurements and the proposed method
	Optimization design method for six order transmission error[124]	Herringbone gear coupling	Reduction of RMS acceleration of 40% in resonance velocity of six order transmission error compared with second-order transmission error

Transmission element	Method	Application	Results
Spiral bevel gear	Local synthesis algorithm for reducing transmission error [112]	Gear pair	Reduced level of transmission error for prototypes of optimized gear drives studied
	Seventh-order polynomial function of transmission error [113]	Gear pair	Advantages in load sharing curves and tensile stress
	Optimization process to reduce the transmission error [114]	Gear pair	30% reduction in the quasi-static transmission error
	seventh-order transmission error for HCR spiral bevel gears [115]	Gear pair	Improvements in the dynamics meshing quality of spiral bevel gears
	High order transmission error for HCR spiral bevel gears [116]	Gear pair	Reduction of transmission errors for different load conditions
	Synthesis, TCA, and stress analysis [117]	Gear pair	Reduction of the shift of bearing contact caused by misalignment
	Integrated computerized approach of design through a Five-Cut Process [118]	Gear pair	Uniform evolution of contact and bending stresses
Bearing	Hybrid genetic algorithm [119]	Two journal bearings	Optimum values of bearing length and bearing clearance
	Design of crowning [120]	Linear ball bearing	Reduction of 33% in the amplitude of displacement for the maximum linear velocity tested
	Design of journal bearing with variable geometry [125]	Journal bearings	Decrease in the vibration amplitude at resonance by up to 70% compared to a conventional journal bearing

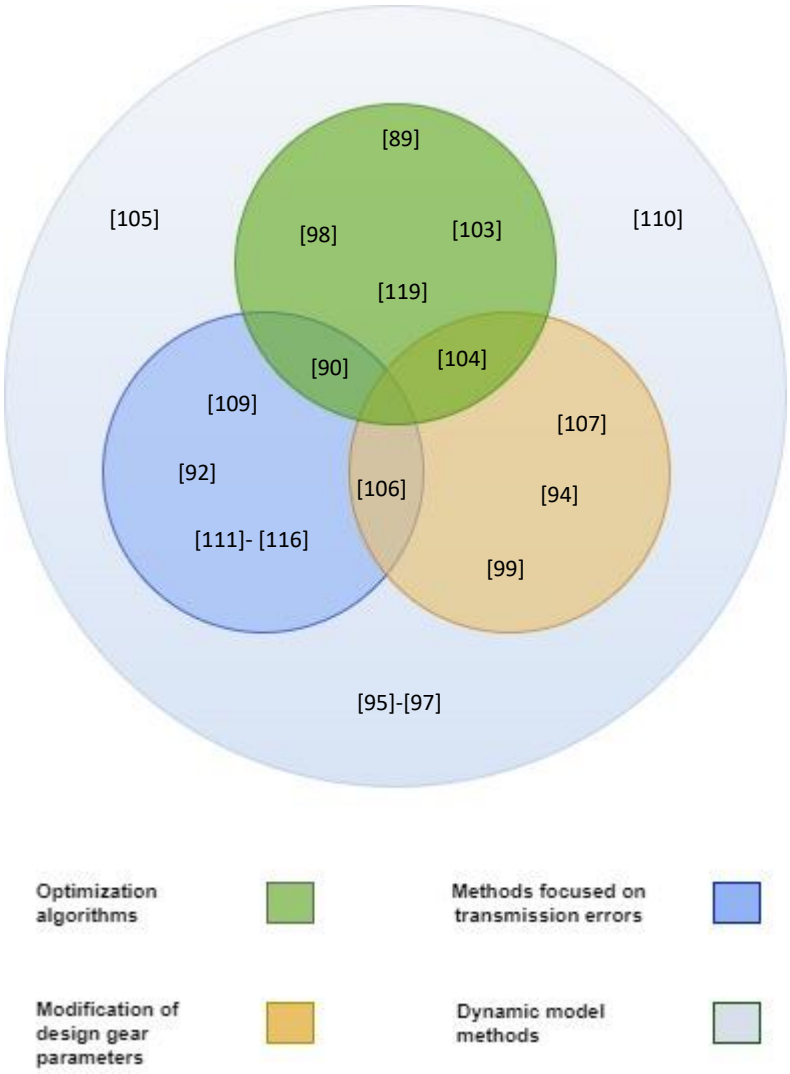

Figure 5. Principal papers found grouped by the approach used to solve the problem of minimizing vibrations from the design stage in geared systems.

Conclusions

It was shown the main design studies carried out in the last 20 years considering vibrations of power transmission elements such as gears and bearings. There are clear design methodologies for gears and gearboxes, that take into account vibrations. The methods found begin with the initial specifications, and they are optimized taking into account the vibrations and other restrictions, to finally obtain the design parameters. Although in some of these papers was found that the final design values are functional and generate lower vibrations than the initial ones, there is no robust methodology that can be applied to more general cases. Some of the studies found apply a method of optimization and prove their efficiency in reducing vibrations.

In the case of bearings, the process is less systematic, and there are fewer papers related to the design, taking into account vibrations. They mainly focus on making modifications in the bearings and then validating the reduction in vibrations generated. Gear design, according to the analysis shown in Figure 2., is an emergent topic. Mesh stiffness and TE are some of the principal variables for gears design considering vibrations. Because the *Vibration* cluster is a motor topic, future research could be directed in developing design methodologies of gears that emphasize the analysis of mesh stiffness and reducing TE. Although helical gears are of particular interest recently, the development of robust design methodologies should not be left aside for spur gears.

Research problem

According to the state of the art, there are some design methodologies that take into account vibrations for gears and gearboxes. The works found start from initial specifications, an optimization is made taking into account the vibrations and other restrictions and finally, the final design parameters are obtained. Although in some of these works it is found that the final design values are functional and generate lower vibrations than the initial ones; there is no robust methodology that can be applied to more general cases. The works more approximate to the design apply a method of optimization and prove their efficiency in the reduction of vibrations.

In the case of bearings, the process is less systematic and there are fewer works related to the design taking into account vibrations. The works are mainly focused on making modifications in the bearings and then validating the decreases in the levels of vibrations generated. Gear design according to the analysis shown in Figure *2* is an emergent topic; mesh stiffness and transmission error are one of the principal variables for the design of gears taking into account vibrations. Because *Vibration* cluster is a motor topic, future works could be directed in developing design methodologies of gears which special emphasis on the analysis of mesh stiffness and reducing the transmission error. Although helical gears are of special interest recently, the development of robust design methodologies for spur gears should not be left aside.

Transmission error is defined as the departure from uniform angular velocity of the gear pair [126]. Transmission error is caused by the tooth profile error, gear tooth deflections caused by the transmitted load and the gear misalignment on the line of action, which means that it is zero if the gear pair has a perfect involute gear geometry, infinite stiffness and no misalignment. Improvements in the design of the tooth profile have been studied and mesh stiffness has been extensively studied, however vibration and the noise characteristics in gear meshing under different shaft misalignments is not comprehensively discussed in the available literature. Most of the studies helped to determine the strength of gears under misalignment but no explain about the gear dynamic responses. Numerical and experimental studies based on vibrations of misaligned gears are relatively new [127] and [128]. M.A. Khan et al. [129] studied vibration in gear mesh under different shaft misalignments through condition indicators like RMS energy, Kurtosis and Skewness. They proposed regression models to predict the degree and type of the shaft misalignment for each type of misalignment (radial, axial, yaw and pitch) under constant load and fixed running speed. The regressions give information about misalignment in terms of the relative loss in the teeth meshing area. More experimental works must be done in order to improve

the regression models. It is also important to consider, not only a type of misalignment but the combination of these, which is more in line with reality. Also, studies under variable loads and different running speeds should be carried out, in time domain and frequency domain. The extension of the study of vibrations in the meshing zone to different combinations of misalignments, under variable load and different speeds would not only improve the diagnosis of misalignment conditions in mechanical transmission of spur gears, but also serve as a considerable contribution to the design of this type of transmissions if the deformations of the teeth are studied to determine the stresses in the meshing zone. In this way, the following research question is posed: What contributions to gearbox design can be derived from bearing vibration measurements when shafts exhibit combined misalignment?

Research Objectives

General Objective

Develop guidelines for the design of spur gear power transmission systems considering the combined misalignment of the shafts.

Specific Objectives

1) Propose a theoretical model for the projected contact area in spur gears subjected to combined misalignments.
2) Develop an experimental and semi analytic approach for the study of vibrations and bending stress in a single-stage spur gear system under combined misalignments.
3) Develop design recommendations for spur gear transmission systems from the results obtained from the combined misalignment analysis.

Structure of the thesis

As previously established, the origin of this thesis derives from the idea of little methodological integration in the design process of gear power transmission systems, taking into account their vibratory behavior. This affirmation was corroborated with the systematic bibliographic search in which it was shown that although there are some significant investigations in the field, there is still a long way to go and there are unexplored themes.

One of these themes is the development of design guidelines from the study of the effects of combined misalignments in the shafts of single-stage transmission systems. This is an unexplored topic because even the study of vibrations under combined misalignments, which are more in line with reality, has not yet been studied or reported in scientific articles. The little information that exists is fundamentally related to individual misalignments. This thesis aims to be the first reported work related to the subject, so that a first analysis of the effects of the combined misalignments is made in the measurements of the vibrations measured in the base of the bearings and in the bending stress of the teeth of the gears. Based on this analysis, design recommendations will be proposed that take into account the variables studied here.

A first experimental approach is carried out. For this stage, a misalignment test bench was designed, built and fine-tuned. This test bench allows generating radial, axial and angular misalignments in a single stage spur gear transmission system. In order to study trends in the vibration response when there are combined misalignments, a first experimental study is carried out evaluating all possible combinations of extreme levels of misalignment for a pair of spur gears. In order to find a relationship between the contact area and the vibratory response, a theoretical model for the projected contact area is proposed. Through an indicator that allows determining the percentage of change of two spectra, it was possible to determine the influence of each type of misalignment and its combinations in the vibration measurements and it was possible to find the areas of greatest interest.

A hybrid model was developed to estimate the accelerations in the bearings. The model is based on a finite element model to estimate the bending stress in the teeth and the force at the point of contact between a gear and its shaft; this force signal is the input of an analytical model that allows the estimation of the vibration signals in the bearings. With this model it was possible to explore a wider range of work and when contrasting it with the experimental results a high correlation was found, which validates the proposed model. With the found results of stress and vibration, some design recommendations were proposed that take into account the work areas found here and that allow the simplified

application of the methodology developed in this research. In the final part, the conclusions found are shown and future work related to the subject is proposed.

Experimental approach

It is intended to study, through experimentation, the effects of the combination of axial, radial and yaw misalignments in the measurements of vibrations, in the bending stresses in the gears in a single stage gear transmission system. This was achieved through the design and construction of a misalignment test bench and the execution of different tests that allowed estimating the effect of the combined misalignments in a wide range of work.

Testing workbench

A testing workbench was designed and manufactured for generate different misalignments conditions in a single stage gear transmission system and evaluate vibration condition in the support bearings and deformations in gears. With the testing workbench is possible get three types of misalignment: radial, axial and angular (yaw). Compared with the alignment condition, in radial misalignment, center to center distance of the gear increases and the shafts remain parallel. In axial misalignment, center to center distance of the gear remains the same but one gear moves forward or backward in the direction of its shaft. In yaw misalignment there is a non-zero angle between the two shafts in the horizontal plane. These three types of misalignments are shown in Figure 6.

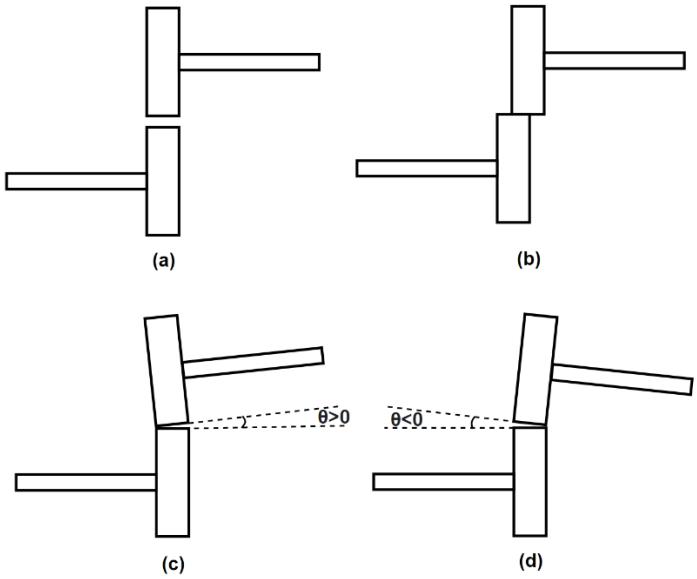

Figure 6. Sides view of misalignments investigated. (a) Radial (b) Axial (c) Positive yaw (d) Negative yaw

Testing workbench is formed by two parts: the motor side, Figure 7 (a), and the reactive side, Figure 7 (b). On the motor side the power supply is given by a 2 hp three-phase AC motor, Figure 7 (n), connected to a frequency variator that allows to regulate the speed of rotation in the motor. The reactive side is responsible for providing the reactive load in the

system through a positive displacement gear pump, Figure 7 (c), in which the fluid pressure is controlled through a hydraulic bank connected to the pump. The motor side is supported by a lower base plate, Figure 7 (d), that is bolted to the machine bed, Figure 7 (e). Four L plates, Figure 7 (f), are mounted on this base plate. The vertical side of the L-plates is slotted to allow displacement of the circular support bars that support an upper base plate, Figure 7 (g). These slots allow movement of the top plate to generate radial and angular misalignments. The top plate supports the base of the motor and the base of the two support bearings. The motor side shaft supports the pinion gear and is supported by two bearings, this shaft is connected to the motor shaft through a flexible coupling, Figure 7 (h). Three vertical screws, Figure 7 (i), go through the top plate and serve as top support for different heights. The slots in the L-plate on the motor side allow axial movement of the upper plate in a range of 3 cm and a yaw misalignment of 4,3°.

The reactive side is formed by a base plate bolted to the machine bed, Figure 7 (j). Four hubs, Figure 7 (k), are mounted on the base plate for support to vertical circular bars that support a top plate, Figure 7 (l). The four vertical circular bars have a nut-locknut mechanism to achieve different heights according to the diameter of the driven gear. The top plate supports the base of the pump and the base of the two support bearings. The reactive side shaft supports the driven gear and is supported by two bearings. As in the motor side this shaft is connected to the pump shaft through a flexible coupling, Figure 7 (m). The pump is connected to a hydraulic bench in which the pump, driven by the engine, sucks from the bench tank and the oil that comes out of the pump is regulated through a valve that controls the fluid pressure. The reactive side base plate moves along the bed through a screw mounted to a fixed base on the bed that pushes or retracts the reactive side to generate axial misalignments up to 5 cm, Figure 7 (o). Ranges of the testing workbench are shown in Table 3. The shafts that support the gears are each mounted on two UC 205 ball bearings.

Table 3. Workbench displacement ranges.

Workbench ranges	
Radial misalignment	0 - 3 cm
Axial misalignment	0 - 5 cm
Yaw misalignment	-4,3° - 4,3°

The motor power is 1,5 kW, therefore at the nominal speed of 1500 rpm, 9.5 Nm can be generated. IMI accelerometers of 100 mv/g sensitivity and a range of 0-10 khz are mounted on the bench, positioned on the bearing bases in the vertical, horizontal, and axial directions as it is shown in Figure 8. The accelerometers are connected by coaxial cable to a National Instrument (NI) 9234 acquisition card. This card has four analog input channels and an anti-aliasing filter for regulating to the sample rate specified. NI 9234 is connected to a computer in which the information is recorded through Signal Express© from LabVIEW©.

Operation of the testing workbench

The two lower bases on both sides are grooved with a 90° L-shaped profile so that it can be coupled to the bedplate and axial displacement can be generated. The motor side is fixed to the base with bolts. The reactive side can be displaced on the bed along the axial direction through the system shown in the Figure 7 (o). By turning the screw with a wrench, the reactive side can be pulled or pushed. The pitch of this screw is 1.5 mm, therefore by turning the screw a quarter of a turn, an axial displacement of 0.375 mm can be achieved. Once the desired displacement is obtained, the fixing screws to the bedplate are tightened for the correct operation.

As mentioned above, the vertical slots in the drive side L-plates allow movement of the top plate, however this movement affects both vertical and angular displacement, i.e. it affects radial and yaw misalignment. Therefore, by means of trigonometric relations, it is necessary to estimate how much the horizontal screws must be displaced on each side. The nuts on the vertical L plates must be loose so that the upper base can move. To achieve a certain height, it is necessary to hold the nut at the top of the upper base and turn the heads of the vertical screws. Once the desired heights have been achieved, all the nuts on the motor side must be tightened.

As mentioned above, the test bench has acceleration IMI sensors with a sensitivity of 100 mv/g and a range of 0 to 10 kHz connected to the NI 9234 card. Another acquisition card, the NI 9215, is used to acquire the other accelerometer signals. This card has four channels and a BNC front connector. An ammeter clamp was also installed to measure the current in one of the motor phases. A laser tachometer was installed to measure the rotational speed of the shaft on the motor side and on the reactive side. Signals from the ammeter clamp and the tachometer are received on the NI 9215. A slip ring was installed on the pinion shaft to transmit strain gauge signals on the pinion gear teeth to an NI 9237 acquisition card. This is a four-channel special card for strain acquisition.

Figure 7. Testing workbench for misalignments. (a) Reactive side (b) Motor side (c) Gear pump (d) Lower base plate (motor) (e) Machine bed (f) L plates (g) Upper base plate (motor) (h) Flexible coupling (motor) (i) Vertical screws (motor) (j) Base plate (reactive side) (k) Support hubs (j) Top plate (reactive side) (k) Flexible coupling (reactive side) (l) Motor power (m) System for axial movement of the reactive side.

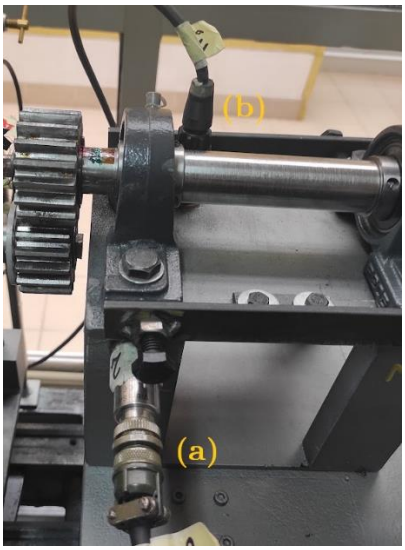

Figure 8. Accelerometers on the motor side. (a) Horizontal position (b) Vertical position.

Shafts alignment

In order not to induce forces in the motor or the pump, the shafts of these equipments must be aligned with the shafts of the gears. The alignment procedure was carried out with dial comparators in the vertical plane and in the horizontal plane as shown in Figure 9. For each plane, 4 points spaced at 90° were measured. Measurements were taken at each of the four

points and through trigonometric ratios it was determined how much the motor or pump should move vertically and horizontally, with the help of shims at the base. After various adjustments, alignment was achieved with the values shown in the Table 4.

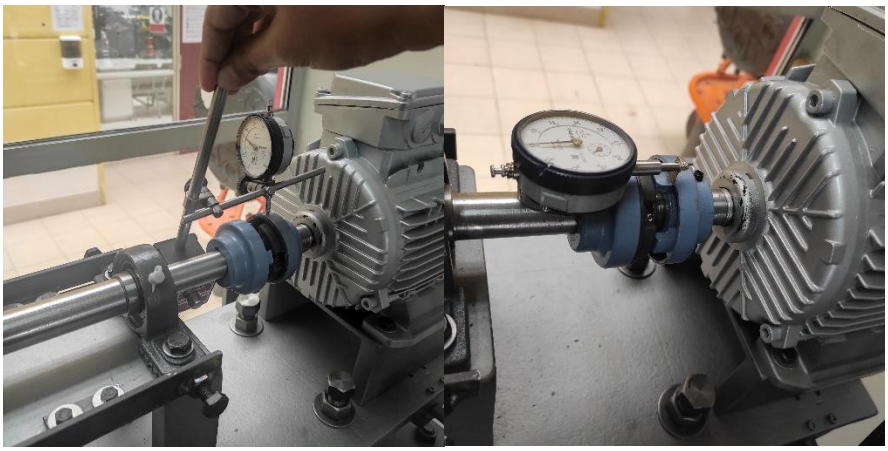

Figure 9. Alignment of the motor axis in the horizontal and vertical plane.

Table 4. Final alignment values for the motor

Angle (degrees)	Radial measurement (mm)	Angular measurement (mm)
0	0	0
90	0	-0,2
180	-0,03	-0,3
270	0,01	-0,01

Experimental runs

As mentioned above, to achieve the misalignments, the upper base must be moved on both the motor side and the reactive side. This will allow relative movement of one gear with respect to the other in 3 directions: axial, radial and yaw. The main cause of misalignment in gears is due to faults in assembly or operation, so these factors were considered to determine the maximum ranges for each variable. The parameters of the pinion gear and the driven gear are shown in the Table 5. Considering these parameters, the ranges were established for each misalignment. In the aligned condition the radial, axial and angular misalignment values are zero. Radial misalignment starts from zero to 1.5 mm; this value was taken since the module is 3, and in this case a displacement of half the module is a considerable misalignment. From the Equation (1), the contact ratio for the alignment condition is 1.53. Contact ratio is the most used variable for checking the continuity of action in the gears [130]; to guarantee a contact for at least one pair of teeth in any moment of the

movement, contact ratio must be greater than one; in this way with a radial misalignment of 1.5 mm, contact ratio is 1.07. Radial misalignment greater than 1.5 mm produces a contact ratio smaller than one, this could produce impact on the tooth and the effects on vibration will be different from what we want to address in this research.

Axial misalignment is not very common in the gear transmission systems, it is most common when the gear moves on its shaft. In this way, large axial misalignment is not very frequent. For experimentation, approximately 13% of the total possible misalignment was taken as the maximum working value. The total possible axial misalignment is given by the tooth face width; in this case the 13% is 4 mm. Although 4mm of axial misalignment is a high value and quite noticeable to the naked eye, it was taken because even with such a large value, the continuous contact of the teeth is guaranteed since the contact ratio is not affected. In addition, it is preferable to have levels of experimentation far enough apart so that the changes in the response variables are noticeable; very close levels between them could not show substantial changes in the response variables.

For setting the levels of yaw misalignment is need to consider that negative values have a different effect than positive angles on vibration measurements [129]. So, for a complete estimation of the effect of combined misalignments is needed to establish an extreme negative value and an extreme positive value for yaw misalignment. These extreme values were set experimentally. Since the main objective is to study the effect of combined misalignments on different output variables, it must be guaranteed that the extreme values of each type of misalignment allow their combination, that is, that any combination of extreme values is an operative experimental point in the workbench. -2,69° and 2,69° satisfy that condition; those misalignments are so high, but they were chosen for the same reason that axial and radial misalignment: they are extreme values far from each other and fall within an operating zone. In this research the pitch misalignment is not studied. To reduce the effect of pitch misalignment, a pair of gears with zero backlash was used. The extreme values for the misalignment studied are shown in Table 6.

Table 5. Parameters of the gears used in the misalignment bench.

	Pinion	Driven gear
Module	3	3
Teeth	18	18
Pressure angle (°)	20	20
Face width (mm)	30	30

$$m_p = \frac{Z}{p_b} \tag{1}$$

$$Z = \sqrt{\left(r_p + a_p\right)^2 - \left(r_p \cos\phi\right)^2} + \sqrt{\left(r_g + a_g\right)^2 - \left(r_g \cos\phi\right)^2} - C \sin\phi$$

m_p = contact ratio
Z = length of the line of action
p_b = base pitch
r_p = pinion pitch radius
r_g = driven gear pitch radius
a_p = pinion addendum
a_g = driven gear addendum
ϕ = pressure angle
C = nominal distance between centers

Table 6. Extreme values for each type of misalignment for the experimental analysis.

Type of misalignment	Extreme values	
Radial (mm)	0	1,5
Axial (mm)	0	4
Yaw (°)	-2,69	2,69

One of the purposes of the experimental analysis is estimate the effect of each type of misalignment in the vibration measurements and the effect of the combination of them. The effects are of greater interest than establishing a regression model since this model would be valid only for the case studied in the workbench under the given conditions, while the effects of the variables and their combinations can be extrapolated to other cases. A first valid approximation to estimate these effects is to combine all the extreme values and analyze the change in a response variable associated with the measured vibrations. In other words, experimental runs will be made of all the possible combinations of misalignments in their extreme values and the change in the response variable that occurs when moving from one experimental point to another will be evaluated. Since there are three variables and two extreme values will be studied for each one, the combination possibilities are $2^3 = 8$ and they are shown in the Table 7.

Table 7. Experimental points considering all possible combinations.

Radial (mm)	Axial (mm)	Yaw (°)
0	0	-2,69
0	0	2,69
0	4	-2,69
0	4	2,69
1,5	0	-2,69
1,5	0	2,69
1,5	4	-2,69
1,5	4	2,69

Although the main objective is not to establish a model from the collected data, it is important to aim for a constant variance in the experimental execution, that is, to guarantee the assumption of independence, for which the experimental runs must be randomized. The order of the runs is shown in the Table 8. Since the main objective is to show the change in vibration measurements due to misalignment, a reference must be taken from the vibration signals of the aligned condition. In practice it is difficult to have a perfectly aligned condition, that is, zero in all types of misalignments, however, a fairly close point was analyzed. Adjusting the vertical and horizontal bolts brings the gears to the desired position. This position is checked through vernier caliper measurements on the gears. Figure 10 shows a representation of the aligned gears and gears with yaw misalignment. Because the pitch diameter of the pinion and driven gears used is 57 mm, distance 1, d1, and distance 2, d2, must be 114 mm for the aligned condition; 114,11 mm and 114,03 mm were the values get for d1 and d2 respectively. The nominal speed of rotation for the runs was 282 rpm and the torque applied by the pump was 3,25 Nm. Seven experimental runs were made for the alignment condition. The acquisition rate was 10 kHz. The signal time from the horizontal accelerometer mounted on the bearing closest to the pinion gear is shown in Figure 11. For checking the distribution of the values, a histogram of the signal time is made. Construction of histogram requires the estimation of bin width to establish the number of bins. The expression proposed by Scott[131] was used (Equation (2)), where h is bin width, s is an estimate of the standard deviation, and n is the number of samples. For the aligned condition seven runs were made and averaged.

$$h = 3{,}49sn^{-\frac{1}{3}} \qquad h = 3{,}49 \times 0{,}1124 \times (60000)^{-\frac{1}{3}} \qquad h = 0{,}01 \tag{2}$$

Therefore, the number of bins b is given by Equation (3) where y_{max} and y_{min} are the maximum and minimum amplitude value for the values, respectively.

. Expression for number of bins.

$$b = \frac{y_{max} - y_{min}}{h} \qquad b = \frac{0{,}4526 - 8{,}03 \times 10^{-6}}{0{,}01} \qquad b \approx 45 \tag{3}$$

Table 8. Order of experimentation.

Possible combination	Radial (mm)	Axial (mm)	Yaw (°)
1	0	0	-2,69
2	0	0	2,69
3	4	0	2,69
4	0	1,5	-2,69
5	4	1,5	-2,69
6	4	0	-2,69
7	4	1,5	2,69
8	0	1,5	2,69

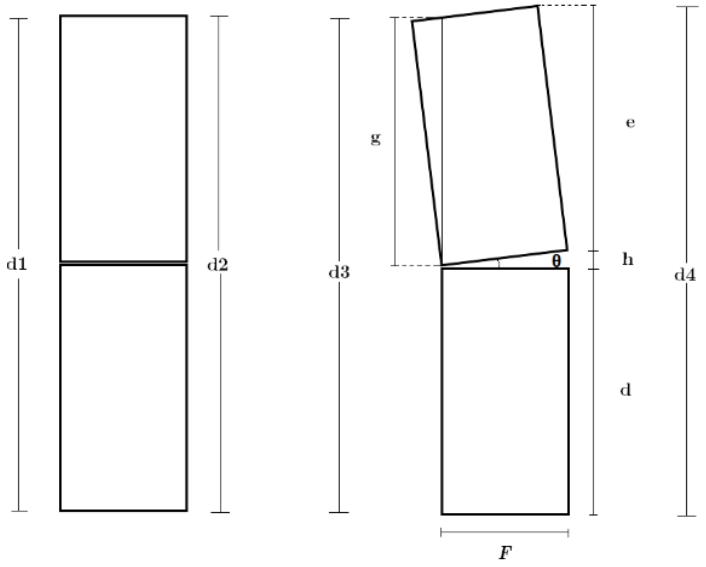

Figure 10. Measurement distances for the aligned condition (left), d1 and d2 and a positive angular misaligned condition (right), d3 and d4. Side view.

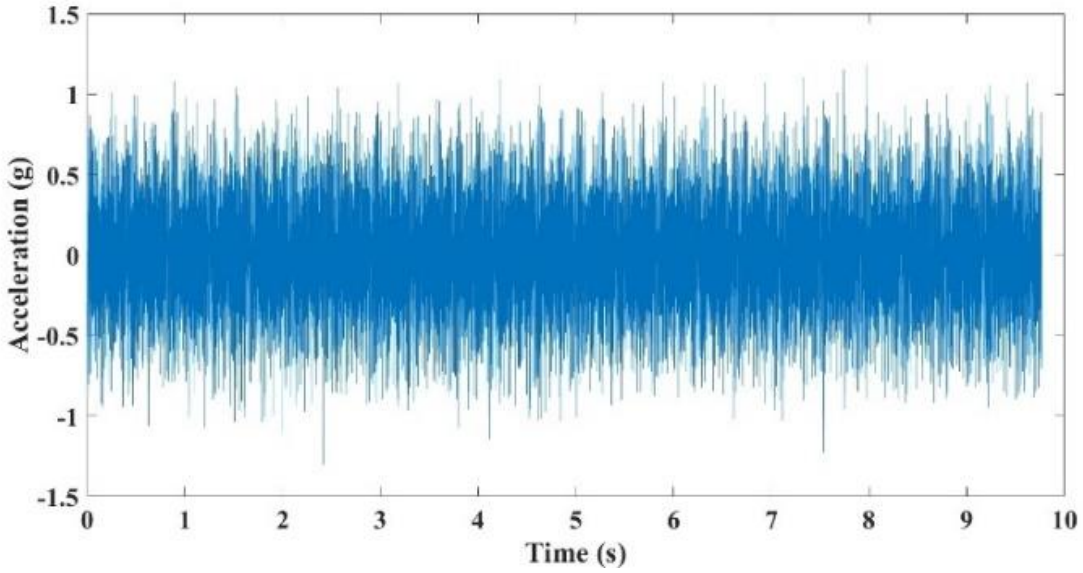

Figure 11. Signal time for one of the runs in the alignment condition for the horizontal accelerometer in the motor side.

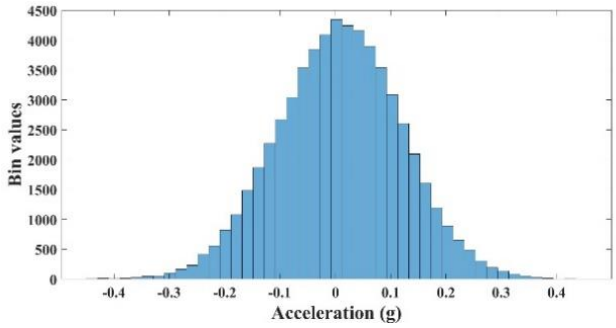

Figure 12. Histogram for the alignment condition for the horizontal accelerometer in the motor side.

As expected in the aligned condition, Figure 12 shows that the highest concentration of values is close to zero. To support this statement quantitatively, it is possible to calculate the kurtosis of the data. Kurtosis is a statistical parameter used to determine the degree of concentration of values around the central distribution zone, that is, it allows knowing how pointed or flattened a distribution is. Kurtosis is defined as the standardized fourth moment about the mean, the expression is shown in Equation (4), where b is kurtosis, y_i is the value of the sample, $\bar{y}$ is the sample mean and n is the number of samples. A kurtosis value of 3 corresponds to that of a normal distribution; values less than three imply in general terms a flatter curve than normal distribution and values greater than 3 imply a more pointed curve than normal. Kurtosis for the aligned condition according to Equation (4) is 3,05. Since the normal distribution has a kurtosis of 3 and the calculated value is very close to 3, it can be stated that in the aligned condition the values have a normal distribution. Runs were made

in the order shown in Table 8. Six runs were made by each experimental point, and the signal time was averaged. Kurtosis in signal times from misalignment cases was researched experimentally in the work of M. A. Khan *et al* [129]; they studied individually the effect of each misalignment on kurtosis response, and they found that for axial, radial and yaw misalignment the kurtosis decreases with the increasing of these misalignments. Although in our work the combined misalignments will be studied fundamentally, with the chosen experimental points the individual effect of each type of misalignment can be analyzed. For this, it will be calculated the effect for each misalignment. The effect can be defined as the change in response produced by a change in the level of the studied factor averaged over the levels of the other factors analyzed [132]. For the case of three factors that move at two levels, which is the one studied, the effect is calculated through the Equation (5) where A is the variable studied, n is the number of samples, (1) is the point with all the factors in their lowest level, *a* is the point with the factor A in the highest level and the other two factors in the lowest level, *b* is the point with the highest level in a B factor and the lowest level in the other two factors, *ab* is the point with the highest level for A and B factor and the lowest level for the other factor, *c* is the point with the highest level for C and the lowest factor por the other two factors, *ac* is the point with the highest level for A and C and the lowest level for the other factor, *bc* is the point with the highest level for B and C and the lowest level for the other factor, and *abc* is the point with all the factors in their highest level. Kurtosis values for the time signals in each experimental point are shown in Table 9. The standardized effect is the effect in which the lower and upper levels of each factor are normalized to -1 and 1 respectively, in such a way that the values of the effects can be compared with each other.to According to the Equation (5) effect for axial, radial and yaw misalignment are -0,023025; -0,102225 and 0,109725 respectively. The negative sign in the effects means that by increasing the value of the axial and radial misalignments, the kurtosis value decreases, which coincides with the results found in the work of M. A. Khan *et al* [129]. Increasing the values of axial and radial misalignment implies a decrease in the contact area of the meshing gears, which decreases the energy levels in vibration measurements. Because kurtosis gives an idea about the intensity of gear meshing energy, it is expected that as these misalignments increase, the kurtosis decreases. The increasing of yaw misalignment also produces a decreasing in kurtosis values. The positive value the calculate effect for yaw misalignment is because the sign convention for this work is opposite to that of M. A. Khan *et al* [129]. When the pinion is displaced towards the driven gear the asperities increase, increasing the energy levels in vibration measurements, this configuration in this work is the positive yaw angle. When the pinion is displaced away the driven gear the asperities decrease, decreasing the energy levels in vibration measurements, this configuration in this work is the negative yaw angle. The percentage of contribution of axial, radial and yaw misalignments in the response variable, kurtosis in this case are 0,88%; 17,39% and 20%. These values coincide with those previously reported [129], since the values of change in kurtosis for axial misalignments are very low compared to radial and yaw misalignments, which have a

relatively similar contribution. Another statistical parameter for preliminar analysis in time domain on vibrations measurements is the skewness. Skewness give us an idea of the simmetry of the amplitude distribution of the vibration. A positive value means that right tail is longer, and a negative value means that left tail is longer; this means that a value of skewness greater than other implies higher vibration levels, so the increasing of axial, radial and yaw misalignments should produces a decreasing in skewness values. Expression for skewness is shown in Equation (6) and the values are shown in Table 9. The effect of each misalignmentes were calculated in the same way that for kurtosis values. Standarized effect os screwness for axial, radial and yaw misalignments are -0,0077; -0,0026 and 0,0097 respectively; percentaje of contribution are 0,5%; 4,22% and 6,64%. This concordance in the trend of the contributions of individual misalignments to the reduction of vibrations, establishes a basis that validates the analysis of results that will be shown for the combined misalignment.

$$b = \frac{\sum(y_i - \bar{y})^4/n}{(\sum(y_i - \bar{y})^2/n)^2} \tag{4}$$

$$A = \frac{1}{4n}[a - (1) + ab - b + ac - c + abc - bc] \tag{5}$$

$$skewness = \frac{n\sum(y_i - \bar{y})^3}{(\sum(y_i - \bar{y})^2)^{3/2}} \tag{6}$$

Table 9. Kurtosis and skewness values for time signals.

Radial (mm)	Axial (mm)	Yaw (°)	Kurtosis	Skewness
0	0	0	3,05	-0,043
0	0	-2,69	2,8605	-0,0334
0	0	2,69	2,8382	0,0248
0	4	-2,69	2,9572	-0,0023
0	4	2,69	2,853	-0,0133
1,5	0	-2,69	2,675	-0,0262
1,5	0	2,69	2,9743	0,000445
1,5	4	-2,69	2,5898	0,0027
1,5	4	2,69	2,8584	-0,0322

Frequency analysis will be made for study the effect of combined misalignment on vibration measurement. The Fast Fourier Transformation (FFT) is applied to the signal time for reading the acquired signal on frequency domain. When reviewing the frequency spectrum of the signals, it is observed that the relevant information is found up to 1000 Hz. As the speed of rotation is 5 Hz, for a better visualization, frequency windows are taken every 5 Hz and the highest value in that window is taken. The superposition of several runs for the same experimental point is shown in Figure 13. The first peak observed occurs at 60 Hz, this peak is related to the positive displacement pump. Since it is a pump in which each gear has 12 teeth and the speed of rotation is 5 Hz, then the gear mesh frequency of the pump is 5 Hz x 12 = 60 Hz. Second peak is related with the gear mesh frequency of the gears. Pinion and driven gear have 18 teeth each, therefore the gear frequency is 5 Hz x 18 = 90 Hz. The rest of the peaks that are observed in the spectrum correspond to multiples of the gear mesh frequency and multiples of the gear rotational frequency. The way to compare frequency spectrum and analyze trends is not very well defined for the case of the misalignments studied in this work; for parallel misalignment in two coupled shafts is common compare the 1X and 2X frequencies, a machine in which vibration at 2X running speed is greater than 150% of the 1X indicates a severe misalignment [133]. V. Skrickij and M. Bogdevicius found relations of increasing and decreasing for pair and nonpair frequency peaks [134]. An indicator for compare the change of the spectrum values with the spectrum of the aligned condition was proposed, see Equation (7). This equation expresses the change for each peak between the spectrum to be compared with the base spectrum. In Equation (7). n is the number of samples; y are the values of the spectrum to be compared, and z are the value of the base spectrum. Due to the way in which this indicator is developed, it allows us to estimate the changes, whether positive or negative, between one spectrum and another. Percentage of change for each experimental point is shown in Table 10. The standardized effects and percentages of contribution of each variable and their combinations were calculated, see Table *11*. The highest contributions are those of radial and the angular interactions. It was to be expected that the radial misalignments would have an important contribution in the measurement of the vibrations because the radial misalignment affect the tangential force which is one of the most important variables that affect the vibrations measurements, since in this case the measured vibrations were in the horizontal axis and the configurations of gears was vertical; another important thing to highlight in these results is the high contribution that the interaction of variables has. This value of contribution allows us to clearly see that the vibratory response of a system subjected to misalignment is not linear in the sense that it is not only the sum of the effects of the individual misalignments but of the combined ones. The sum of the contributions of the interaction of radial-angular and axial-radial-angular is about 27%. In this way omitting these interactions could generate considerable errors. As it was expected, axial misalignments don't produce a significant change in the aligned spectrum, this is because the axial misalignments don't

change considerably the horizontal forces, which are what the horizontal accelerometer captures.

$$\%Change\ of\ spectrum = \frac{\sum_{i=1}^{n}(y_i - z_i)}{\sum_{i=1}^{n} z_i} \times 100 \quad (7)$$

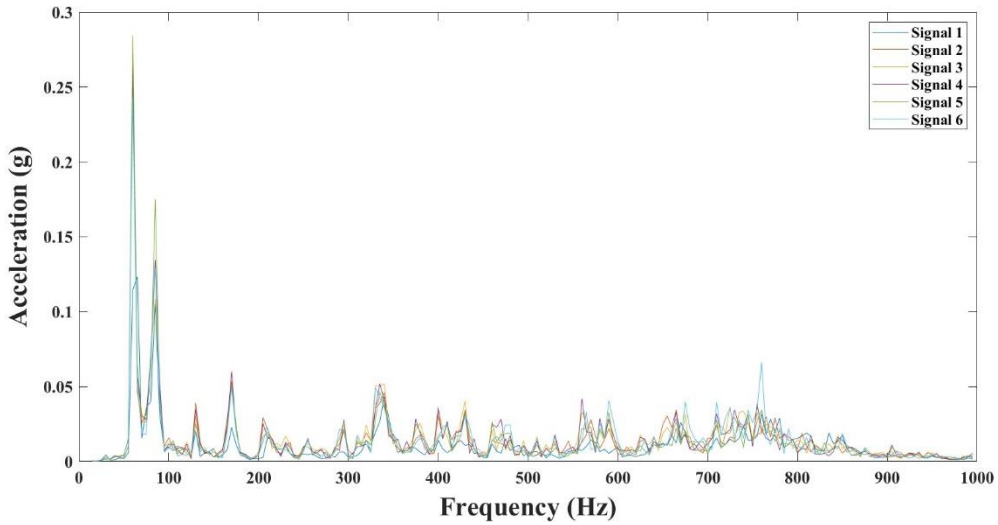

Figure 13. Frequency spectrums for the six runs of the point (Axial = 0, Radial = 0, Yaw = -2,69°). Values on the x-axis are in Hz and on the y-axis in g.

Table 10. Percentage of change of spectrum for different experimental point for the horizontal accelerometer in the motor side.

Axial (mm)	Radial (mm)	Yaw (°)	%Change of spectrum
0	1,5	-2,69	-40,8
4	0	-2,69	-31,6
4	1,5	-2,69	-49
0	0	2,69	-16,5
4	0	2,69	-16,7
0	0	-2,69	-41,3
4	1,5	2,69	-41,2
0	1,5	2,69	-53,3

Table 11. Standardized effect and percentage of contribution for axial, radial and yaw misalignment on vibration measurements.

Variable	Standardized effect	%Contribution
A-Axial	3,35	1,7
B-Radial	-19,55	58
C-Yaw	8,75	11,6
AB	-1,4	0,29
BC	-11,1	18,7
AC	2,6	1
ABC	7,55	8,6

The contact area in meshing gears is important in the vibratory response when there are radial, axial, and angular (yaw) misalignments and therefore it will also be important in their combinations. An increase in these types of misalignments implies a reduction in contact area. In this sense, it is possible to relate the percentage of reduction in the contact area with an indicator of the vibrations produced. For this, mathematical expressions will be developed to estimate the contact area based on combination of radial, axial and angular (yaw) misalignments. A previous work was made to estimate the effect of gear misalignment on contact area through theoretical and experimental validation [135]. However, in this case the same equations cannot be used since for the case of angular misalignment the reference axis in our case is the pitch line while for them it was the pinion axis of rotation, also in P. Kumar et. al. work only considered individual misalignments, not combined.

The contact area in this case will be taken as the projection of the contact area of the teeth on a plane perpendicular to the face of the gears that contains the gear axes. A representation of the contact area for aligned and individual misalignments conditions is shown in Figure 14. The pinion gear is in the top position and the driven gear is in the bottom position. Rap and Rad are the addendum radio of the pinion and the driven gear respectively; CD is the distance between the axis of the pinion and the axis of the driven gear; h is the contact height, TW is the teeth width, PL is the picth line, X is the pinion axis of rotation, Y is the driven gear axis of rotation in the aligned condition and Y' is the new driven gear axis for a misaligned condition. Figure 14 (a) shows the aligned condition, Figure 14 (b) shows the da axial misalignment, Figure 14 (c) shows the dr radial misalignment, in this case the driven gear axial rotation is displaced a dr distance, Figure 14 (d) is the representation of yaw misalignment of θ degrees with respect to the pitch line. In the aligned condition and for axial and radial misalignments, the contact area is rectangular; in yaw misalignment the area is a trapezius and could be a triangle for high values of misalignments. That case will not be considered here since such high misalignments are not frequent. Although not

shown, negative yaw misalignment also generates a trapezoidal shaped contact area. For combined misalignment, Figure 15 (a), (b), (c), (d), (e) show the contact area of different possible combinations of two types of misalignments and Figure 15 (f), (g) show the contact area when three types of misalignment are present.

Contact area for the aligned case, A_0, (Figure 14 (a)), is the rectangle of height h and length TW.

$$A_0 = TW \times h = TW \times \left(R_{ap} + R_{ad} - CD\right) \tag{8}$$

For the axial misalignment, Figure 14 (b), contact area A_a is

$$A_a = (TW - da) \times h = (TW - da) \times \left(R_{ap} + R_{ad} - CD\right) \tag{9}$$

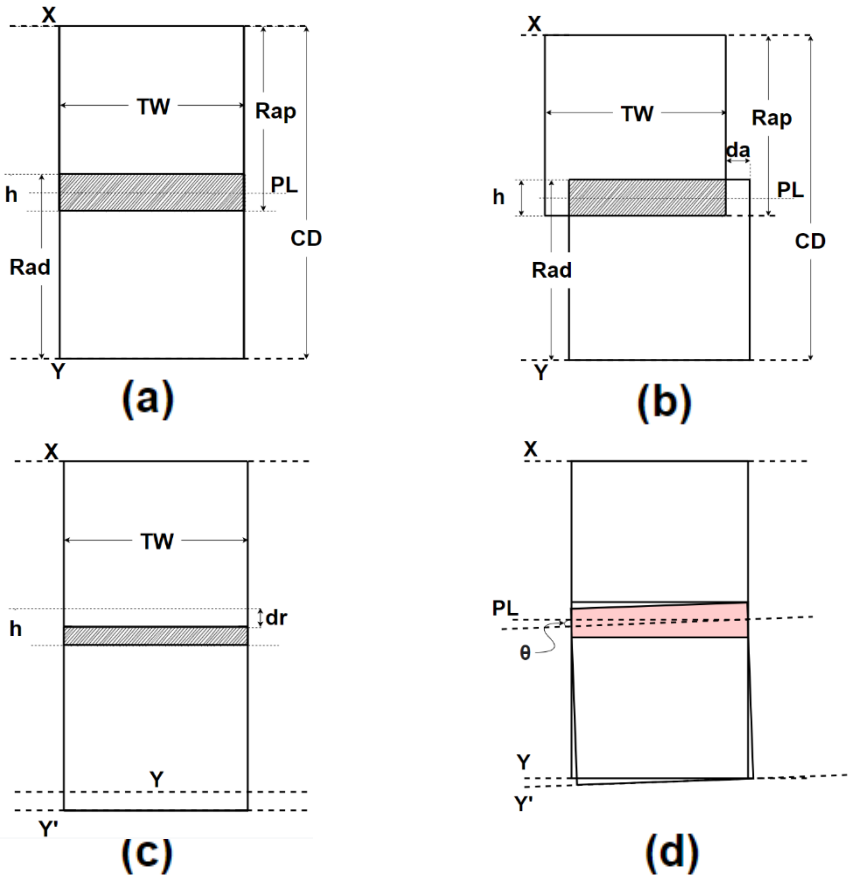

Figure 14. Contact area on a pair of aligned and individual misaligned teeth. (a) aligned condition (b) axial misalignment (c) radial misalignment (d) positive yaw misalignment.

For the radial misalignment, Figure 14 (c), contact area A_r is

$$A_r = TW \times (h - dr) = TW \times \left(R_{ap} + R_{ad} - CD - dr\right) \quad (10)$$

The contact area for positive yaw misalignment, A_{y+}, (Figure 14 (d)), is the area of the aligned condition minus the area of the superior triangle formed by the inclination of the driven gear. The expression is the same for the negative yaw misalignment

$$A_{y+} = TW \times h - \frac{1}{2}(TW \times tan\theta)(TW) = TW \times \left(R_{ap} + R_{ad} - CD\right) - \frac{1}{2}(TW \times tan\theta)(TW) \quad (11)$$

When axial and radial misalignments are present, Figure 15 (a), the contact area, $A_{ar,}$ is given by the expression

$$A_{ar} = (TW - da) \times (h - dr) = (TW - da) \times \left(R_{ap} + R_{ad} - CD - dr\right) \quad (12)$$

For the contact area for axial and yaw misalignments, A_{ay} , (Figure 15 (a), (b)) a zoom is made in Figure 16. The area is calculated by subtracting the area of the upper trapezoid, A_{t1} (gray color) and the area of the lower left trapezoid, A_{t2} (orange color) from the area in the aligned condition.

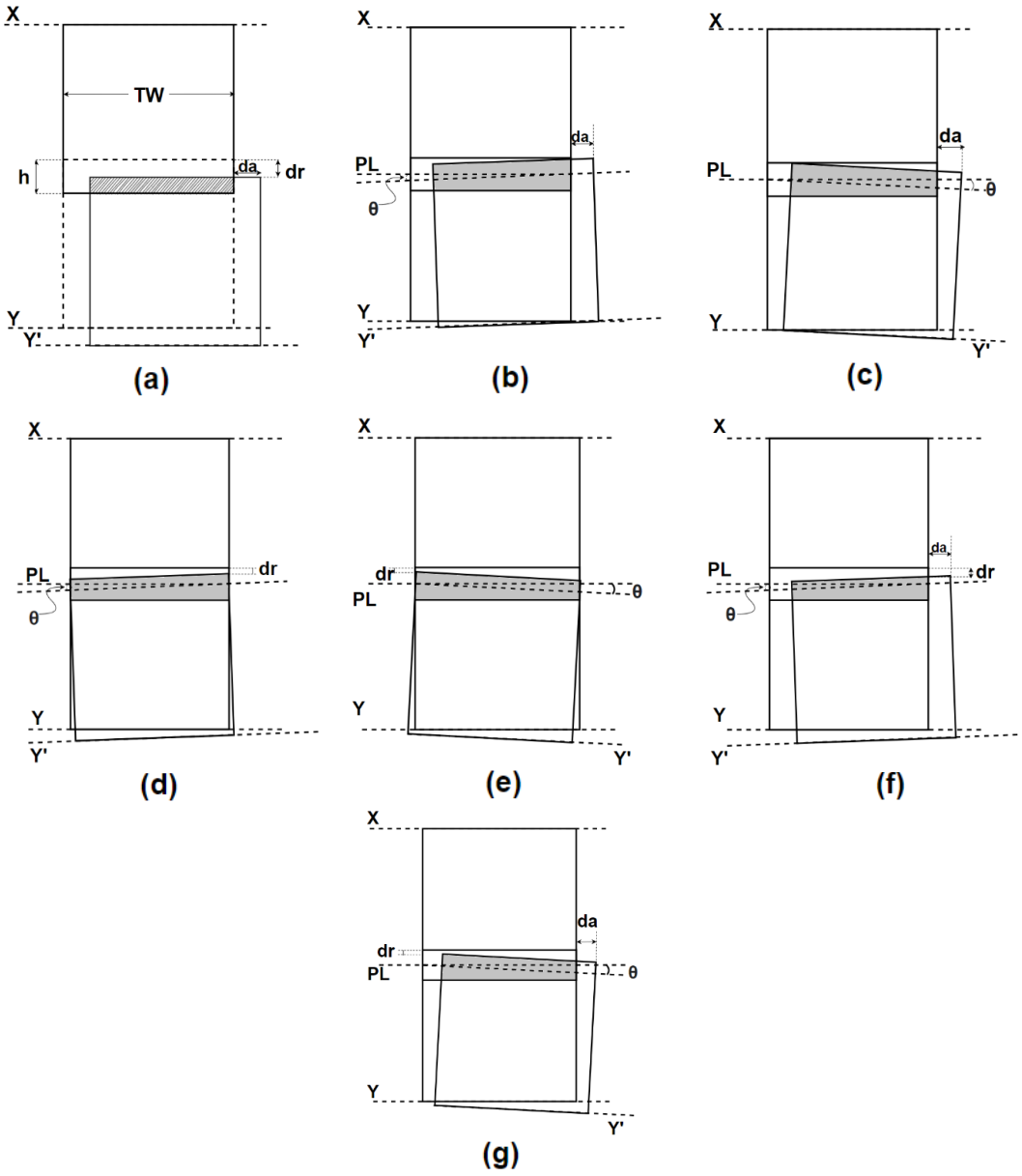

Figure 15. Contact area on a pair of combined misaligned teeth. (a) Axial-Radial (b)Axial-Angular (+) (c) Axial-Angular (-) (d) Radial-Angular (+) (e) Radial-Angular (-) (f) Radial-Axial-Angular (+) (g) Radial-Axial-Angular (-)

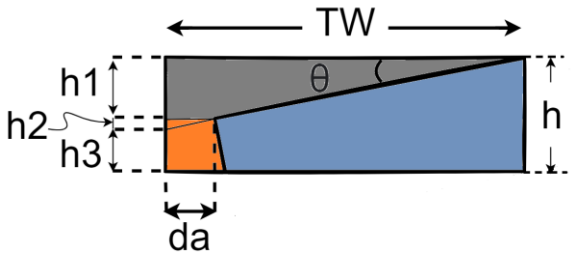

Figure 16. Zoom for contact area on axial-positive yaw misalignment.

$$A_{ay} = (TW \times h) - A_{t1} - A_{t2} = TW \times \left(R_{ap} + R_{ad} - CD\right) - A_{t1} - A_{t2} \quad (13)$$

To calculate A_{t1} and A_{t2} it is necessary to know h1, h2 and h3.

$$h1 + h2 = TW \times tan\theta \quad (14)$$

$$h2 = da \times tan\theta \quad (15)$$

$$h3 = h - h1 - h2 \quad (16)$$

Substituting Equation (15) in (14), (14) and (15) in (16)

$$h3 = \left(R_{ap} + R_{ad} - CD\right) - (TW \times tan\theta) \quad (17)$$

The area of the upper trapezoid, A_{t1} (gray color) and the area of the lower left trapezoid, A_{t2} (orange color) is given by:

$$A_{t1} = \frac{1}{2}(d_a + TW) \times h1 = \frac{1}{2}(d_a + TW) \times (TW \times tan\theta - da \times tan\theta \ \ ) \quad (18)$$

$$A_{t2} = \frac{1}{2}(d_a + h3 \times tan\theta + d_a) \times h3 \quad (19)$$

After putting the value of h3 of the Equation (17) in (19), A_{t2} becomes

$$A_{t2} = \frac{1}{2}\{2d_a + \left[\left(R_{ap} + R_{ad} - CD\right) - (TW \times tan\theta)\right] \times tan\theta\} \times \left[\left(R_{ap} + R_{ad} - CD\right) - (TW \times tan\theta)\right] \quad (20)$$

Substituting (18) and (20) in (13), the expression for contact area in axial-yaw misalignment is given by

$$A_{ay} = [TW \times (R\_ap + R\_ad - CD)] - \left[\frac{1}{2}(d_a + TW) \times (TW \times tan\theta - da \times tan\theta \ \ )\right] - \left[\frac{1}{2}\{2d_a + \left[\left(R_{ap} + R_{ad} - CD\right) - (TW \times tan\theta)\right] \times tan\theta\} \times \left[\left(R_{ap} + R_{ad} - CD\right) - (TW \times tan\theta)\right]\right] \quad (21)$$

The contact area for radial-yaw misalignment, A_{ry} , is the shown in Figure 15 (d), (e); a zoom for a better visualization is shown in Figure 17. The contact area (blue region) is the area in aligned condition without the area of up trapezoid (gray zone), A_{t3}.

$$A_{ry} = (TW \times h) - A_{t3} = TW \times \left(R_{ap} + R_{ad} - CD\right) - \left[\frac{1}{2}(dr + dr + TW \times tan\theta) \times TW\right] \quad (22)$$

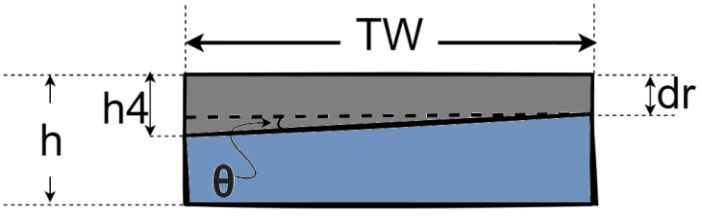

Figure 17. Zoom for contact area on radial-positive yaw misalignment.

The contact area for the three types of combined misalignments, A_{ary}, is shown in Figure 16 (f), (g). As in the previous cases a zoom, Figure 18 , is made for a better visualization and for calculate the expression for the contact area. Subtracting the area of the upper pentagon (gray color), A_p, and the area of the lower left trapezoid (orange color), A_{t4}, from the area of the aligned condition, the contact area for this scenario (blue color) can be obtained.

$$A_{ary} = (TW \times h) - A_p - A_{t4} \tag{23}$$

$$A_{ary} = TW \times (R_{ap} + R_{ad} - CD) - \left[TW \times dr + (TW - da) \times tan\theta \times da + \frac{1}{2} \times (TW - da) \times tan\theta \times (TW - da)\right] - \left[[da \times (h - dr - (TW - da) \times tan\theta)] + \left[\frac{1}{2} \times [h - dr - (TW - da) \times tan\theta] \times tan\theta\right] \times [h - dr - (TW - da) \times tan\theta]\right] \tag{24}$$

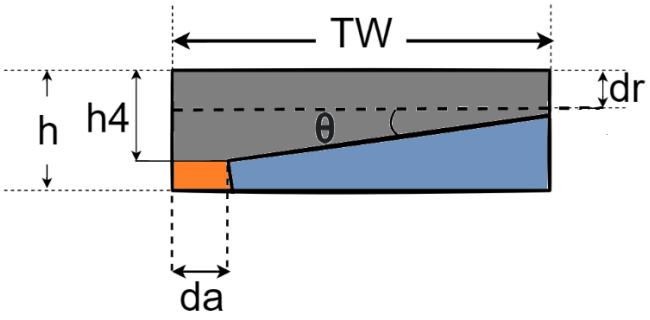

Figure 18. Zoom for contact area on axial-radial-positive yaw misalignment.

With the expressions (8), (11), (21), (22) and (24) is possible calculate the contact area for the experimental points in this work. Input variables need for estimate the area is shown in Table 12. Equation (25) allows to calculate the percentaje of change of contact area (%CA) comparing each misaligned area (A_m) with the area in the aligned condition (A_0). The values of change in contact area for each experimental point are shown in Table 13. The contact area is an important factor in the case of individual misalignments. The objective of knowing the contact area at each point of experimentation is to determine how influential the projected contact area is in the vibratory behavior when there are combined misalignments.

Table 12. Input parameter for estimate the contact area in different misalignment conditions.

Input parameter	Value
TW	30 mm
Rap	30 mm
Rad	30 mm
CD	54 mm
dr	0 - 1,5 mm
da	0 - 4 mm
θ	2,69°

$$\%CA = \frac{A_m - A_o}{A_o} \%CA = \frac{A_m - A_o}{A_o} \times 100 \quad (25)$$

Table 13. Percentage of change of contact area for each experimental point.

Axial (mm)	Radial (mm)	Yaw (°)	%CA
0	1,5	-2,69	-37%
4	0	-2,69	-22%
4	1,5	-2,69	-44%
0	0	2,69	-12%
4	0	2,69	-22%
0	0	-2,69	-12%
4	1,5	2,69	-44%
0	1,5	2,69	-37%

Due to the adopted coordinate system, the contact area in positive angular misalignments is the same as in negative ones. The vibratory behavior for positive angular misalignments is different from the one that occurs in negative ones according to the results of Table 10; this could imply that what happens in the positive zone is different from what happens in the negative zone, for which the positive standardized effect of the yaw factor shown in Table 11 must be taken with care.

What this positive value of the effect for angular misalignment is actually showing is that when going from the negative angular misalignment experienced to the positive there is an increase in the vibration measurements but it does not imply that in the area of positive misalignment when increasing the value of misalignments increase the proposed indicator of change in the spectra. The standardized effect of the axial-angular combination is negative and the contribution percentage is 10,9%, the sign implies that when the two types of misalignment increase, the proposed vibration indicator decreases. Angular misalignment has a 58% of contribution, and the sign is positive, this means that for the sign convention adopted when the positive misalignment increases the percentaje of change increases too, and when the negative misalignment increases the percentaje of change increases too. When correlating the percentage of change in contact area with the values obtained for the vibration spectra change indicator at the points with positive angular misalignment, a clear trend is observed in Figure 19. For positive yaw misalignments, a greater decrease in the contact area is reflected in a greater decrease in the proposed vibration indicator, regardless of whether only yaw misalignment is present or if it is combined with radial and/or axial misalignment. For negative yaw misalignments, the contact area does not seem to have a significant effect. These results suggest that the smaller

the projected contact area, the lower the vibration levels, either for individual misalignments or combined misalignments in the positive zone of angular misalignments. Mesh stiffness affects the vibration levels. When the misalignment increases, the mesh stiffness is reduced becasuse the reduction of contact area of the teeth [136]. If the mesh stiffness decreases, it is expected that the vibration levels increase, however, friction plays an important role and if the system is not lubricated, the decrease in friction as misalignment increases causes the vibration indicator to decrease. Another reason for that is related with the transmited force to the shaft; in general terms when the centers distance increase the force on shat due to the gear meshing decreases. The reason for this is linked to the torque to be transmitted; If the reaction torque remains constant, as it was in this case, increasing the center distance to maintain the same torque requires less tangential force. Whether the effect of mesh stiffness or force prevails will depend on the magnitude of the applied load and the elastic modulus of the gear materials; for low or medium loads and steel gears, the conclusions that the proposed vibration indicator decreases with increasing misalignments are valid.

In some cases vibration measurements could be related with the gears contact ratio. To estimate that effect, for each experimental condition a contact ratio (Equation (1)) is calculated in the initial point of contact and the final point of contact; the values are averaged and they are ploted with the results of the proposed vibration indicator as it is shown in Figure 20. A decrease in the contact ratio implies fewer teeth in contact and therefore less contact area, therefore the contact area and the contact radius are dependent variables. A contact ratio less than one implies that there are instants of time in which there are no pairs of teeth in contact, which could cause impact loads, however in this case, although there are values less than one, they are not so low, and the dynamic loads do not exceed the effect of the friction force on vibrations. From Figure 19 and Figure 20 it can be deduced that for positive yaw misalignment, increasing the area reduction percentage and decreasing the contact ratio decreases the percentage of change of the spectrum with respect to the base signal. For negative yaw misalignment, the effect of the average contact ratio does not seem to have an influence on the change of the frequency spectrum.

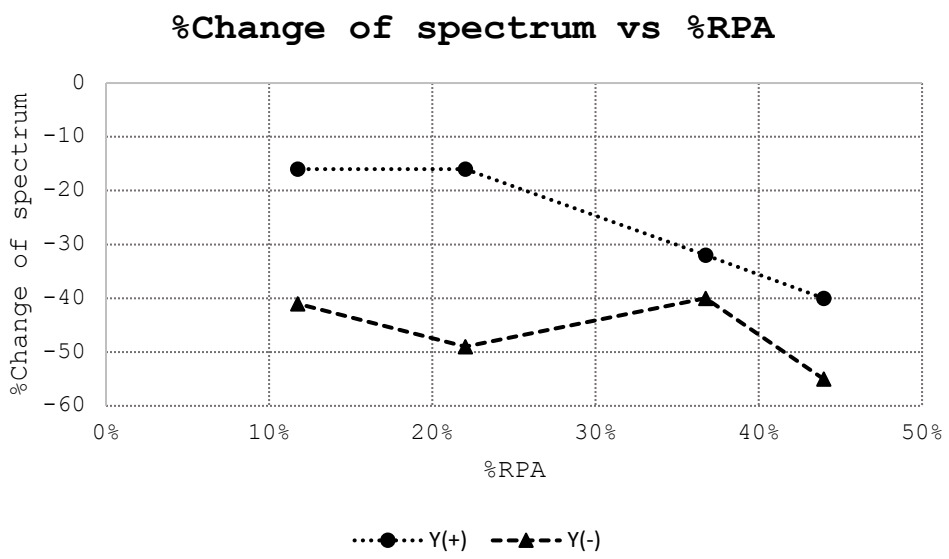

Figure 19. Percentaje of change of spectrum vs percentaje of reduction of projected area (%RPA) for positive yaw misalignments y(+) and negative yaw misalignments. y(+).

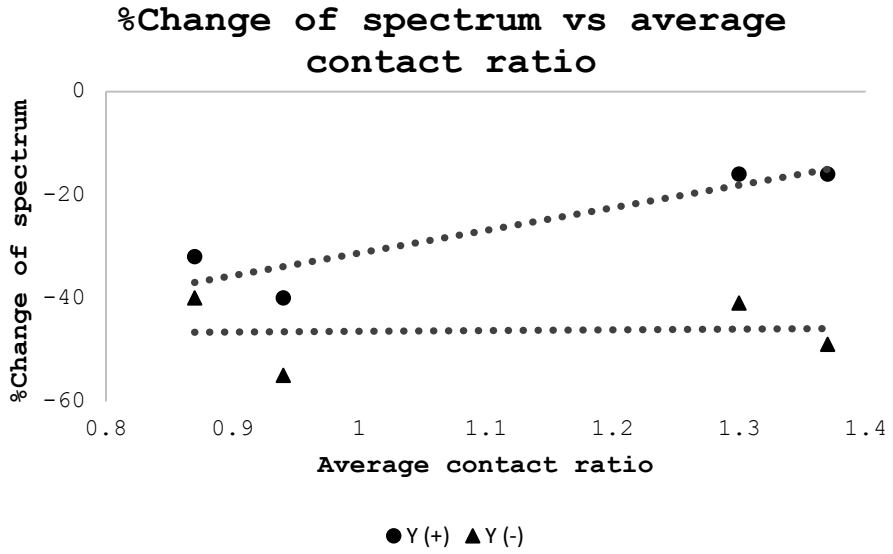

Figure 20. %Change of spectrum vs average contact ratio for positive yaw misalignments y(+) and negative yaw misalignments y(-).

Chapter conclusions

An experimental analysis has been developed to understand the effect of combined misalignment on vibration measurements in a single-stage spur gear transmission system. Axial, radial, yaw, and pitch are the types of individual misalignments that could appear in that kind of system. Misalignments in a real application can be expressed as the combination of individual ones; therefore, the study of combined misalignments is pertinent for fault diagnosis and design. In this research, a preliminary experimental study has been made combining axial, radial, and angular (yaw) misalignments. Each type of misalignment was studied between two extreme values in such a way that the meshed system was operative, and they were chosen far enough apart to be able to detect significant changes in the vibratory response. All possible combinations were made at those extreme values.
As reported by M. A. Khan et al [129], the increase in individual axial, radial, and yaw misalignment generates a decrease in kurtosis and skewness. This result was corroborated in our work, which validates the results found for the combinations made. The analysis in the frequency domain allowed us to observe the rotational frequency of the pump used to apply the load. In turn, the rotational frequencies of the shaft, the gear frequency, and their multiples could be seen. To determine the vibrational behavior measured at the base of the bearings, it was necessary to compare the spectra of the misaligned conditions with the base spectrum in the aligned condition. Since patterns could not be identified, such as the increase or decrease of certain representative peaks in the gear mesh frequency or its multiples or the increase in sidebands in these frequencies, an indicator was proposed that would allow the comparison of the entire spectrum. This indicator takes each peak value of the spectrum to be evaluated and subtracts it with its corresponding peak in the aligned spectrum, this result is divided by the peak of the aligned spectrum at that frequency and multiplied by 100 to calculate the percentage deviation, then averages these percentages and that average is the percentage of spectrum change. Once this percentage of change was found for each evaluated condition, it was found that the most significant misalignments are yaw, radial, axial, and the yaw-axial combination, the yaw is the one with the greatest contribution to the final vibratory response.

Vibration for radial, axial, and yaw misalignments is related to the contact area of the teeth. To estimate the effect in combined misalignments cases, analytical expressions were developed for the contact area. Analyzing the values of reduction in the contact area and percentage of change in spectra, it was shown that the relationship is linearly negative for positive angles; that is, the higher percentage of area reduction, the lower percentage of change in the spectrum. For negative yaw, there is not an apparent relation between these two variables. The contact ratio is also related with the vibration levels: for positive yaw misalignments decreasing the average contact ratio implies lower percentages of change in the vibration spectrum; and for negative yaw misalignments decreasing the average contact

ratio in a specific degree of misalignment does not implies a significative change on the frequency spectrums for that degree of misalignment.

More experimental works should be developed in which the effect of combined misalignments on vibrations at variable speeds and loads is evaluated. To obtain a wider working range numerical simulation can be used. Efforts should also be directed at developing analytical models that allow estimating the vibratory behavior under different conditions of load, speed, and configuration of the transmission system.

Dynamic model

As it was explained in previous chapter, vibration on bearing units due to misalignments of the shafts is not a linear process. That means: total vibration of a combined misalignment is not the sum of the effects of individual misalignments. That conclusion was obtained through experimental research on a test bench.

The possibility of having a test bench that allows evaluating a large number of parameters such as type of gears, transmission ratio, applied load, speed, bearing arrangement configuration, types of bearings, among others is minimal. If the case is in a design stage the chances are even less. So, in order to predict the influence of misalignments on the vibration behavior of a transmission system, a dynamic model would be very useful, either for a problem in a design stage or for a problem in an existing transmission.

A good classification of the characteristics of a dynamic model is the used by Marafona et al [137]; they proposed four parameters for evaluate a model: accuracy, computation time, implementation procedure and resources. Accuracy refers to the ability of the model to give results that are fairly close to the true value. Computation time is related to the computational cost needed to solve the model. The implementation procedure includes the steps necessary to solve the model and the skills and knowledge required either in finite elements, mathematics , programming or the phenomenon itself. Resources refers to the computational power necessary for solving the model.

There are four types of possible models for estimate the dynamic behavior of a mechanical system: analytical, finite element, hybrid, and approximated analytical. The choice of one or the other will depend on the available computational resources, the expertise in the physical model, knowledge of mathematics, finite elements, and simulation software, how crucial the solution time is and how replicable it is expected to be. If the principal goal is the accuracy and there are enough computational resources, expertise in the physical problem and the solution time is not a problem, the finite element models are the best to predict the dynamic response. If the time is a critical factor and the accuracy is not the most important, approximate analytical model could be useful. To select a new model a fifth parameter can be added, this is the ease of the development.

Table 14 shows a valuation from 1 to 4 for the different types of models according to the 5 parameters mentioned before. The model with a valuation of 4 in accuracy is the model with the best accuracy, the model with a valuation of 1 is the model with the worst accuracy. The model with a valuation of 4 in computation time is the model with the lowest computational cost and the model with a valuation of 1 is the model with the highest computational cost. The model with a valuation of 4 in implementation procedure is the model with the minimum steps and the model with a valuation of 1 is the model with the maximum steps.

Finally, the model with a valuation of 4 in ease of development is the model easiest of develop, the model with a valuation of 1 is the model hardest to build. Although there are not previous models for estimate the vibrations due to combined misalignments the quantification of each type of model was carried out based on general dynamics models of spur gear transmission system. Accuracy is often the most desirable parameter in a model. Finite element models are those that have shown the best accuracy in dynamic power transmission systems, however in general, they require a high knowledge of the physical process, in mathematics and programming, and the use of software and robust computing equipment.

Since the idea is to understand the effects of the combined misalignments on the vibrational behavior of the system to make contributions in the design stage, equal weighting was given to the accuracy of the model and to the ease of development of the new model, this weighting being the most high assigned with 30%. The second parameter with the most weight chosen was the computation time with 20% and finally the parameters of the implementation procedure and resources were assigned 10% each as it is shown in Table 14. According to the previous evaluation, the hybrid model is the best option for this research. A hybrid model is composed of a finite element part and an analytical or an approximate analytical part. The hybrid model represents a good option when it is difficult to develop a highly accurate analytical model. It is the balance between precision, computational requirements, and execution time.

Table 14. Selection of the type of dynamic model to develop.

	Parameters					
	Accuracy	Computation time	Implementation procedure	Resources	Ease of development	
Ponderation	30%	20%	10%	10%	30%	Total evaluation
Model						
Analytical	2	3	3	3	1	2,1
Finite element	4	1	2	1	3	2,6
Hybrid	3	2	1	2	4	2,8
Approximated analytical	1	4	4	4	2	2,5

Vibrations are produced for the excitation that produces a force in a system. Vibrations measured in bearing units are generated by the force exerted by the shaft on them; this force in a simple spur gear transmission system depends on the force that the engaged gear exerts on the gear mounted on the shaft in question. For a complete analytic model, the

determination of that force is required and for an alignment case is relatively easy to calculate; when there are misalignments the contact and tangential forces changes because of the change in contact area. In the alignment case the tangential force is applied along a line whose magnitude is the width of the face of the teeth. The position of this line changes on the tooth face but in an absolute coordinate system it remains constant so that the distance from the center of the axis to the point of force application also remains constant whereby the value of the forces acting on an aligned gear pair is relatively constant over time with small variations. In combined misalignment case the line of the meshing forces changes in size, inclination, and position, so the average value of the force changes as well as its variations in time.

As the forces transmitted to the shaft due to misalignments are difficult to predict through analytical procedures, it is proposed in this work get these forces through finite element simulation. The forces get by simulation will be inputs for an analytical model which predicts the acceleration in the bearing units.

The finite element method has been widely used to study stress and strain in power transmission systems. One of the most recently used methodologies for finite element analysis of gears is the one proposed by Litvin F and Fuentes A [138] ; authors proposed the discretization of three teeth including the rim. Three teeth are sufficient for the study of stress and strain in pairs of gears whose contact ratio is less than two. In the mesh of 3 pairs of teeth, there is a complete cycle from the moment a tooth comes into contact with the other gear until this contact ends. Most spur gear pairs have a contact radius of less than two; high contact ratios occur in more specific applications. So, the discretization of three teeth with their rims is so far the most optimal solution for a finite element model of a pair of gears; the discretization of the entire gear would imply a high computational cost that in a strict sense would not be necessary.

Litvin F and Fuentes A [138] suggest the use of six auxiliary intermediate surfaces to divide the tooth into six parts. That division let a major control for the discretization of the six subvolumes. For the application of boundary condition and load is possible use rigid surfaces at the interior and lateral part of the discretized teeth coupled to a reference points which in this case are the center of the gears in the position of the shafts. Although the authors proposed and analytical procedure for generate the gear surfaces and discretization, in this work the model was developed firstly through Solidworks® for get the CAD of the model and the discretization was made in Abaqus® due to the good meshing quality offered by this software.

The use of tetrahedral elements of first order for tensional analysis of tridimensional geometries is not recommendable because of the high rigid response to bending stresses. This could be solved using higher order element, for example a second order tetrahedral element, nevertheless, a first order hexahedral element is most suitable because it can get

the same precision of the second order tetrahedral element with a lower computational cost [139]; so, the chosen element in Abaqus is C3D8 which has eight nodes and 24 degrees of freedom. The finite element model for the analyzed spur gear pair is the shown in Figure 21. RP-1 is the reference point for the driven gear which is coupled to the internal and lateral surfaces of the driven gear, in this point is applied a constant torque and the rotation in z direction is let. RP-2 is the reference point for the pinion which is coupled to the internal and lateral surfaces of the pinion, in this point is applied a specific angular displacement in z direction. The gear parameters for the pinion and the driven gear of the simulation are the same used for the experimental analysis, these are the shown in Table *5*.

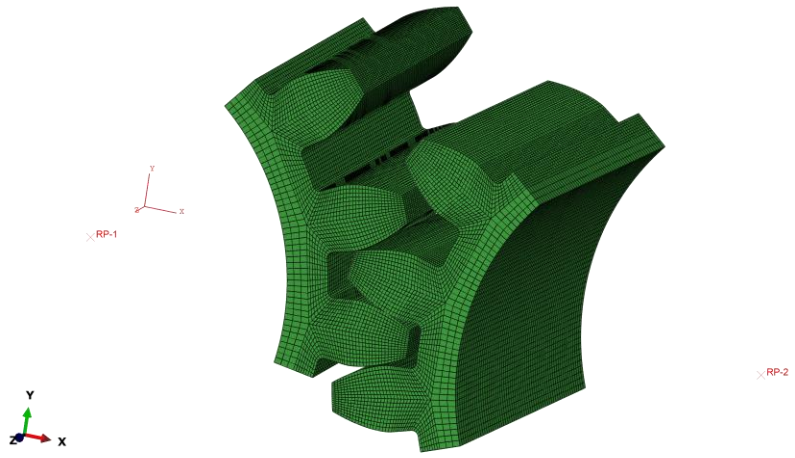

Figure 21. Finite element model for the analyzed spur gear pair.

For the contact discretization method there are two options: node to surface and surface to surface. Although the surface to surface method is generally more accurate, for a refined mesh the differences are not significant between the two methods. In this sense, the node to surface method was chosen because its computational cost is lower. If the transmission model included the shafts and bearings, a transient dynamic analysis would be more appropriate to predict the accelerations in the system, however, since the main objective is to obtain the forces that the shafts receive due to the interaction of the gears under aligned and misaligned conditions, a static analysis will be performed. This type of analysis reduces computational cost, and it is appropriate as an input in the analytical model for estimate the tendency in acceleration behavior of the bearing units in different misalignments condition. The friction formulation and the contact property used were frictionless and tangential respectively. A constant torque of 3,25 Nm is applied in the reference point RP-1 as the react load. In the reference point RP-2 is applied an angular displacement of 0,71 rad through a ramp function, which is sufficient for a complete meshing cycle.

The model was developed for different misalignment conditions for the pair of spur gears with the parameters shown in Table *5*. Each experimental condition evaluated is the combination of three types of misalignments: axial, radial and yaw (angular). Three levels of each type of misalignment were selected, so the number of simulations were $3^3 = 27$. The levels for each factor of the simulation analysis are shown in Table 15. The different combinations of misalignment were gotten through the module assembly in Abaqus®, Figure 22 shows some of the configurations used; the sign convention for the misalignments are those shown in Figure 6 .

Table 15. Values of each type of misalignment for the simulation analysis.

Type of misalignment	Values		
Radial (mm)	0	0,75	1,5
Axial (mm)	0	2	4
Yaw (°)	-2,69	0	2,69

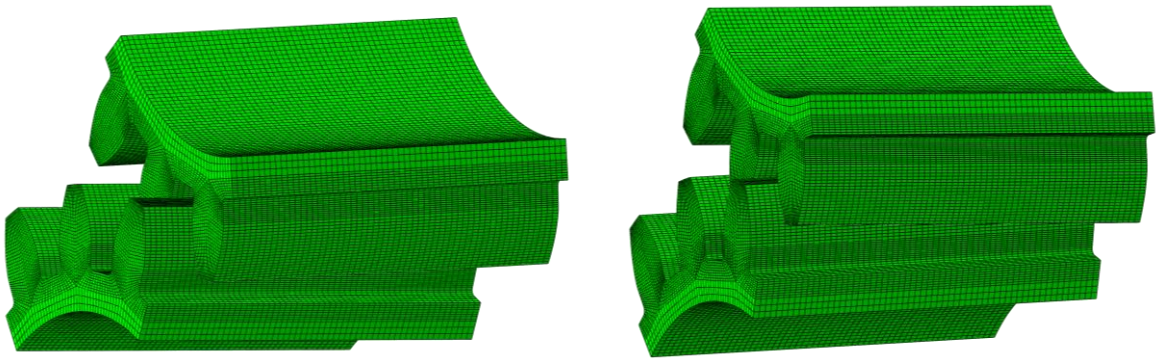

Figure 22. Pair of spur gears with 1,5 mm, 4 mm and 2,69° of radial, axial and yaw misalignment respectively (left) and 1,5 mm, 2 mm and -2,69° of radial, axial and yaw misalignment respectively (right).

Because of the pressure angle of 20°, the vertical component of the force at the contact of the gears is greater than the horizontal component. So, in this sense, since the acceleration response depends to a great extent on that force, to appreciate more significant changes in the vibration response, the vertical force will be chosen for the analysis. The average value of the vertical force that is transmitted to the shaft that supports the pinion is 120 N as it is shown in Figure 23. In the figure is shown also the vertical force of a misalignment point. The time in Figure 23 is the time for a complete meshing cycle for a shaft speed of 282 rpm. All the force values for the different configurations were get and the signal was replicated until a time of 60 seconds was achieved for analysis. This time is necessary to achieve stabilization of the response variable in the analytical model.

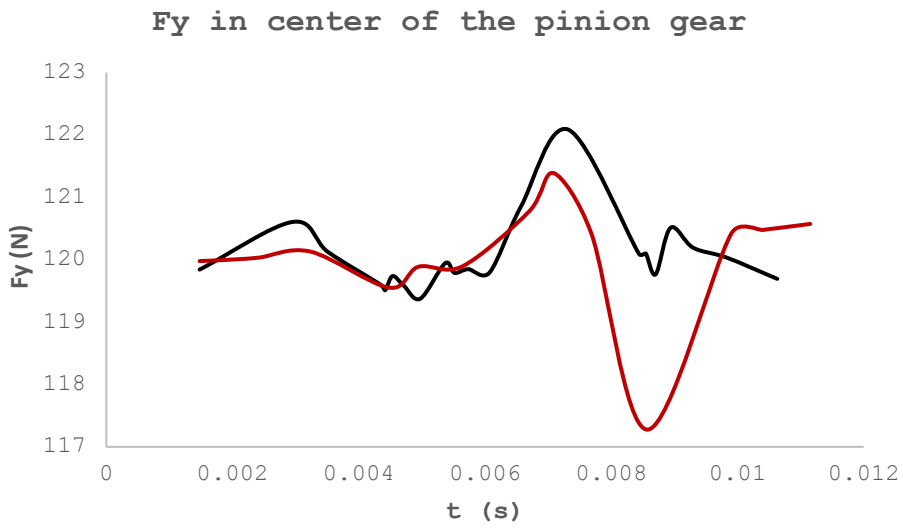

Figure 23. Vertical force (Fy) in the center of the pinion gear (RP-2) in a period of meshing for the aligned condition (black) and an angular misalignment condition with 2,69° (red).

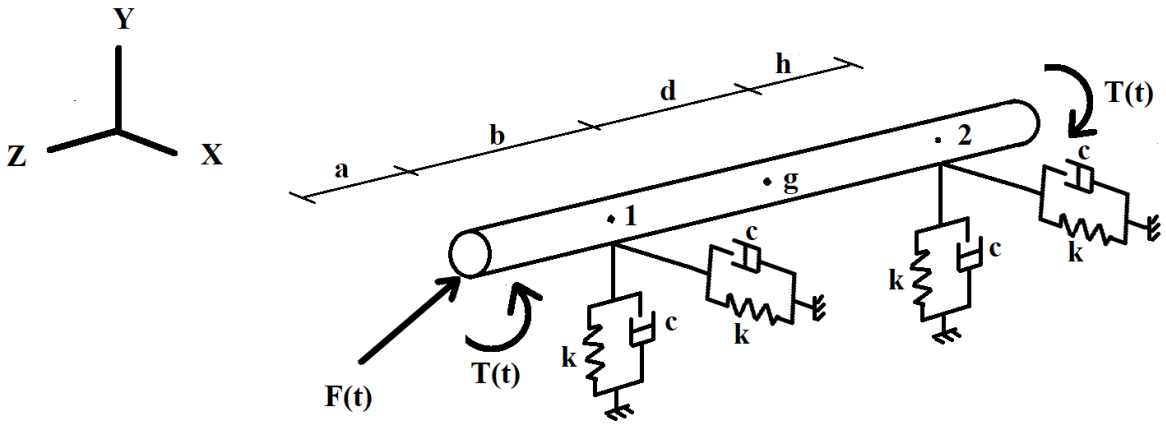

Figure 24. Simplified dynamic model to predict the vibratory behavior in bearings 1 and 2 of the shaft that supports the pinion gear in a single stage spur gear transmission system.

As it was said before, the hybrid model consists of a simulation component to get the forces transmitted to the shaft which supports the pinion gear. The processed force signals are the inputs for the analytical model. A model is proposed that considers the shaft and the external loads that act on it. Figure 24 shows the shaft on which the force F(t) product of the meshing and the reaction torque T(t) act at one of its ends. At the other end of the shaft, the torque is applied by the motor coupled to the system. Since a cantilevered one-stage

transmission system is being analyzed, between the two ends of the shaft there are two bearings that can be represented by an equivalent system of stiffness k and damping c in vertical and horizontal components. To find the velocity and the acceleration of the system in the x direction in the points 1 of the Figure 24 which represents the bearing unit near to the pinion gear, the sum of forces in the x direction and the sum of moments about the center of gravity g are developed as shown in the equations (26) - (45) as follows:

$$\sum F_x = m \cdot \ddot{x_g} \qquad F_x(t) - k \cdot x_1 - c \cdot \dot{x_1} - k \cdot x_2 - c \cdot \dot{x_2} = m \cdot \ddot{x_g} \tag{26}$$

$$\sum M_g = I \cdot \ddot{\theta} \qquad -F_x(t)(a+b) + k \cdot x_1 \cdot b + c \cdot \dot{x_1} \cdot b - k \cdot x_2 \cdot d - c \cdot \dot{x_2} \cdot d = I \cdot \ddot{\theta} \tag{27}$$

Kinematic analysis considering small angle θ

$$x_2 = d \cdot \theta + x_g \tag{28} \qquad x_1 = -b \cdot \theta + x_g \tag{29}$$

Deriving equations (28) and (29) we get:

$$\dot{x_2} = d \cdot \dot{\theta} + \dot{x_g} \tag{30} \qquad \dot{x_1} = -b \cdot \dot{\theta} + \dot{x_g} \tag{31}$$

From Equation (29) $$x_g = x_1 + b \cdot \theta \tag{32}$$

Substituting Equation (32) in (28) we get:

$$x_2 = d \cdot \theta + x_1 + b \cdot \theta \tag{33} \qquad x_2 = (d+b) \cdot \theta + x_1 \tag{34}$$

If $f = d + b$ $$x_2 = f \cdot \theta + x_1 \tag{35}$$

Deriving equations (32) and (35)

$$\dot{x_g} = \dot{x_1} + b \cdot \dot{\theta} \tag{36} \qquad \ddot{x_g} = \ddot{x_1} + b \cdot \ddot{\theta} \tag{37}$$

$$\dot{x_2} = f \cdot \dot{\theta} + \dot{x_1} \tag{38} \qquad \ddot{x_2} = f \cdot \ddot{\theta} + \ddot{x_1} \tag{39}$$

Substituting equations (35), (38) and (37) in (26)

$$F_x(t) - k \cdot x_1 - c \cdot \dot{x_1} - k \cdot (f \cdot \theta + x_1) - c \cdot \left(f \cdot \dot{\theta} + \dot{x_1}\right) = m \cdot \left(\ddot{x_1} + b \cdot \ddot{\theta}\right) \tag{40}$$

$$F_x(t) - k \cdot x_1 - c \cdot \dot{x_1} - k \cdot f \cdot \theta - k \cdot x_1 - c \cdot f \cdot \dot{\theta} - c \cdot \dot{x_1} = m \cdot \ddot{x_1} + m \cdot b \cdot \ddot{\theta} \tag{41}$$

$$m \cdot \ddot{x_1} + 2 \cdot c \cdot \dot{x_1} + 2k \cdot x_1 + m \cdot b \cdot \ddot{\theta} + c \cdot f \cdot \dot{\theta} + k \cdot f \cdot \theta - F_x(t) = 0 \tag{42}$$

If $e = a + b$ and substituting equations (35) and (38) in (27)

$$-e \cdot F_x(t) + k \cdot b \cdot x_1 + c \cdot b \cdot \dot{x_1} - k \cdot d \cdot (f \cdot \theta + x_1) - c \cdot d \cdot \left(f \cdot \dot{\theta} + \dot{x_1}\right) = I \cdot \ddot{\theta} \tag{43}$$

$$-e \cdot F_x(t) + k \cdot b \cdot x_1 + c \cdot b \cdot \dot{x_1} - k \cdot d \cdot f \cdot \theta - k \cdot d \cdot x_1 - c \cdot d \cdot f \cdot \dot{\theta} - c \cdot d \cdot \dot{x_1} = I \cdot \ddot{\theta} \tag{44}$$

$$-e \cdot F_x(t) + (c \cdot b - c \cdot d) \cdot \dot{x_1} + (k \cdot b - k \cdot d) \cdot x_1 - I \cdot \ddot{\theta} - c \cdot d \cdot f \cdot \dot{\theta} - k \cdot d \cdot f \cdot \theta = 0 \tag{45}$$

Equations (42) and (45) are a system of equations in which the variables are x_1 and θ. For solving that system is need estimate the stiffness and damping of the bearings. The stiffness

of a bearing depends on the type of bearing being used. The deep-grove ball bearing is one of the most used and therefore this will be the selected for the model. Referent research for the calculation of the stiffness of that type of bearing is the work of H. R. El-Sayed [140]. He developed analytical expressions for estimate the stiffness from available bearing dimensions and he made experimental verification with a high grade of coincidence. There are subsequent works in which the stiffness of different types of bearings is determined analytically, by experimentation or through simulation, taking into account the lubricant, the applied loads, the rotational speed, among other factors [141],[142],[143] and [144]. However, the work of H. R. El-Sayed continues to be a reference; for this research it allows calculating an estimated value of the stiffness of the selected bearing given that the speed and load used is low; for very high speeds and loads, the stiffness value changes considerably [145] .

Radial stiffness (λ) according to H. R. El-Sayed [140] is calculated through the Equation (46). W is the load on bearing and L is the stiffness factor which depends on the bearing dimensions. D_0 and D_i used in the Equation (47) are the outside and inside diameter of the bearing in mm, respectively. C_i and C_0 are the curvatures of the ball and raceway in the rolling and the perpendicular planes, inner and outer race respectively. M_i/m_i and M_0/m_0 are constants which depend on Poisson's ratio of the inner and outer races material respectively, according to the Figure 25 . The ball bearing selected for the model was the UCP 205 which is a bearing for a shaft of 25,4 mm of diameter. The necessary parameters of the UCP 205 bearing for the estimation of the radial stiffness are shown in the Table 16. Since the stiffness value depends on the applied load, a stiffness curve for radial as a function of load was obtained. Figure 26 shows the radial stiffness for the selected bearing in a range of loads. A constant torque of 3,25 Nm was taken as the reaction torque, therefore the estimated load on each bearing is close to 60 N. In this sense, the stiffness that will be taken for the model is $2{,}18 \times 10^7 N/m$ according to Figure 26.

Damping of the bearings is another parameter need for the model. Calculation of the real damping is not a simple process, depends on lubricant and friction at contact points due to internal movements. Although there are several researches for the estimation of bearing's damping, most of them are specific for the application studied. A rough estimation is the proposed by Krämer E [146] , he concluded that bearings damping is in the range $c = (0{,}25\ to\ 2{,}5)10^{-5}k\ \left({}^{Ns}/_{m}\right)$ where k is the stiffness of the bearing in ${}^{N}/_{m}$. The minimum value in that range was selected for the model, so c = 54,5 ${}^{Ns}/_{m}$.

$$\lambda = LW^{\frac{1}{3}} \tag{46}$$

$$L = \left\{531{,}6\left(\frac{2{,}4D_0+d_i}{D_0-d_i}\right)^{\frac{2}{3}}\right\}\left(\frac{M_i}{m_i}C_i^{\frac{1}{3}} + \frac{M_0}{m_0}C_0^{\frac{1}{3}}\right)^{-1} \tag{47}$$

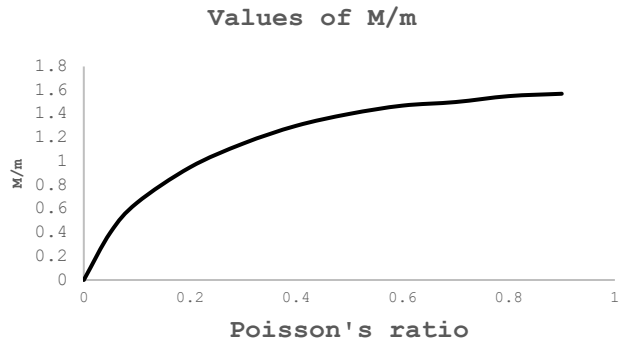

Figure 25. Values of M/m according to the work of H. R. El-Sayed [140]

Table 16. UCP 205 bearing's parameter

Parameter	Value
Poisson's ratio	0,3 mm/mm
Do	46,52 mm
Di	25,4 mm
Ball radius (r)	3,98 mm
Inner race radius (Ri)	16,87 mm
Outer race radius (Ro)	22,68 mm
Radius of curvature of the bearing race (r_i)	3,98 mm

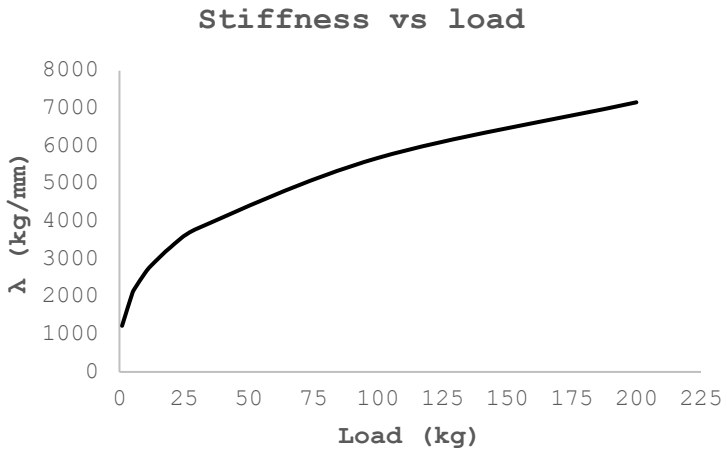

Figure 26. Radial stiffness of the UCP 205 ball bearing

The system of non-homogeneous second-degree differential equations (42) and (45) are solved through Simulink from Matlab® as it is shown in Figure 27. Parameters such as shaft mass, inertia, and the geometric lengths shown in the figure are required for the model. In

this case, m = 1,225 kg; I = 0,0105 kgm^2 ; a = 0,11m and b= 0,05m are included in the model shown in Figure *27*.

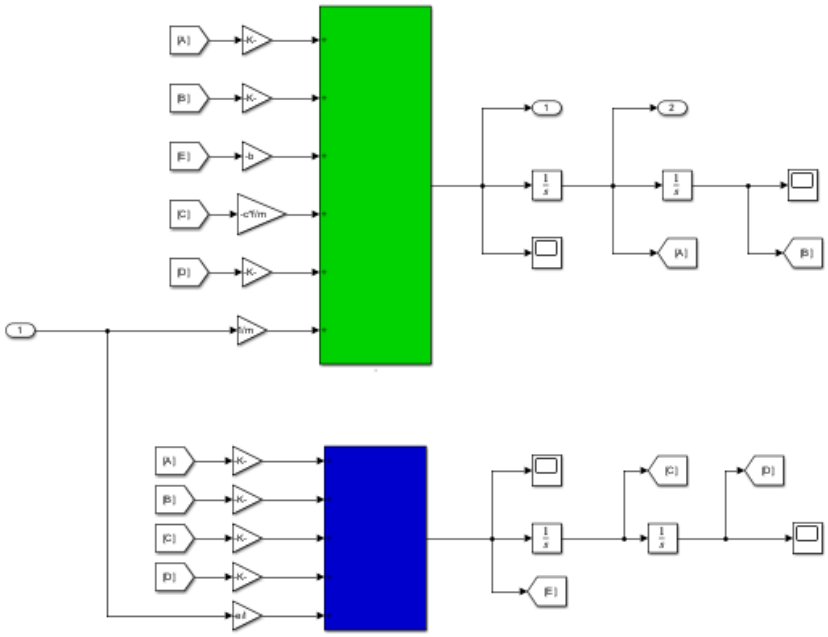

Figure 27. Schematic diagram in Simulink Matlab® for the solution of the system of non-homogeneous second-degree differential equations (42) and (45). The green block gives the solution for $\ddot{x_1}$ and the blue block gives the solution for $\ddot{\theta}$.

FFT is applied to the $\ddot{x_1}$ output signal time in order to see the frequency peaks for each simulated condition. As expected, there are well-differentiated peaks at the gear mesh frequency (GMF) of 84,7 Hz and its multiples as it is shown in Figure 28. The aligned frequency spectrum is the base for compare the misalignment conditions. The proposed indicator in the experimental approach is used for compare the misaligned spectrums with the aligned spectrum. This indicator, shown in the Equation (7) calculates the peaks deviation of two spectrums. These spectra are previously smoothed, so that the peaks at the turning frequencies and their multiples and at the gear frequencies and their multiples stand out. For this, the maximum value is taken every 5 Hz, thereby omitting the information that is not of interest, which may be noise in the signal and that could affect the real value of the indicator if they are not suppressed. Combinations of axial and radial misalignments with no angular misalignment were made. A surface response for the selected levels is shown in Figure 29. As it was reported in the work of Khan et al [129] , increasing just radial misalignment decreases vibration levels. In this case the changes of spectrum are considerable (15%) when the radial misalignment is 1,5 mm, this is half the module. For combination of axial and radial misalignment that tendence remains. All of combinations of axial-radial misalignment, including the zero, generates a decreasing in the percentage of change of area as it is shown in Figure 29. This verifies the initial hypothesis that the increase

or decrease in vibration levels is strongly related to the force received by the shaft due to the contact of the gears: in the case of radial misalignment, this force would have to decrease if the distance between centers is increased since the torque remains constant. Since the acceleration signals obtained are in the vertical direction, it is understandable that the effect of axial misalignment is not significant, as can be seen in Figure 29. The change of zero radial misalignment to 1,5 mm radial misalignment with any axial misalignment generates an increasing of the area of acceleration spectrum compared with the base spectrum of 15% approximately. 1.5 mm in this case is half the module used, which means that through modeling or vibration measurements, radial misalignment can be diagnosed either when it acts alone or when it is combined with the axial through the determination or reading of vibrations in one of the bearings in the vertical direction, for horizontal configuration of the gears. It is interesting that unlike misalignments due to deflection or deformation in the teeth, which generate an increase in vibrations, in the misalignments studied, which are products of position changes in the shafts, the effect is generally inverse, that is, vibration levels are lowered. Although the percentage change of acceleration spectrum decreases in axial-radial combinations, it is not desirable to have misalignments in the system due to transmission errors and increased stress that they can generate.

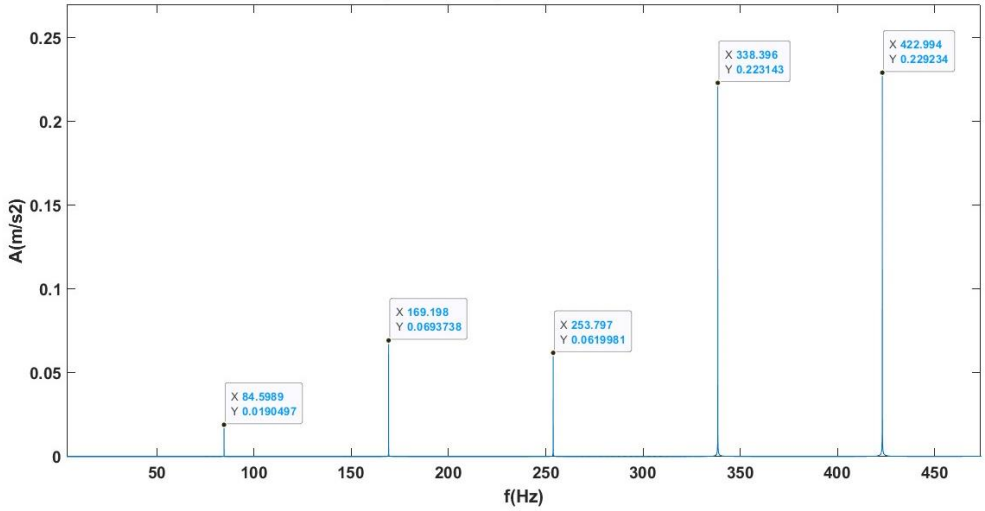

Figure 28. Frequency spectrum for the simulated acceleration signal in the aligned condition. Peaks are observed at GMF and at 2X, 3X, 4X and 5X multiples.

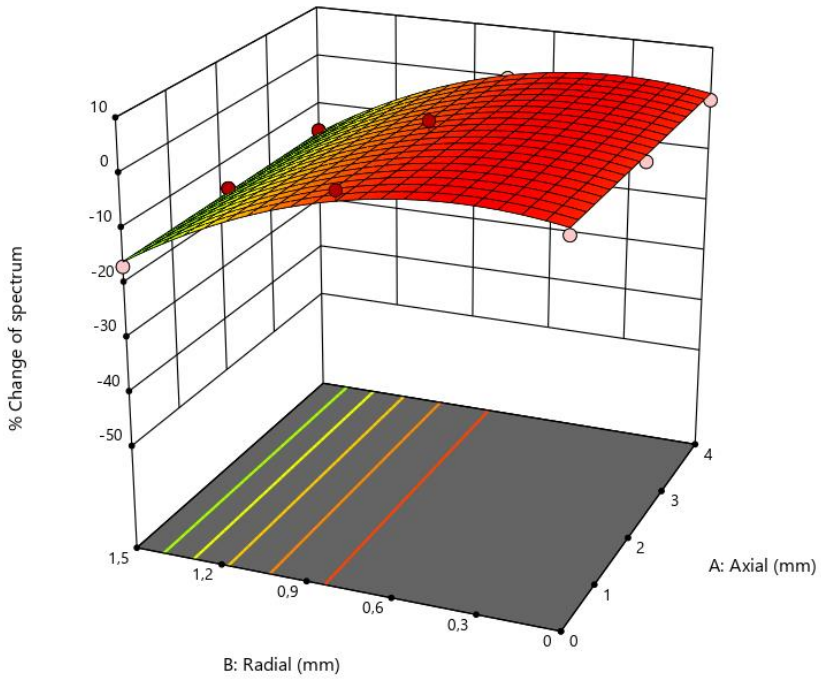

Figure 29. Surface response of percentage of change of spectrum for combination of axial and radial misalignment without yaw misalignment.

And analysis of variance (ANOVA) of all the results of the combinations of the levels studied in Table 15 were made to estimate the significant variables and interactions. The variables with a p-value less than 0,05 were radial (B), interaction radial-angular (BC), the radial variable squared (B^2), the angular variable squared (C^2), and the interaction axial squared multiplied by angular (A^2C). Equation (49) is a regression which predicts the change of area of spectrum for the combined misalignments researched with a coefficient of determination of 0,87. The equation is codified, this means the high level of the factors are coded as +1 and the low levels are coded as -1, this is important to compare the effect of each element in the regression.

Beyond the exact prediction of the vibrations, what is important are the conclusions regarding the trends that can be deduced. For example, the negative sign of the coefficient of the radial variable means that increasing only the radial misalignment causes a decrease in the acceleration spectrum. The negative sign that accompanies the angular variable squared (C^2) means that as the angular misalignment increases, the acceleration spectrum, compared to the base, decreases. That means that the increasing of positive yaw misalignments decreases the percentage of change of the spectrum, and the increases in absolute value of negative angular misalignments generate a decrease in the percentage change of the spectrum. Value of the coefficient of each element in the regressions is related with the contribution of that element to the response variable; the sum of the contributions of the elements where the angular misalignment appears is the largest. As expected, axial

misalignment does not have a significant effect on vertical vibrations, for a horizontal gear configuration, which is why it does not appear as an individual variable in the regression.

$$\%Change\ of\ spectrum = 0{,}4630 - 8{,}44B - 3{,}28BC - 7{,}64B^2 - 16{,}33C^2 + 3{,}61A^2C \quad (48)$$

Figure 30 shows the percentage of change of spectrum for two angles, a positive angle (2,69°) and a negative angle (-2,69°) for the values obtained in the hybrid model developed. The figures are response surfaces of Equation (49). The regression of the percentage of change of spectrum shown in Equation (49) comes from the combination of the three levels of each of the three factors shown in Table 15, that is, a total of 27 conditions. The operating conditions and the misalignment values of the combinations of the extreme values of these runs coincide with the misalignment values analyzed experimentally, that is the experimental runs shown in Table *6*. The indicator to compare the change of a spectrum from a misaligned condition to an aligned one was the same for both the experimental runs and for the points evaluated in the hybrid model. Therefore, in order to validate the proposed model, the results of the experimental runs can be compared with the points of the model through the percentage of spectrum change. All of the experimental points were compared with the values obtained in the model, and the results are shown in Figure 31. The eight points that were taken to compare are shown on the x-axis and correspond to those shown in Table 10 in the same order. In order to quantitatively compare the experimental results with those obtained by the proposed model, the Pearson correlation coefficient for samples (r_{xy}) is calculated, through Equation (49). n is the number of samples, x is one of the data to compare and y is the second one, $\bar{x}$ and $\bar{y}$ are their respective means. This coefficient allows estimating how much two variables vary together; it can take values from -1 to 1. Positive values indicate a direct relationship and negative coefficients indicate an inverse relationship; if the absolute value approaches one it indicates a strong correlation. In this case the correlation is 0.98, which indicates a robust correlation in the same direction of change. This correlation value shows the validity of the model to describe the trend of the proposed indicator of spectrum change percentage of a misaligned condition with respect to a baseline aligned condition. The differences between the predictions and the experimental values are due to the simplifications that are made in the model and in any case no difference exceeds a value of 15% and the average of the differences is 10.5%.

$$r_{xy} = \frac{\sum_{i=1}^{n}(x_i-\bar{x})\,(y_i-\bar{y})}{\sqrt{\sum_{i=1}^{n}(x_i-\bar{x})^2}\sqrt{\sum_{i=1}^{n}(y_i-\bar{y})^2}} \quad (49)$$

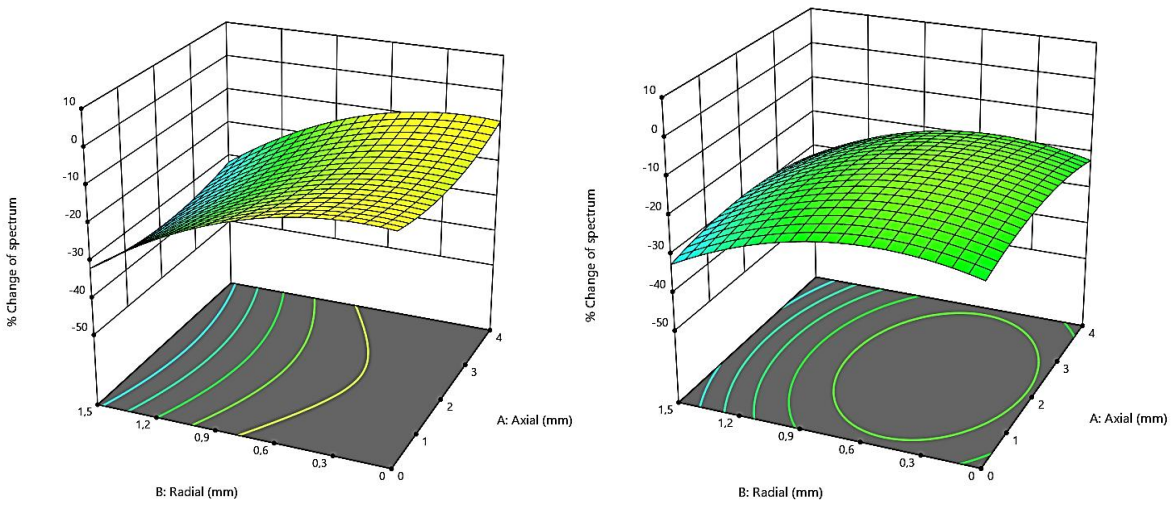

Figure 30. Percentage of change of spectrum for a 2,69° of yaw misalignment (left) and -2,69° of yaw misalignment (right) in the developed hybrid model.

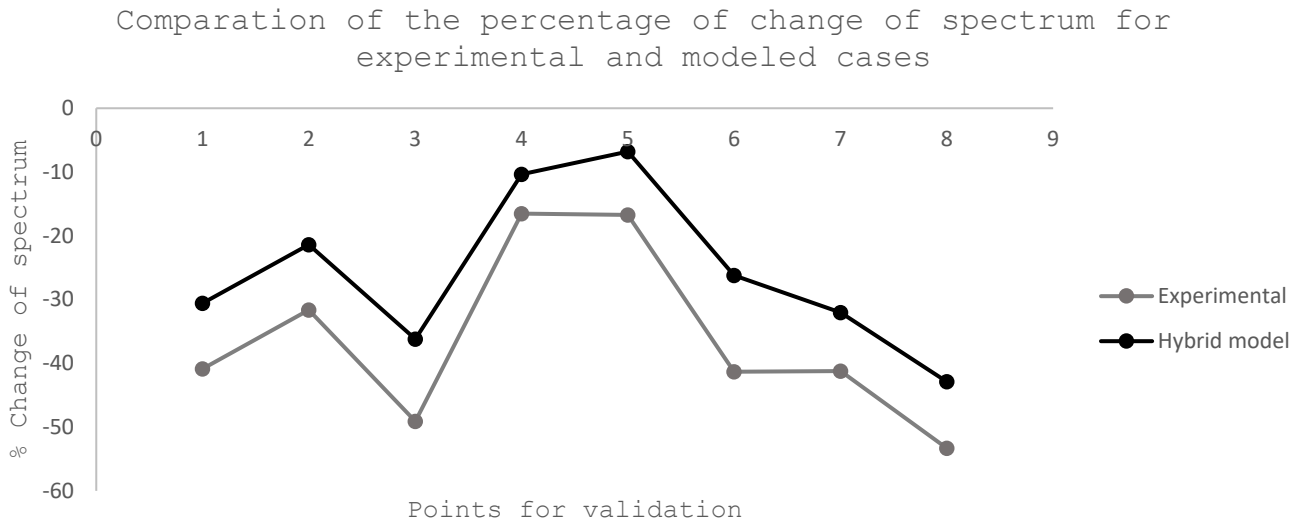

Figure 31. Comparation of the percentage of change of spectrum for experimental and modeled cases. The points in x-axis are those shown in Table 10 in the same order.

Stress analysis

One of the principal variables to consider for designing a gear transmission is the stresses on the teeth. The stress at the root of the tooth is one of the most critical. For the misaligned cases, if the reaction torque is kept constant, it is not easy to predict the maximum stress at the root of the teeth since the misalignment changes the value of the force between the teeth and the position and magnitude of the line of action. So, through simulation by finite elements, the maximum stresses in the root of the tooth will be analyzed for all the combined cases studied in Table *15*; Abaqus® will be used for the analysis with the geometric parameter, discretization conditions and the boundary conditions already explained in the dynamic model section. Figure *32* shows the maximum principal stresses along the root of the pinion gear tooth due to the different combinations of misalignment studied. Figure *32*.a shows the stress for the combination of radial-axial misalignment without yaw misalignment. A slight increase in the stresses is observed when the axial misalignment increases. The radial misalignment does not generate important changes in the stresses, and the axial-radial interaction is not relevant. Figure *32*.b shows the stress for the combination axial-radial with 2,69° of yaw misalignment. According to the Figure *32*.b for a positive yaw misalignment, the increase of radial misalignment produces a slight decrease in the stresses. In that condition axial misalignment does not have a significant influence on changing normal stress value. For a negative yaw misalignment (-2,69°), axial misalignment generates a decrease in the stress values, as it is shown in Figure *32*.c . The results of the simulated stresses show that the most important variable of the studied variables influencing the stresses values is the yaw misalignment. The stresses increase considerably for negative or positive misalignment compared with no yaw misalignment for any combination of radial-axial misalignment. For zero yaw misalignment the stresses values are between 7,8 MPa and 8,7 MPa; for positive yaw misalignment the stresses values are between 31,7 MPa and 32,7 MPa, and for negative yaw misalignment the stresses values are between 21 MPa and 31 MPa. So, the increment of the average values for the positive misalignment taken in this work is four times the value in the aligned condition. The increment for the stress values in the negative misalignment is between 2,6 and 4,3 times the value in the aligned condition.

A misalignment bending stress increase factor K_{mis} can be calculated for each of the simulated conditions by dividing each stress value (σ_{mis}) by the bending stress value in the aligned condition (σ_{alig}) as shown in Equation (50). A response surface for the variable K_{mis} is shown in Figure *33*. The response surface regression model has a coefficient of determination of 0,99 and all of its terms have a p-value less than 0,05. Figure *33* shows the K_{mis} factor for the aligned condition, and for the 2.69° and -2,69° of misaligned conditions.

$$K_{mis} = \frac{\sigma_{mis}}{\sigma_{alig}} \tag{50}$$

Since, according to the Figure *33*, a different behavior is observed for positive and negative angles, two regression models are shown. Equation (51) and Equation (52) are the regression models in coded variables for positive and negative yaw misalignment respectively. *A, B* and *C* are axial, radial and yaw misalignment respectively. The coded variables means that extreme values in equation go from -1 to 1. For positive cases axial values go from 0 to 4, radial values go from 0 to 1,5 and yaw values go from 0 to 2,69°. For negative cases axial values go from 0 to 4, radial values go from 0 to 1,5 and yaw values go from 0 to -2,69°.

$$K_{mis(+)} = 1{,}04 + 0{,}0526A + 2{,}94C - 0{,}0708AC - 0{,}0842BC \quad (51)$$

$$K_{mis(-)} = 1{,}04 + 0{,}0526A - 2{,}29C + 0{,}0423AB + 0{,}7717AC + 0{,}0885BC \quad (52)$$

From equations (51) and (52), the strong and almost predominant influence of angular misalignment can be seen for the combinations of misalignments in which positive angular misalignment is present. The combinations of misalignments in which negative misalignments is present are influence strongly by the angular misalignment but also by the axial misalignment.

In order to compare the effect of misalignment on bending stress, it is shown in Figure 34, Figure 35 and Figure 36 the relation between the bending stress and the area reduction percentage. As the misalignment generate a meshing area reduction it is interesting to analyze if there is a relation between the meshing area and the stresses. Figure 34 and Figure 35 show that there is not a clear relation between contact area and bending stresses for negative yaw misalignments or for zero yaw misalignment. Figure 36 shows that the relation is approximately linear and when the area reduction increases the bending stresses decrease.

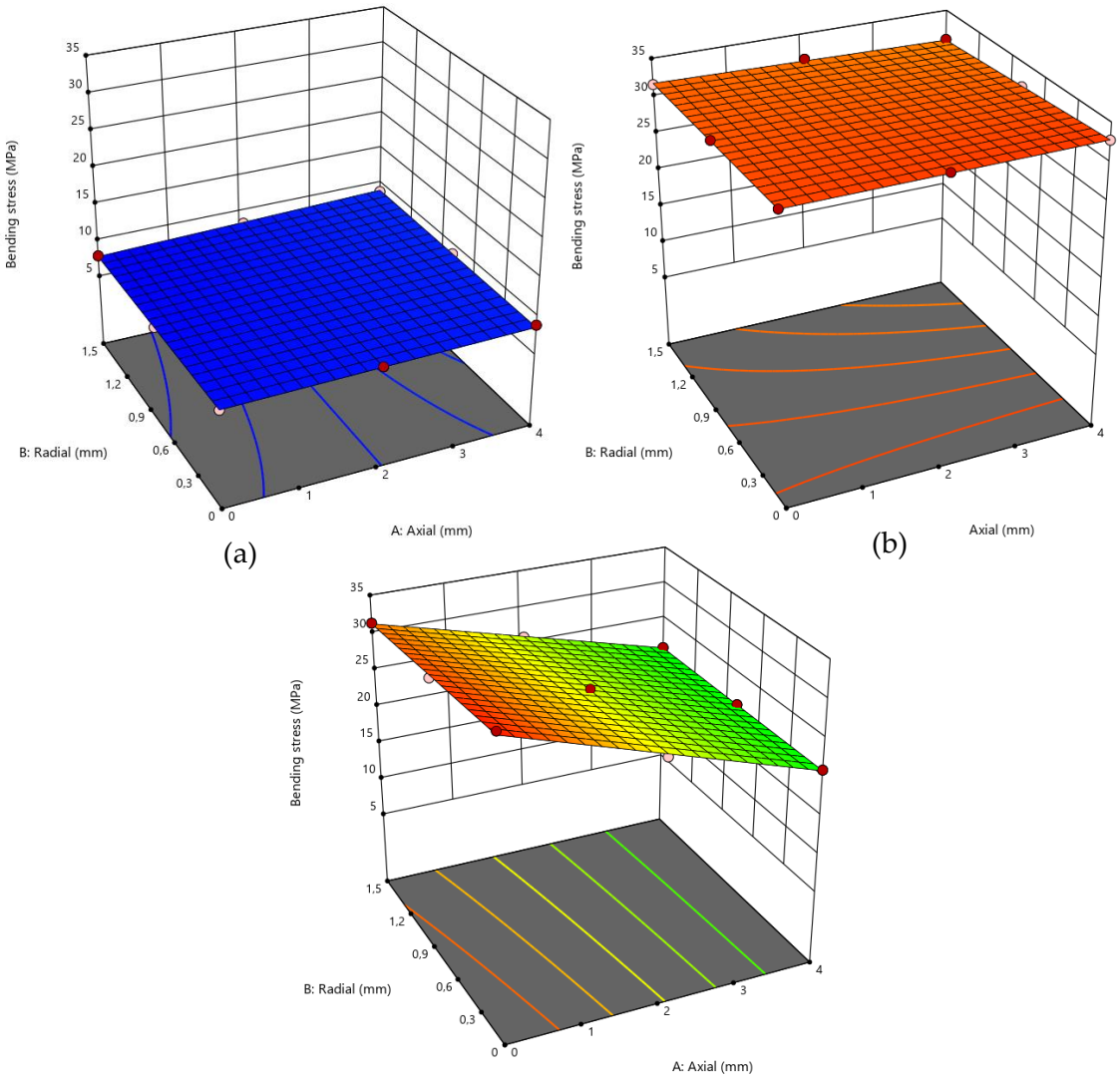

Figure 32. Maximum principal stresses at the root of the tooth for simulated combined misalignments. a) yaw = 0° b) yaw = 2,69° c) -2,69°

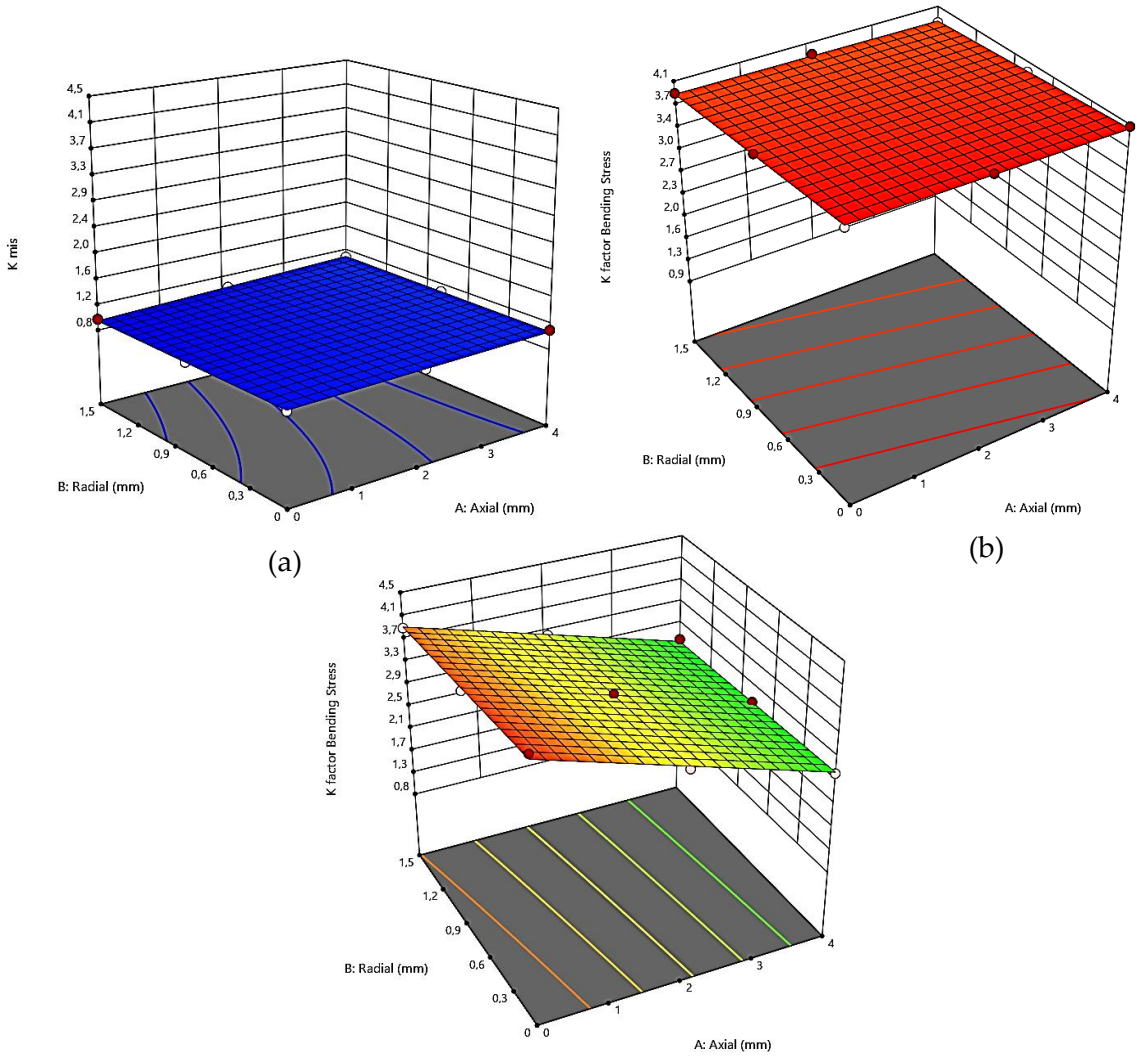

Figure 33. Misalignment bending stress increase factor K_{mis}. a) yaw = 0° b) yaw = 2,69° c) -2,69°

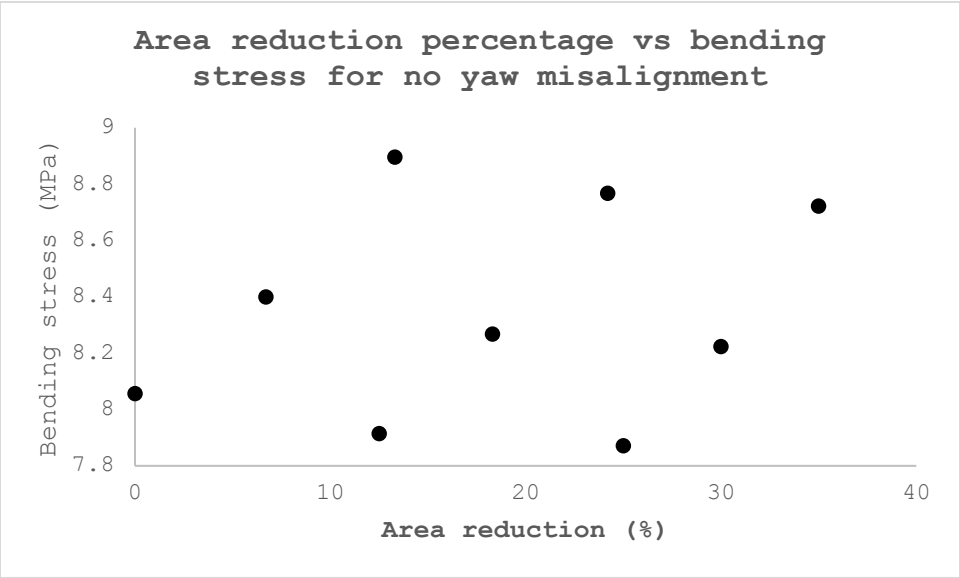

Figure 34. Meshing area reduction percentage vs bending stress for no yaw misalignment

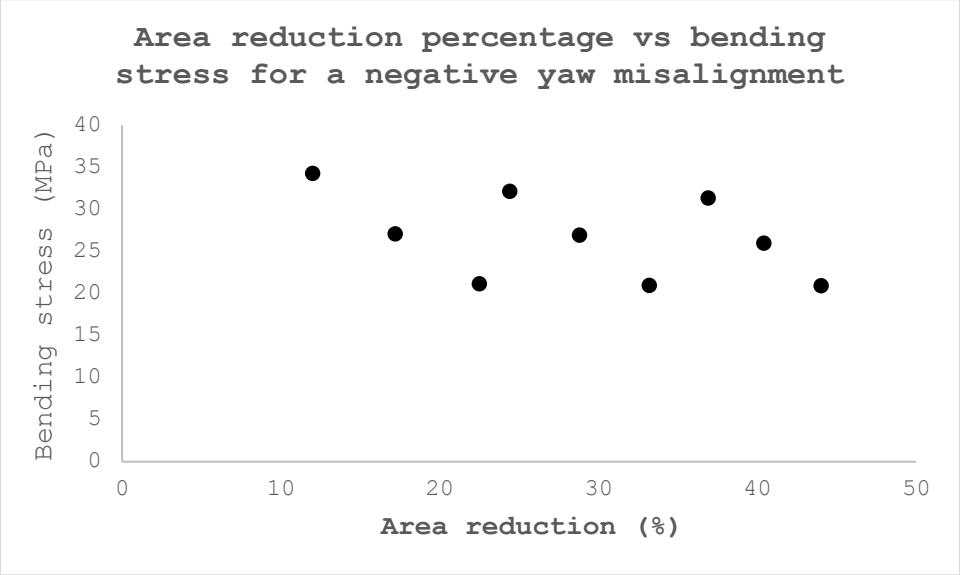

Figure 35. Meshing area reduction percentage vs bending stress for -2,69° of yaw misalignment

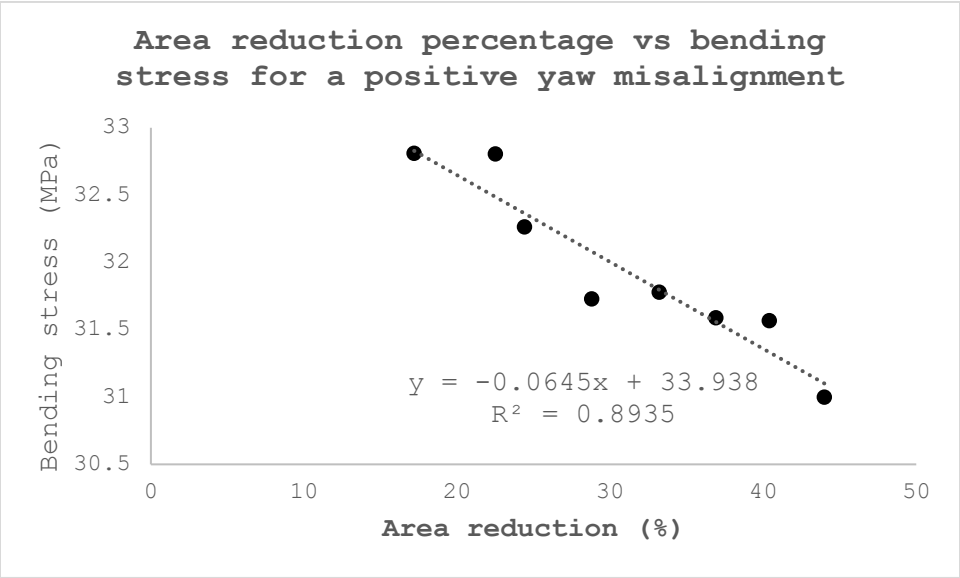

Figure 36. Meshing area reduction percentage vs bending stress for 2,69° of yaw misalignment

Guidelines for spur gear power transmission considering shaft misalignments

The misalignments studied in this work are due to changes in the theoretic position of the shafts in a transmission system of a spur gear stage. These changes in practice are due to errors in the assembly or due to failures in the operation.

As it was said before it is really hard to get a perfect alignment between two spur gear in the assembly stage. Although the intention of the designer or the assembly technician is to achieve zero misalignment in the assembly, there are errors due to the measuring instruments, the available technology, the expertise of the assembly personnel, among others.

Shaft misalignments in a spur gear transmission system is not desirable because of the increase in the tooth bending stress, surface stress and transmission error. Although it was not researched in this work, the surface stress is one of the most affected stresses when there are misalignments. Because of the meshing reduction area, the surface stresses increase. Dudley [130] suggests that in order to compensate for misalignments due to assembly, superficial modifications should be made to the teeth when they are manufactured, with this it is possible to reduce the contact and bending stresses due to the expected alignment errors. In the last year numerous works have been related with surface modification in order to reduce the transmission error and therefore to improve the efficiency of the transmission in the event of possible misalignment of the shafts. As this is not the objective of this work, we will focus on those recommendations related to bending stresses.

- For a spur gear transmission with zero backlash, the misalignments that could be present are the axial, radial, yaw and their combinations. As it was shown in this work the yaw misalignment is the most critical for the bending stress, in general terms an increase of the positive yaw misalignments increase the bending stress for any combinations of the axial and radial misalignments. An increase in the absolute value of the negative misalignments in any combination of axial and radial misalignments results in an increase in bending stresses. Therefore, when assembling spur gear transmission systems, yaw misalignments must be avoided as much as possible.

- Good control over the surfaces on which the bearing units rest can ensure minimal yaw misalignments. For this, these surfaces would have to be parallel.

- Even if the surfaces supporting the bearing units were made to be parallel, there is the possibility of axial and radial misalignment. As shown in this work, when there is no angular misalignment, radial misalignment is not as significant in bending stresses as axial, therefore it must be avoided by ensuring that the gear faces are in the same plane.

- Although the radial misalignment is the least influential in the maximum bending stress, care must be taken to allow high values in the assembly, since this is the one that most influences the contact ratio. Having a contact ratio less than one at all contact points would result in tooth impacts that would increase dynamic loads and transmission noise.

- Although the misalignment of the shafts does not generate an increase in vibrations, it is possible to take this variable as a diagnostic variable. Therefore, taking into account the previous recommendations, the following procedure is suggested once the highest possible level of alignment has been achieved:

  1) Preliminary gear design.

  In the case of a single spur gear system that is being designed, it must start with a preliminary design. From this stage, the torque, the materials of the gears, the module (m), the number of teeth (N), the diameter of the shafts and the face width for both the pinion and the driven gear must be obtained. With the diameter of the shafts and with the other parameters, the thickness of the ring can be calculated and a geometric configuration of the gears can be obtained.

  2) Gear mounting configuration.

  For a single spur gear system four type of mounting configuration are possible:

  a) Pinion and driven gear in a straddle mounting.
  b) Pinion and driven gear in overhang mounting.
  c) The pinion in a straddle mounting and the driven gear in overhang mounting.
  d) The pinion in overhang mounting and the driven gear in a straddle mounting.

  In this stage a gear mounting configuration have to be chosen.

  3) Another preliminary design information.
  Also required: shaft material, shaft overall length, bearing type, bearing spacing, gear to bearing spacing, bearing stiffness and damping factor.

4) Computer Aided Design (CAD)

With the information obtained up to this stage a 3D model of the pinion and driven gear can be made in drawing software such as SolidWorks or any other available.

5) Finite element model of gears.

Software like Ansys or Abaqus can be used for finite element analysis of gears. In this case, the latter was used due to the quality of the mesh that can be obtained. For the analysis, it is enough to select three teeth of each gear, since with them a complete meshing cycle of a tooth can be simulated, thus optimizing the computational resource.
Regarding the ring, it is suggested to calculate the thickness of the ring and check if it is 1.2 times greater than the total working depth of the tooth, h_t. If so, the bending stress will not be affected by this value as reported by the AGMA standard [147]. Therefore, if the thickness of the ring is greater than 1.2 h_t, it is suggested that the thickness of the model be 1.2 h_t, which saves computational resources without generating a change in the bending stress results.
It is suggested to divide the tooth into six parts through six auxiliary intermediate surfaces. First order hexahedral element is the most recommended for this application because it has good precision with a lower computational cost. The assembly of the pinion and driven gear must be according to the misalignment condition to be studied.
Two reference points are taken coincident with the center of the gears that would correspond to the point of connection with the shafts. These reference points are coupled to the internal and lateral surfaces of the pinion and driven gear. The torque to be transmitted is applied at the reference point associated with the driven gear. At the reference point associated with the pinion, an angle of rotation equivalent to the complete cycle of the meshing of a tooth is applied.
For the contact discretization method can be node to surface and surface to surface. Node to surface method has a lower computational cost.
The outputs of this stage are the force on the shaft in the direction of the tangential force on the gears and the maximum stresses at the base of the teeth.

6) Analytical model.
For this stage the force signals from the previous stage are required. Since the forces obtained are from one meshing cycle of a tooth, these signals have to be replicated a number of times n so as to obtain a signal that allows the stabilization of the model in a given time.

The model requires the following inputs that can be obtained from the previous stages: bearing stiffness, damping factor, mass of the shaft, moment of inertia of the shaft, and geometric configuration of the transmission stage. The model presented in this work is for a pinion in overhang mounting, but it could be adjusted for other types of configurations.
The output of this stage is a signal of acceleration in time for the bearing closest to the pinion.

7) Signal processing.

The signals of acceleration in time are transformed to signals in frequency through the fast Fourier transform (FFT). From this spectrum, the proposed indicator of percentage change of spectra with respect to a base spectrum is calculated, which in this case corresponds to the spectrum of the aligned condition. Therefore, the first spectrum to be generated is that of the aligned condition. The proposed indicator compares the peak values of the aligned spectrum and compares it with the values at those corresponding frequencies in the misaligned spectrum.
The output of this stage is the percentage change of the acceleration spectrum. The methodology described here is shown in Figure 37.

- As shown in this work, a decrease in the proposed indicator of spectrum change indicates a misalignment in the axes. However, with the tools and information available it is not possible to accurately predict the types and amount of misalignment present from a bearing vibration measurement. What is feasible in a design stage is to estimate through the proposed methodology what would be the largest change in the indicator for the most critical misalignment condition. According to the case study worked on, the condition that produces the most significant changes is the maximum angular combination, either positive or negative, with the maximum radial in any axial combination.

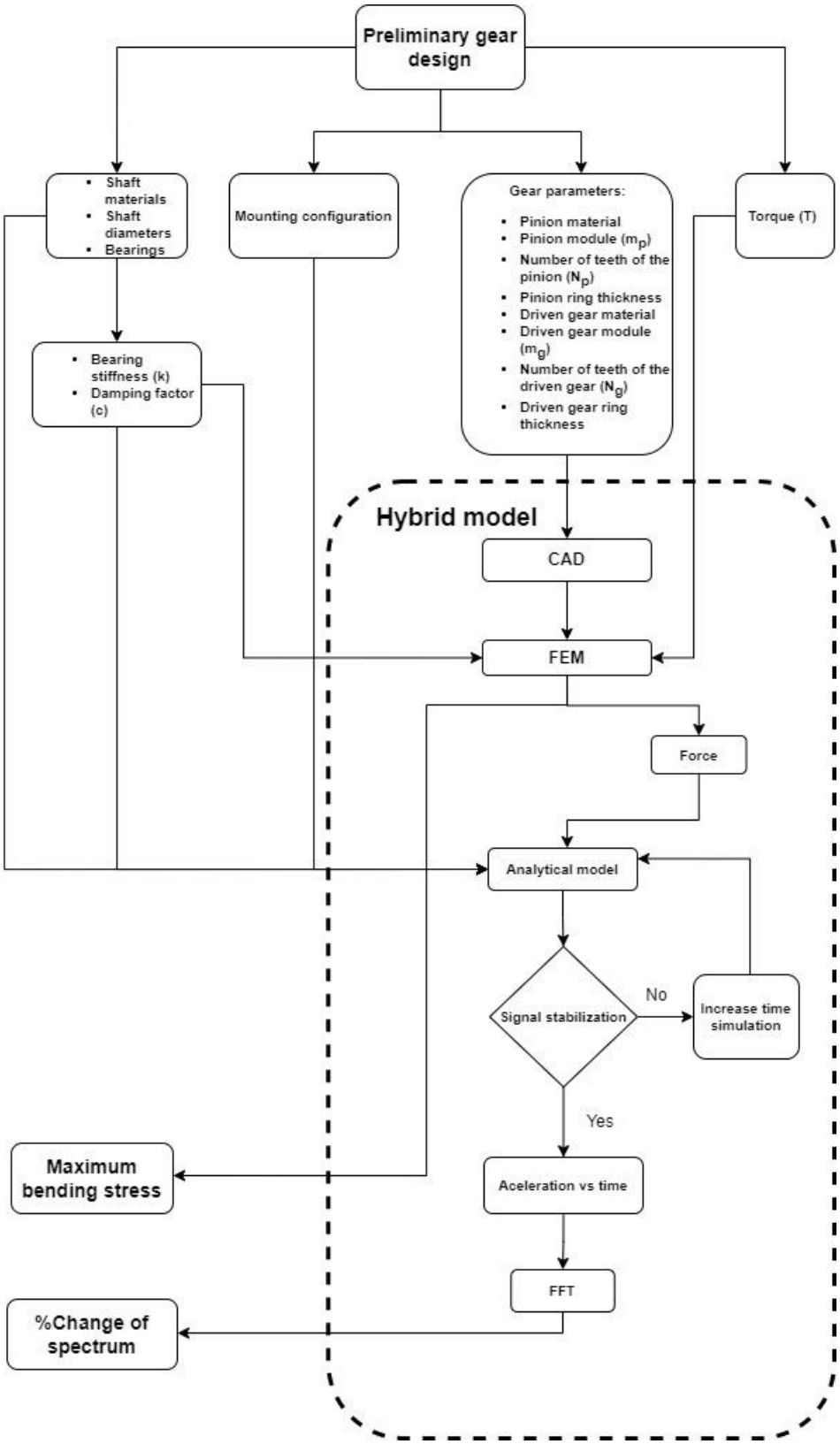

Figure 37. Proposed methodology for the estimation of bending stresses and changes in vibration signals in single-stage spur gear transmission systems under shaft misalignment.

Therefore, in a previous stage of design this percentage change of spectrum area change can be estimated taking a particular combined misalignment condition (yaw - radial - axial). Since bending stress is one of the critical variables in gears, a permissible limit value of misalignment could be the one that generates a certain level of stress. As shown in this research, the misalignment that has the most influence on the bending stresses is the yaw one. Therefore it is possible start with an exaggerated angular misalignment condition to estimate the relationship between angular misalignment and stresses; this is a simplification of equations (51) and (52) for a preliminary estimate. A first value of angular misalignment could be the one that is formed when one of the ends of the gear does not rest on the pitch circle but on the addendum circle of the other gear. Once this assembly is determined, the proposed model can be used to determine the stress increase factor K at this point and estimate a preliminary relationship between stress and angular misalignment as shown in the Equation (53). This relationship is based on the trends found in equations (51) and (52). y is the yaw misalignment in codified variable (0 to 1), zero for no misalignment and 1 for the yaw misalignment chosen. σ_{mis} is the bending stress for the yaw misalignment chosen.

$$K_{mis} = 1 + r.y \qquad where\ r = \frac{\sigma_{mis}}{\sigma_{aligned}} - 1 \tag{53}$$

Equation (53) is a rough estimation of bending stresses by yaw misalignments. For a more accurate approximation two or more angles can be taken and the regression equation can be made with these values. With this equation it is possible to calculate the stress increase factor for a given yaw misalignment, or inversely, the misalignment required to achieve a given increase factor. For the angles worked in this work, the increase factors were in the order of 3 to 4, which is too high. At this stage the designer must determine how much he will allow the bending stresses to increase due to misalignment. For example, if he will allow an increase of 20%, in Equation (53) he must replace K_{mis} by 1.2, with this he will determine the angular misalignment in a coded variable and he will be able to find the angular misalignment in a real variable. This will be the maximum angular misalignment that he will allow in his design.

With the maximum permissible angular misalignment, the maximum permissible radial misalignment can now be determined, which could be calculated taking into account that a contact ratio of less than 1.2 is not reached.

Once the combined misalignment point formed by angular and radial misalignment has been determined, the percentage change in the acceleration spectrum that it would generate is evaluated, through the previously described methodology (Figure 37). In order to use this value as a diagnostic limit value, the actual spectrum of the aligned condition must first be obtained, which can be done when mounting the transmission. In this way, in a future operation the spectrum can be obtained and the spectrum change percentage indicator can be calculated. The previous procedure is shown in Figure 38.

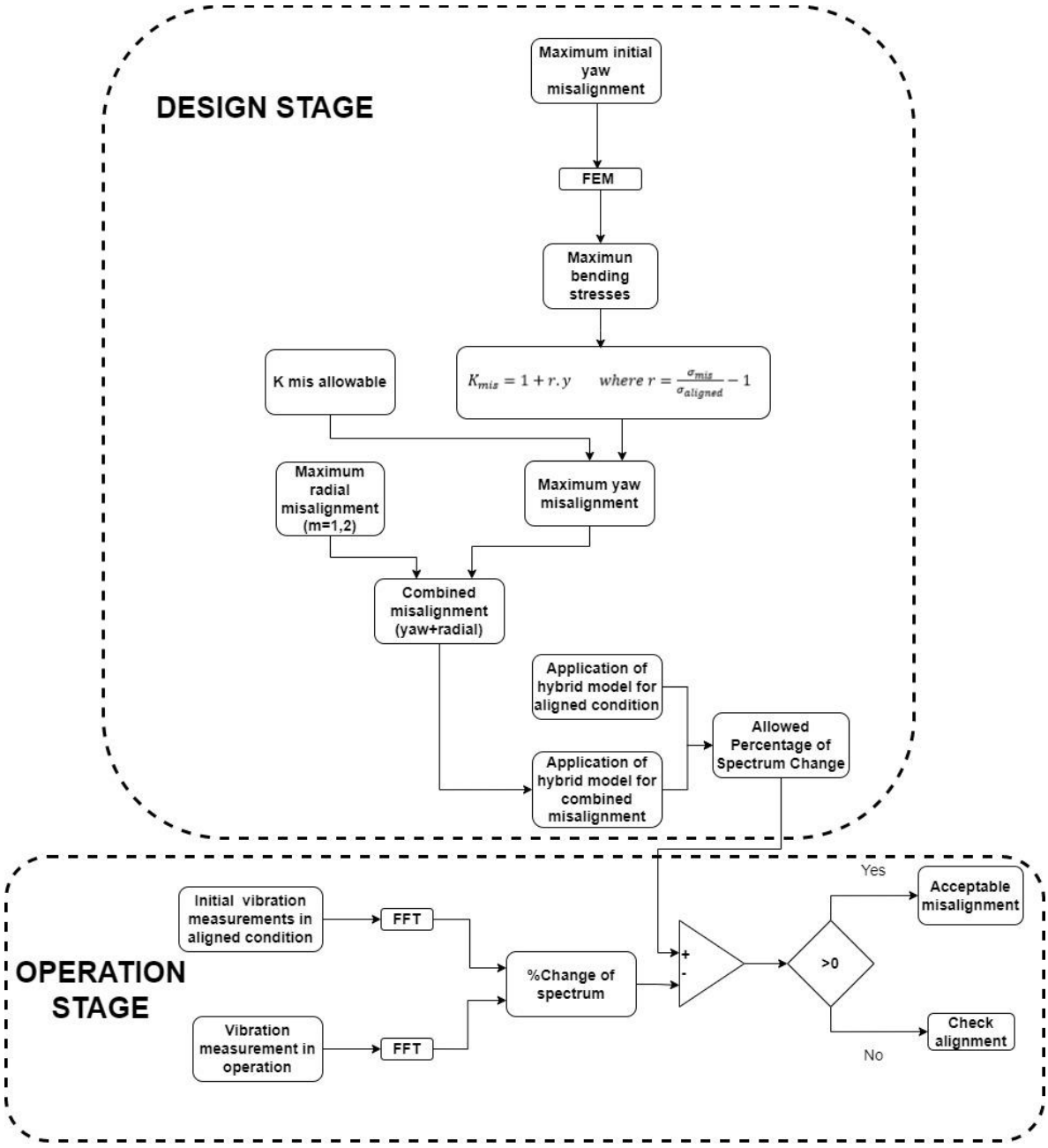

Figure 38. Proposed methodology to set a maximum level of spectrum change percentage from the design stage.

Conclusions

The study of the effect of misalignment of spur gears, on stresses and vibrations, either experimentally or analytically, is relatively recent. The main conclusions and contributions achieved with the development of this research are shown below.

- Starting from the original idea of integrating the areas of vibration and design in power transmission systems, through a systematic search for the state of the art, it was possible to successfully delimit the problem and a gap could be found that consists of the lack of study related to misalignments and their effects on vibrations. If the knowledge in this area is not extensive, much less will it be related to design methodologies that integrate these two areas. In this sense, this work is the first step in this line of research.

- Misalignments in a transmission system can come from different sources. In this work, the misalignments due to changes in the position of the shafts due to assembly or operation errors whose origin is not deflection were studied.

- A test bench was designed and built for the generation of radial, axial and angular misalignments and the combination of these. The bench allows changing gears to work with different gear ratios and other geometric parameters. The bench is instrumented to measure vibrations in the bases of the bearings.

- An experimental exploration was carried out working with all possible combinations of extreme levels of radial, axial and angular misalignment in a single stage transmission system for a given pair of gears. The work consisted of measuring the vibrations at the base of the bearing closest to the pinion, with the aim of screening and understanding some trends and effects of misalignment and their interactions.

- The peaks of interest in the acceleration spectrum are the peaks at the rotational frequency and its multiples and the peaks at the gear mesh frequency and its multiples. Because these peaks are numerous, which makes it difficult to immediately analyze the spectrum change from an aligned condition to a misaligned one, a spectrum change indicator was proposed that evaluates the deviation of the main peaks, for which smoothed spectra are required.

- A hybrid model was proposed for the estimation of bending stresses and acceleration spectra at the base of one of the bearings of a one-stage spur gear transmission system in which the pinion and the driven gear are in overhang

mounting. The model is based on a simulation in a finite element software for the estimation of the bending stresses in the teeth and the force that the gears transmit to the shaft. This force signal is one of the inputs into an analytical model that predicts the vibrations in one of the bearing bases. With this model, more points were explored than those that were worked on experimentally.

- The experimental results and those obtained by the model coincided with a correlation of 0.98. The differences obtained do not exceed 15% in each evaluated value. In this way, the proposed methodology for the estimation of the change in the acceleration spectrum in the bearing bases of one-stage transmission systems with shaft misalignment constitutes a good way to estimate this variable. Running a fully simulated model through dynamic analysis would require much more computational resources and time.

- Although regression models were obtained for the bending stress and the percentage of change of spectrum, what is important to emphasize are the contributions of each type of misalignment and their interactions. For combined misalignments, the percentage change of spectra is mainly influenced by angular and radial misalignment and their quadratic effects. This is to be expected since axial misalignments do not generate significant changes in the tangential force of the gears. For bending stresses, it was found that the most influential factor is the angular one, which is why it is the type of misalignment that should be avoided the most.

- With the results obtained, guidelines were proposed for the design and assembly of spur gear transmission systems, as well as a methodology to set a maximum permissible value of the percentage change of acceleration spectra from the design stage.

Future works

The work shown here is a preliminary study of the combined misalignments in a single-stage spur gear transmission system in overhang mounting for pinion and driven gear. The effects of these misalignments on bending stresses and vibrations were investigated through a hybrid model that was validated experimentally. This exploration allowed us to know the significant variables and interactions, which allowed us to propose design recommendations. The following works are proposed:

- To make other design recommendations, it is proposed to expand the working range in order to include positive and negative intermediate angles. That is, evaluate the proposed model in combinations of misalignments with positive and negative intermediate angles and validate them experimentally.

- Investigate the effect of torque variation on measured vibrations for a given gear configuration with combined misalignments.

- Develop fully analytical models that allow estimating bending stresses and vibrations in a spur gear transmission system with combined misalignments.

- Study the effect of combined misalignments in spur gear transmission systems on surface stresses on the teeth.

- Investigate the effect of combined misalignments on transmission error and take it as a critical design variable to make design recommendations.

- Develop more accurate misalignment prediction models by measuring vibrations in the bearing bases. This can be achieved with vibration measurements in more than one direction.

- The misalignments studied here cause a reduction in the percentage of spectrum change, while other types of failures in transmission systems, such as misalignments due to shaft deflection due to overloads, increase vibration measurements. Thus, if there is misalignment due to a change of position in the shafts and due to deflection, it is possible that the vibration measurements will increase, which would not reflect the misalignment due to a change of position. Therefore, it is proposed to develop investigations that include different types of typical failures that occur in transmission systems at the same time to develop better predictive models.

- Extend the study of misalignments to other types of gears such as helical and bevel gears.

References

[1] P. Henriquez, J. B. Alonso, M. A. Ferrer, and C. M. Travieso, "Review of automatic fault diagnosis systems using audio and vibration signals," *IEEE Transactions on Systems, Man, and Cybernetics: Systems*, vol. 44, no. 5. Institute of Electrical and Electronics Engineers Inc., pp. 642–652, 2014. doi: 10.1109/TSMCC.2013.2257752.

[2] S. Sheng, "Gearbox Typical Failure Modes, Detection, and Mitigation Methods (Presentation), NREL (National Renewable Energy Laboratory)," 2014.

[3] D. Wang, K. L. Tsui, and Q. Miao, "Prognostics and Health Management: A Review of Vibration Based Bearing and Gear Health Indicators," *IEEE Access*, vol. 6, pp. 665–676, Nov. 2017, doi: 10.1109/ACCESS.2017.2774261.

[4] C. Riba and A. Molina, "Ingeniería Concurrente : Una metodología integradora," 2006.

[5] I. Zupic and T. Čater, "Bibliometric Methods in Management and Organization," *Organ Res Methods*, vol. 18, no. 3, pp. 429–472, 2015, doi: 10.1177/1094428114562629.

[6] H. C. Lin and Y. C. Ye, "Reviews of bearing vibration measurement using fast Fourier transform and enhanced fast Fourier transform algorithms," *Advances in Mechanical Engineering*, vol. 11, no. 1, pp. 1–12, 2019, doi: 10.1177/1687814018816751.

[7] B. J. Olson, S. W. Shaw, C. Shi, C. Pierre, and R. G. Parker, "Circulant matrices and their application to vibration analysis," *Appl Mech Rev*, vol. 66, no. 4, p. 040803, Jun. 2014, doi: 10.1115/1.4027722.

[8] R. Yan, R. X. Gao, and X. Chen, "Wavelets for fault diagnosis of rotary machines: A review with applications," *Signal Processing*, vol. 96, no. PART A, pp. 1–15, 2014, doi: 10.1016/j.sigpro.2013.04.015.

[9] L. Prášil and J. Mackerle, "Finite element analyses and simulations of gears and gear drives," *Eng Comput (Swansea)*, vol. 25, no. 3, pp. 196–219, 2008, doi: 10.1108/02644400810857056.

[10] J. Su, L. Zheng, Z. Deng, and Y. Jiang, "Research progress on high-intermediate frequency extension methods of SEA," *Shock and Vibration*, vol. 2019, 2019, doi: 10.1155/2019/4192437.

[11] F. Li, Y. Qin, L. Ge, Z. Pang, S. Liu, and D. Lin, "Influences of planetary gear parameters on the dynamic characteristics – a review," *Journal of Vibroengineering*, vol. 17, no. 2, pp. 574–586, 2015.

[12] K. M. Mohan, K. Srinivasan, and V. Ramamurti, "Dynamics of machine tool drive housings," *Proc Inst Mech Eng B J Eng Manuf*, vol. 224, no. 11, pp. 1619–1630, 2010, doi: 10.1243/09544054JEM1873.

[13] Q. Gao, W. Chen, L. Lu, D. Huo, and K. Cheng, “Aerostatic bearings design and analysis with the application to precision engineering: State-of-the-art and future perspectives,” *Tribol Int*, vol. 135, no. November 2018, pp. 1–17, 2019, doi: 10.1016/j.triboint.2019.02.020.

[14] F. Al-Bender, “On the modelling of the dynamic characteristics of aerostatic bearing films: From stability analysis to active compensation,” *Precis Eng*, vol. 33, no. 2, pp. 117–126, 2009, doi: 10.1016/j.precisioneng.2008.06.003.

[15] S. W. Hong and V. C. Tong, “Rolling-element bearing modeling: A review,” *International Journal of Precision Engineering and Manufacturing*, vol. 17, no. 12, pp. 1729–1749, 2016, doi: 10.1007/s12541-016-0200-z.

[16] H. Mahdisoozani *et al.*, “Performance Enhancement of Internal Combustion Engines through Vibration Control: State of the Art and Challenges,” *Applied Sciences*, vol. 9, no. 3, p. 406, Jan. 2019, doi: 10.3390/app9030406.

[17] S. Sharma, E. B. Coetzee, M. H. Lowenberg, S. A. Neild, and B. Krauskopf, “Numerical continuation and bifurcation analysis in aircraft design: An industrial perspective,” *Philosophical Transactions of the Royal Society A: Mathematical, Physical and Engineering Sciences*, vol. 373, no. 2051, 2015, doi: 10.1098/rsta.2014.0406.

[18] T. Wang, Q. Han, F. Chu, and Z. Feng, “Vibration based condition monitoring and fault diagnosis of wind turbine planetary gearbox: A review,” *Mech Syst Signal Process*, vol. 126, pp. 662–685, Jul. 2019, doi: 10.1016/j.ymssp.2019.02.051.

[19] C. K. T. and L. M. S.-C. Tan, Y.M.Lai, “Sliding mode voltage controller for basic DC-DC converter in discontinuous conduction mode,” *IET Electr.Power Appl. Vol. 1, No. 1*, vol. 67, no. 4, pp. 263–270, 2001, doi: 10.1049/iet-epa.

[20] P. D. Samuel and D. J. Pines, *A review of vibration-based techniques for helicopter transmission diagnostics*, vol. 282, no. 1–2. Academic Press, 2005. doi: 10.1016/j.jsv.2004.02.058.

[21] A. S. Sekhar, “Multiple cracks effects and identification,” *Mech Syst Signal Process*, vol. 22, no. 4, pp. 845–878, 2008, doi: 10.1016/j.ymssp.2007.11.008.

[22] M. S. Patil, J. Mathew, and P. K. R. Kumar, “Bearing signature analysis as a medium for fault detection: A review,” *J Tribol*, vol. 130, no. 1, pp. 1–7, 2008, doi: 10.1115/1.2805445.

[23] L. L. Gonçalves, A. P. Vieira, and E. P. De Moura, “Fluctuation analyses for pattern classification in nondestructive materials inspection,” *EURASIP J Adv Signal Process*, vol. 2010, 2010, doi: 10.1155/2010/262869.

[24] R. B. Randall and J. Antoni, “Rolling element bearing diagnostics-A tutorial,” *Mech Syst Signal Process*, vol. 25, no. 2, pp. 485–520, 2011, doi: 10.1016/j.ymssp.2010.07.017.

[25] J. Cibulka, M. K. Ebbesen, G. Hovland, K. G. Robbersmyr, and M. R. Hansen, “A review on approaches for condition based maintenance in applications with induction machines located offshore,” *Modeling, Identification and Control*, vol. 33, no. 2, pp. 69–86, 2012, doi: 10.4173/mic.2012.2.4.

[26] Z. Feng, M. Liang, and F. Chu, “Recent advances in time-frequency analysis methods for machinery fault diagnosis: A review with application examples,” *Mech Syst Signal Process*, vol. 38, no. 1, pp. 165–205, 2013, doi: 10.1016/j.ymssp.2013.01.017.

[27] Y. Lei, J. Lin, M. J. Zuo, and Z. He, “Condition monitoring and fault diagnosis of planetary gearboxes: A review,” *Measurement (Lond)*, vol. 48, no. 1, pp. 292–305, 2014, doi: 10.1016/j.measurement.2013.11.012.

[28] W. A. Smith and R. B. Randall, “Rolling element bearing diagnostics using the Case Western Reserve University data: A benchmark study,” *Mech Syst Signal Process*, vol. 64–65, pp. 100–131, 2015, doi: 10.1016/j.ymssp.2015.04.021.

[29] W. Y. Liu, B. P. Tang, J. G. Han, X. N. Lu, N. N. Hu, and Z. Z. He, “The structure healthy condition monitoring and fault diagnosis methods in wind turbines: A review,” *Renewable and Sustainable Energy Reviews*, vol. 44, pp. 466–472, 2015, doi: 10.1016/j.rser.2014.12.005.

[30] I. Antoniadou, N. Dervilis, E. Papatheou, A. E. Maguire, and K. Worden, “Aspects of structural health and condition monitoring of offshore wind turbines,” *Philosophical Transactions of the Royal Society A: Mathematical, Physical and Engineering Sciences*, vol. 373, no. 2035, pp. 1–14, 2015, doi: 10.1098/rsta.2014.0075.

[31] I. El-Thalji and E. Jantunen, “A summary of fault modelling and predictive health monitoring of rolling element bearings,” *Mech Syst Signal Process*, vol. 60, pp. 252–272, 2015, doi: 10.1016/j.ymssp.2015.02.008.

[32] T. Narendiranath Babu, T. Manvel Raj, and T. Lakshmanan, “A Review on Application of Dynamic Parameters of Journal Bearing for Vibration and Condition Monitoring,” *Journal of Mechanics*, vol. 31, no. 4, pp. 391–416, 2015, doi: 10.1017/jmech.2015.6.

[33] M. J. Gómez, C. Castejón, and J. C. García-Prada, “Review of recent advances in the application of the wavelet transform to diagnose cracked rotors,” *Algorithms*, vol. 9, no. 1, 2016, doi: 10.3390/a9010019.

[34] D. Goyal and B. S. Pabla, “The Vibration Monitoring Methods and Signal Processing Techniques for Structural Health Monitoring: A Review,” *Archives of Computational Methods in Engineering*, vol. 23, no. 4, pp. 585–594, Dec. 2016, doi: 10.1007/s11831-015-9145-0.

[35] Y. Wang, J. Xiang, R. Markert, and M. Liang, “Spectral kurtosis for fault detection, diagnosis and prognostics of rotating machines: A review with applications,” *Mech Syst Signal Process*, vol. 66–67, pp. 679–698, 2016, doi: 10.1016/j.ymssp.2015.04.039.

[36] A. Rai and S. H. Upadhyay, “A review on signal processing techniques utilized in the fault diagnosis of rolling element bearings,” *Tribol Int*, vol. 96, pp. 289–306, 2016, doi: 10.1016/j.triboint.2015.12.037.

[37] Z. Li, Y. Jiang, C. Hu, and Z. Peng, “Recent progress on decoupling diagnosis of hybrid failures in gear transmission systems using vibration sensor signal: A review,” *Measurement (Lond)*, vol. 90, pp. 4–19, Aug. 2016, doi: 10.1016/j.measurement.2016.04.036.

[38] H. D. M. De Azevedo, A. M. Araújo, and N. Bouchonneau, “A review of wind turbine bearing condition monitoring: State of the art and challenges,” *Renewable and Sustainable Energy Reviews*, vol. 56, pp. 368–379, 2016, doi: 10.1016/j.rser.2015.11.032.

[39] W. Caesarendra and T. Tjahjowidodo, “A Review of Feature Extraction Methods in Vibration-Based Condition Monitoring and Its Application for Degradation Trend Estimation of Low-Speed Slew Bearing,” *Machines*, vol. 5, no. 4, p. 21, Sep. 2017, doi: 10.3390/machines5040021.

[40] I. Javorskyj, I. Kravets, I. Matsko, and R. Yuzefovych, “Periodically correlated random processes: Application in early diagnostics of mechanical systems,” *Mech Syst Signal Process*, vol. 83, pp. 406–438, 2017, doi: 10.1016/j.ymssp.2016.06.022.

[41] F. Wang, C. Liu, W. Su, Z. Xue, H. Li, and Q. Han, “Condition monitoring and fault diagnosis methods for Low-Speed and Heavy-Load slewing bearings: A literature review,” *Journal of Vibroengineering*, vol. 19, no. 5, pp. 3429–3444, 2017, doi: 10.21595/jve.2017.18454.

[42] X. Tong, A. Palazzolo, and J. Suh, “A Review of the Rotordynamic Thermally Induced Synchronous Instability (Morton) Effect,” *Appl Mech Rev*, vol. 69, no. 6, p. 060801, 2017, doi: 10.1115/1.4037216.

[43] A. Sabato, C. Niezrecki, and G. Fortino, “Wireless MEMS-Based Accelerometer Sensor Boards for Structural Vibration Monitoring: A Review,” *IEEE Sens J*, vol. 17, no. 2, pp. 226–235, 2017, doi: 10.1109/JSEN.2016.2630008.

[44] Y. Liu and A. M. Bazzi, “A review and comparison of fault detection and diagnosis methods for squirrel-cage induction motors: State of the art,” *ISA Trans*, vol. 70, pp. 400–409, 2017, doi: 10.1016/j.isatra.2017.06.001.

[45] X. Xu, H. Wang, N. Zhang, Z. Liu, and X. Wang, “Review of the Fault Mechanism and Diagnostic Techniques for the Range Extender Hybrid Electric Vehicle,” *IEEE Access*, vol. 5, pp. 14234–14244, 2017, doi: 10.1109/ACCESS.2017.2725298.

[46] D. Goyal, Vanraj, B. S. Pabla, and S. S. Dhami, “Condition Monitoring Parameters for Fault Diagnosis of Fixed Axis Gearbox: A Review,” *Archives of Computational Methods in Engineering*, vol. 24, no. 3, pp. 543–556, 2017, doi: 10.1007/s11831-016-9176-1.

[47] S. Li, Y. Nie, and J. Li, “Condition monitoring and diagnosis of power equipment: Review and Prospective,” *High Voltage*, vol. 2, pp. 82–91, 2017, doi: 10.1049/hve.2017.0026.

[48] R. Liu, B. Yang, E. Zio, and X. Chen, “Artificial intelligence for fault diagnosis of rotating machinery: A review,” *Mech Syst Signal Process*, vol. 108, pp. 33–47, 2018, doi: 10.1016/j.ymssp.2018.02.016.

[49] X. Liang, M. J. Zuo, and Z. Feng, “Dynamic modeling of gearbox faults: A review,” *Mech Syst Signal Process*, vol. 98, pp. 852–876, 2018, doi: 10.1016/j.ymssp.2017.05.024.

[50] S. Xu, F. Xing, R. Wang, W. Li, Y. Wang, and X. Wang, “Vibration sensor for the health monitoring of the large rotating machinery: Review and outlook,” *Sensor Review*, vol. 38, no. 1, pp. 44–64, 2018, doi: 10.1108/SR-03-2017-0049.

[51] S. Delvecchio, P. Bonfiglio, and F. Pompoli, “Vibro-acoustic condition monitoring of Internal Combustion Engines: A critical review of existing techniques,” *Mech Syst Signal Process*, vol. 99, pp. 661–683, 2018, doi: 10.1016/j.ymssp.2017.06.033.

[52] R. Siva Srinivas, R. Tiwari, and C. Kannababu, “Application of active magnetic bearings in flexible rotordynamic systems – A state-of-the-art review,” *Mech Syst Signal Process*, vol. 106, pp. 537–572, 2018, doi: 10.1016/j.ymssp.2018.01.010.

[53] T. Touret, C. Changenet, F. Ville, M. Lalmi, and S. Becquerelle, “On the use of temperature for online condition monitoring of geared systems – A review,” *Mech Syst Signal Process*, vol. 101, pp. 197–210, 2018, doi: 10.1016/j.ymssp.2017.07.044.

[54] Y. Ding, P. Ren, H. Zhao, and C. Miao, “Structural health monitoring of a high-speed railway bridge: Five years review and lessons learned,” *Smart Struct Syst*, vol. 21, no. 5, pp. 695–703, 2018, doi: 10.12989/sss.2018.21.5.695.

[55] Y. Li, X. Wang, Z. Liu, X. Liang, and S. Si, “The entropy algorithm and its variants in the fault diagnosis of rotating machinery: A review,” *IEEE Access*, vol. 6, pp. 66723–66741, 2018, doi: 10.1109/ACCESS.2018.2873782.

[56] Z. Qiao, Y. Lei, and N. Li, “Applications of stochastic resonance to machinery fault detection: A review and tutorial,” *Mech Syst Signal Process*, vol. 122, pp. 502–536, 2019, doi: 10.1016/j.ymssp.2018.12.032.

[57] B. A. Zai, M. A. Khan, K. A. Khan, A. Mansoor, A. Shah, and M. Shahzad, “The role of dynamic response parameters in damage prediction,” *Proc Inst Mech Eng C J Mech Eng Sci*, vol. 233, no. 13, pp. 4620–4636, 2019, doi: 10.1177/0954406219841083.

[58] C. Malla and I. Panigrahi, “Review of Condition Monitoring of Rolling Element Bearing Using Vibration Analysis and Other Techniques,” *Journal of Vibration Engineering & Technologies*, vol. 7, no. 4, pp. 407–414, 2019, doi: 10.1007/s42417-019-00119-y.

[59] S. Lu, R. Yan, Y. Liu, and Q. Wang, “Tacholess Speed Estimation in Order Tracking: A Review with Application to Rotating Machine Fault Diagnosis,” *IEEE Trans Instrum Meas*, vol. 68, no. 7, pp. 2315–2332, 2019, doi: 10.1109/TIM.2019.2902806.

[60] A. Kumar and R. Kumar, “Role of Signal Processing, Modeling and Decision Making in the Diagnosis of Rolling Element Bearing Defect: A Review,” *J Nondestr Eval*, vol. 38, no. 1, pp. 1–29, 2019, doi: 10.1007/s10921-018-0543-8.

[61] T. Poompavai and M. Kowsalya, “Control and energy management strategies applied for solar photovoltaic and wind energy fed water pumping system: A review,” *Renewable and Sustainable Energy Reviews*, vol. 107, no. November 2018, pp. 108–122, 2019, doi: 10.1016/j.rser.2019.02.023.

[62] C. A. Papadopoulos, “The strain energy release approach for modeling cracks in rotors: A state of the art review,” *Mech Syst Signal Process*, vol. 22, no. 4, pp. 763–789, 2008, doi: 10.1016/j.ymssp.2007.11.009.

[63] D. W. Barke and W. K. Chiu, “A review of the effects of out-of-round wheels on track and vehicle components,” *Proc Inst Mech Eng F J Rail Rapid Transit*, vol. 219, no. 3, pp. 151–175, 2005, doi: 10.1243/095440905X8853.

[64] Y. Hori and K. Kato, “Studies on tribology,” *Proc Jpn Acad Ser B Phys Biol Sci*, vol. 84, no. 8, pp. 287–320, 2008, doi: 10.2183/pjab.84.287.

[65] R. A. Ibrahim, “Recent advances in nonlinear passive vibration isolators,” *J Sound Vib*, vol. 314, no. 3–5, pp. 371–452, 2008, doi: 10.1016/j.jsv.2008.01.014.

[66] H. Cao, L. Niu, S. Xi, and X. Chen, “Mechanical model development of rolling bearing-rotor systems: A review,” *Mech Syst Signal Process*, vol. 102, pp. 37–58, 2018, doi: 10.1016/j.ymssp.2017.09.023.

[67] J. Liu and Y. Shao, “Overview of dynamic modelling and analysis of rolling element bearings with localized and distributed faults,” *Nonlinear Dyn*, vol. 93, no. 4, pp. 1765–1798, 2018, doi: 10.1007/s11071-018-4314-y.

[68] J. Y. Jang and M. M. Khonsari, “On the characteristics of misaligned journal bearings,” *Lubricants*, vol. 3, no. 1, pp. 27–53, 2015, doi: 10.3390/lubricants3010027.

[69] S. Singh, C. Q. Howard, and C. H. Hansen, “An extensive review of vibration modelling of rolling element bearings with localised and extended defects,” *J Sound Vib*, vol. 357, pp. 300–330, Nov. 2015, doi: 10.1016/j.jsv.2015.04.037.

[70] H. Aboshosha, A. Elawady, A. El Ansary, and A. El Damatty, “Review on dynamic and quasi-static buffeting response of transmission lines under synoptic and non-synoptic winds,” *Eng Struct*, vol. 112, pp. 23–46, 2016, doi: 10.1016/j.engstruct.2016.01.003.

[71] H. Ma, J. Zeng, R. Feng, X. Pang, Q. Wang, and B. Wen, “Review on dynamics of cracked gear systems,” *Eng Fail Anal*, vol. 55, pp. 224–245, 2015, doi: 10.1016/j.engfailanal.2015.06.004.

[72] J. C. Ji, C. H. Hansen, and A. C. Zander, “Journal of Intelligent Material Systems and Structures Nonlinear Dynamics of Magnetic Bearing Systems,” vol. 19, no. 12, pp. 1471–1491, 2008, doi: 10.1177/1045389X08088666.

[73] A. Bovsunovsky and C. Surace, “Non-linearities in the vibrations of elastic structures with a closing crack: A state of the art review,” *Mech Syst Signal Process*, vol. 62, pp. 129–148, Oct. 2015, doi: 10.1016/j.ymssp.2015.01.021.

[74] C. G. Cooley and R. G. Parker, “A review of planetary and epicyclic gear dynamics and vibrations research,” *Appl Mech Rev*, vol. 66, no. 4, pp. 1–15, Jun. 2014, doi: 10.1115/1.4027812.

[75] Q. Wang, J. Zeng, L. Wei, and B. Zhu, “Carbody vibrations of high-speed train caused by dynamic unbalance of underframe suspended equipment,” *Advances in Mechanical Engineering*, vol. 10, no. 12, pp. 1–13, 2018, doi: 10.1177/1687814018818969.

[76] V. del Campo, D. Ragni, D. Micallef, J. Diez, and C. J. Simão Ferreira, “Estimation of loads on a horizontal axis wind turbine,” *Wind Energy*, vol. 18, no. 11, pp. 1875–1891, 2015, doi: 10.1002/we.

[77] A. Sharma, N. Upadhyay, P. K. Kankar, and M. Amarnath, “Nonlinear dynamic investigations on rolling element bearings: A review,” *Advances in Mechanical Engineering*, vol. 10, no. 3, 2018, doi: 10.1177/1687814018764148.

[78] D. Clouteau, R. Cottereau, and G. Lombaert, “Dynamics of structures coupled with elastic media - A review of numerical models and methods,” *J Sound Vib*, vol. 332, no. 10, pp. 2415–2436, 2013, doi: 10.1016/j.jsv.2012.10.011.

[79] R. Uma Maheswari and R. Umamaheswari, “Trends in non-stationary signal processing techniques applied to vibration analysis of wind turbine drive train – A contemporary survey,” *Mech Syst Signal Process*, vol. 85, pp. 296–311, 2017, doi: 10.1016/j.ymssp.2016.07.046.

[80] S. Braun, “The synchronous (time domain) average revisited,” *Proceedings of ISMA 2010 - International Conference on Noise and Vibration Engineering, including USD 2010*, vol. 25, no. 4, pp. 2751–2762, 2010, doi: 10.1016/j.ymssp.2010.07.016.

[81] Y. Lei, J. Lin, Z. He, and M. J. Zuo, “A review on empirical mode decomposition in fault diagnosis of rotating machinery,” *Mech Syst Signal Process*, vol. 35, no. 1–2, pp. 108–126, 2013, doi: 10.1016/j.ymssp.2012.09.015.

[82] P. Gardonio, “Review of Active Techniques for Aerospace Vibro-Acoustic Control_gordonio2002.pdf,” vol. 39, no. 2, 2002.

[83] H. Hanselka, “Adaptronics as a Key Technology for Intelligent Lightweight Structures,” *Adv Eng Mater*, vol. 3, no. 4, pp. 205–215, 2001, doi: 10.1002/1527-2648(200104)3:4<205::aid-adem205>3.3.co;2-8.

[84] I. Santos, “Controllable Sliding Bearings and Controllable Lubrication Principles—An Overview,” *Lubricants*, vol. 6, no. 1, p. 16, 2018, doi: 10.3390/lubricants6010016.

[85] U. Aridogan and I. Basdogan, “A review of active vibration and noise suppression of plate-like structures with piezoelectric transducers,” *J Intell Mater Syst Struct*, vol. 26, no. 12, pp. 1455–1476, 2015, doi: 10.1177/1045389X15585896.

[86] W. Y. Liu, “A review on wind turbine noise mechanism and de-noising techniques,” *Renew Energy*, vol. 108, pp. 311–320, 2017, doi: 10.1016/j.renene.2017.02.034.

[87] L. Ben-Brahim, A. Gastli, T. Yoshino, T. Yokoyama, and A. Kawamura, “Review of Medium Voltage High Power Electric Drives,” *IEEJ Journal of Industry Applications*, vol. 8, no. 1, pp. 1–11, 2019, doi: 10.1541/ieejjia.8.1.

[88] S. Abouel-seoud, “Review Papers Tire and Engine Sources Contribution to Vehicle Interior Noise and Vibration Exposure Levels,” vol. 44, no. 2, pp. 201–214, 2019, doi: 10.24425/aoa.2019.126366.

[89] Y. Abuid, BA; Ameen, “Procedure for optimum design of a two-stage spur gear system.” JSME INTERNATIONAL JOURNAL SERIES C-MECHANICAL SYSTEMS MACHINE ELEMENTS AND MANUFACTURING, pp. 1582–1590, 2003.

[90] D. J. Fonseca, S. Shishoo, T. C. Lim, and D. S. Chen, “A genetic algorithm approach to minimize transmission error of automotive spur gear sets,” *Applied Artificial Intelligence*, vol. 19, no. 2, pp. 153–179, 2005, doi: 10.1080/08839510590901903.

[91] M. S. Tavakoli, “Optimization of Spur Gear Transmission Error Using Profile Modifications,” *The Ohio State University*, no. M.Sc. Thes, 1983.

[92] J. Jiang and Z. Fang, “Design and analysis of modified cylindrical gears with a higher-order transmission error,” *Mech Mach Theory*, vol. 88, pp. 141–152, 2015, doi: 10.1016/j.mechmachtheory.2015.02.006.

[93] Y. Wang, “Optimized tooth profile based on identified gear dynamic model,” *Mech Mach Theory*, vol. 42, no. 8, pp. 1058–1068, 2007, doi: 10.1016/j.mechmachtheory.2006.02.011.

[94] N. Yildirim, G. Gasparini, and S. Sartori, “An improvement on helicopter transmission performance through use of high contact ratio spur gears with suitable profile modification design,” *Proc Inst Mech Eng G J Aerosp Eng*, vol. 222, no. 8, pp. 1193–1210, 2008, doi: 10.1243/09544100JAERO344.

[95] F. Karpat, S. Ekwaro-Osire, K. Cavdar, and F. C. Babalik, “Dynamic analysis of involute spur gears with asymmetric teeth,” *Int J Mech Sci*, vol. 50, no. 12, pp. 1598–1610, 2008, doi: 10.1016/j.ijmecsci.2008.10.004.

[96] T. Ouyang, H. Huang, N. Zhang, C. Mo, and N. Chen, “A model to predict tribo-dynamic performance of a spur gear pair,” *Tribol Int*, vol. 116, no. August, pp. 449–459, 2017, doi: 10.1016/j.triboint.2017.08.005.

[97] T. Ouyang, H. Huang, X. Zhou, M. Pan, N. Chen, and D. Lv, “A finite line contact tribo-dynamic model of a spur gear pair,” *Tribol Int*, vol. 119, no. December 2017, pp. 753–765, 2018, doi: 10.1016/j.triboint.2017.12.010.

[98] R. Ramadani, A. Belsak, M. Kegl, J. Predan, and S. Pehan, “Topology optimization based design of lightweight and low vibration gear bodies,” *International Journal of Simulation Modelling*, vol. 17, no. 1, pp. 92–104, 2018.

[99] L. Xu and N. Chen, “Nonlinear dynamic study and vibration reduction of a power turret gear train with modified design parameters,” *Proc Inst Mech Eng C J Mech Eng Sci*, vol. 229, no. 10, pp. 1745–1749, 2015, doi: 10.1177/0954406214547092.

[100] C.-H. Liou, H. H. Lin, F. B. Oswald, and D. P. Townsend, “Effect of Contact Ratio on Spur Gear Dynamic Load With No Tooth Profile Modifications,” *Journal of Mechanical Design*, vol. 118, no. 3, p. 439, 2008, doi: 10.1115/1.2826905.

[101] A. Andersson, “An Analytical Study of the Effect of the Contact Ratio on the Spur Gear Dynamic Response,” *Journal of Mechanical Design*, vol. 122, no. 4, p. 508, 2002, doi: 10.1115/1.1320819.

[102] K. Theerarangsarit and C. Ratanasumawong, “Parallel-axis gear design methodology for minimization of power loss and its effect on vibration characteristics,” *Engineering Journal*, vol. 21, no. 7, pp. 427–439, 2017, doi: 10.4186/ej.2017.21.7.427.

[103] C. T. Hyong, B. Inho, and A. Kubo, “Multiobjective optimal design of cylindrical gears pairs for the reduction of gear size and meshing vibration,” *JSME International Journal Series C*, vol. 44, no. 1, pp. 291–298, 2001.

[104] M. Komori, A. Kubo, and Y. Suzuki, “Simultaneous optimization of tooth flank form of involute helical gears in terms of both vibration and load carrying capacity,” *Series C JSME International Journal*, vol. 46, no. 4, pp. 1572–1581, 2003.

[105] J. Hedlund and A. Lehtovaara, “A parameterized numerical model for the evaluation of gear mesh stiffness variation of a helical gear pair,” *Proc Inst Mech Eng C J Mech Eng Sci*, vol. 222, no. 7, pp. 1321–1327, 2008, doi: 10.1243/09544062JMES849.

[106] A. Fuentes, H. Nagamoto, F. L. Litvin, I. Gonzalez-Perez, and K. Hayasaka, “Computerized design of modified helical gears finished by plunge shaving,” *Comput Methods Appl Mech Eng*, vol. 199, no. 25–28, pp. 1677–1690, 2010, doi: 10.1016/j.cma.2010.01.023.

[107] Y. jun Wu, J. jun Wang, and Q. kai Han, “Static/dynamic contact FEA and experimental study for tooth profile modification of helical gears,” *Journal of Mechanical Science and Technology*, vol. 26, no. 5, pp. 1409–1417, 2012, doi: 10.1007/s12206-011-1028-1.

[108] C. Wang, H. Y. Cui, Q. P. Zhang, and W. M. Wang, “Modified optimization and experimental investigation of transmission error, vibration and noise for double helical gears,” *JVC/Journal of Vibration and Control*, vol. 22, no. 1, pp. 108–120, 2016, doi: 10.1177/1077546314525216.

[109] J. D. M. Marafona, P. M. T. Marques, R. C. Martins, and J. H. O. Seabra, “Towards constant mesh stiffness helical gears: The influence of integer overlap ratios,” *Mech Mach Theory*, vol. 136, pp. 141–161, 2019, doi: 10.1016/j.mechmachtheory.2019.02.008.

[110] E. TANAKA, H. HOUJOH, D. MUTOH, H. MOTOSHIROMIZU, K. OHNO, and N. TANAKA, “Vibration and Sound-Radiation Analysis for Designing a Low-Noise Gearbox with a Multi-Stage Helical Gear System,” *JSME International Journal Series C*, vol. 46, no. 3. pp. 1178–1185, 2004. doi: 10.1299/jsmec.46.1178.

[111] F. Wang, X. Xu, Z. Fang, and L. Chen, “Design and analysis of herringbone gear with sixth-order transmission error based on meshing vibration optimization,” *Advances in Mechanical Engineering*, vol. 9, no. 6, pp. 1–8, 2017, doi: 10.1177/1687814017704359.

[112] F. L. Litvin, A. Fuentes, and K. Hayasaka, “Design, manufacture, stress analysis, and experimental tests of low-noise high endurance spiral bevel gears,” *Mech Mach Theory*, vol. 41, no. 1, pp. 83–118, 2006, doi: 10.1016/j.mechmachtheory.2005.03.001.

[113] J. Su, Z. Fang, and X. Cai, “Design and analysis of spiral bevel gears with seventh-order function of transmission error,” *Chinese Journal of Aeronautics*, vol. 26, no. 5, pp. 1310–1316, 2013, doi: 10.1016/j.cja.2013.07.012.

[114] J. Astoul, E. Mermoz, M. Sartor, J. M. Linares, and A. Bernard, “New methodology to reduce the transmission error of the spiral bevel gears,” *CIRP Ann Manuf Technol*, vol. 63, no. 1, pp. 165–168, 2014, doi: 10.1016/j.cirp.2014.03.124.

[115] Y. Mu and Z. Fang, “Design and analysis of high contact ratio spiral bevel gears by modified curvature motion method,” *Proc Inst Mech Eng C J Mech Eng Sci*, vol. 232, no. 19, pp. 3396–3409, 2018, doi: 10.1177/0954406217737803.

[116] Y. Mu, W. Li, Z. Fang, and X. Zhang, “A novel tooth surface modification method for spiral bevel gears with higher-order transmission error,” *Mech Mach Theory*, vol. 126, pp. 49–60, 2018, doi: 10.1016/j.mechmachtheory.2018.04.001.

[117] J. Argyris, A. Fuentes, and F. L. Litvin, “Computerized integrated approach for design and stress analysis of spiral bevel gears,” *Comput Methods Appl Mech Eng*, vol. 191, no. 11–12, pp. 1057–1095, 2002, doi: 10.1016/S0045-7825(01)00316-4.

[118] A. Fuentes-Aznar, R. Ruiz-Orzaez, and I. Gonzalez-Perez, “Computational approach to design face-milled spiral bevel gear drives with favorable conditions of meshing and contact,” *Meccanica*, vol. 53, no. 10, pp. 2669–2686, 2018, doi: 10.1007/s11012-018-0841-3.

[119] B. S. Yang, S. P. Choi, and Y. C. Kim, “Vibration reduction optimum design of a steam-turbine rotor-bearing system using a hybrid genetic algorithm,” *Structural and Multidisciplinary Optimization*, vol. 30, no. 1, pp. 43–53, 2005, doi: 10.1007/s00158-004-0513-x.

[120] H. Ohta, S. Kato, J. Matsumoto, and K. Nakano, “A design of crowning to reduce ball passage vibrations of a linear guideway type recirculating linear ball bearing,” pp. 1–7, 2013.

[121] R. G. Kirk *et al.*, “Influence of Turbocharger Bearing Design on Observed Linear and Nonlinear Vibration,” pp. 175–177, 2011, doi: 10.1115/ijtc2010-41021.

[122] A. Chasalevris and F. Dohnal, “A journal bearing with variable geometry for the suppression of vibrations in rotating shafts: Simulation, design, construction and experiment,” *Mech Syst Signal Process*, vol. 52–53, no. 1, pp. 506–528, 2015, doi: 10.1016/j.ymssp.2014.07.002.

[123] J. Cao and P. Allaire, “Reduction of vibration and power loss in industrial,” pp. 1–9, 2015.

[124] F. Wang, X. Xu, Z. Fang, and L. Chen, “Design and analysis of herringbone gear with sixth-order transmission error based on meshing vibration optimization,” *Advances in Mechanical Engineering*, vol. 9, no. 6, pp. 1–8, 2017, doi: 10.1177/1687814017704359.

[125] A. Chasalevris and F. Dohnal, “A journal bearing with variable geometry for the suppression of vibrations in rotating shafts: Simulation, design, construction and experiment,” *Mech*

Syst Signal Process, vol. 52–53, no. 1, pp. 506–528, 2015, doi: 10.1016/j.ymssp.2014.07.002.

[126] Richard G. Budynas and J. N. Keith, *Mechanical engineering design*, Tenth. McGraw-Hill Education, 2015.

[127] S. Y. Ye and S. J. Tsai, "A computerized method for loaded tooth contact analysis of high-contact-ratio spur gears with or without flank modification considering tip corner contact and shaft misalignment," *Mech Mach Theory*, vol. 97, pp. 190–214, 2016, doi: 10.1016/j.mechmachtheory.2015.11.008.

[128] R. G. Jones, "The Mathematical Modelling of Gearbox Vibration under Applied Lateral Misalignment," University of Warwick, 2012.

[129] M. A. Khan *et al.*, "Gear misalignment diagnosis using statistical features of vibration and airborne sound spectrums," *Measurement (Lond)*, vol. 145, pp. 419–435, 2019, doi: 10.1016/j.measurement.2019.05.088.

[130] Stephen P. Radzevich, *DUDLEY's HANDBOOK OF PRACTICAL GEAR DESIGN and MANUFACTURE T H I R D E D I T I O N*.

[131] D. W. Scott, "On optimal and data-based histograms," *Biometrika*, vol. 66, no. 3, pp. 605–610, 1979, doi: 10.2307/2335182.

[132] D. C. Montgomery, "Douglas C. Montgomery-Diseño y Analisis de Experimentos-Limusa-Wiley (2004).pdf." p. 692, 2004.

[133] M. Loeb, "Spectrum Analysis," *J Am Chem Soc*, vol. 20, no. 5, pp. 383–384, 1898, doi: 10.1021/ja02067a010.

[134] V. Skrickij and M. Bogdevicius, "View of Vehicle gearbox dynamics_ Centre distance influence on mesh stiffness and spur gear dynamics.pdf," *Transport*, vol. 25, no. 3, pp. 278–286, 2010.

[135] P. Kumar, H. Hirani, and A. Kumar Agrawal, "Effect of gear misalignment on contact area: Theoretical and experimental studies," *Measurement (Lond)*, vol. 132, pp. 359–368, 2019, doi: 10.1016/j.measurement.2018.09.070.

[136] M. Durali and M. G. Saryazdi, "Three dimensional calculation of meshing stiffness for spur gears," vol. 15, no. 2, pp. 1–5, 2005.

[137] J. D. M. Marafona, P. M. T. Marques, R. C. Martins, and J. H. O. Seabra, "Mesh stiffness models for cylindrical gears: A detailed review," *Mechanism and Machine Theory*, vol. 166. Elsevier Ltd, Dec. 01, 2021. doi: 10.1016/j.mechmachtheory.2021.104472.

[138] F. L. Litvin and A. Fuentes, *Gear geometry and applied theory*, 2nd Edition. Cambridge, 2004.

[139] V. Roda Casanova, “Simulación del engrane y análisis del contacto en sistemas de transmisión por engranajes mediante la modelización avanzada del conjunto ejes-engranajes,” Universitat Jaume, 2015.

[140] H. R. El-Sayed, “STIFFNESS OF DEEP-GROOVE BALL BEARINGS,” Elsevier Sequoia S.A, 1980.

[141] W. Jacobs, R. Boonen, P. Sas, and D. Moens, “The influence of the lubricant film on the stiffness and damping characteristics of a deep groove ball bearing,” *Mech Syst Signal Process*, vol. 42, no. 1–2, pp. 335–350, Jan. 2014, doi: 10.1016/j.ymssp.2013.07.018.

[142] S. W. Hong and V. C. Tong, “Rolling-element bearing modeling: A review,” *International Journal of Precision Engineering and Manufacturing*, vol. 17, no. 12. SpringerOpen, pp. 1729–1749, Dec. 01, 2016. doi: 10.1007/s12541-016-0200-z.

[143] Q. Niu, Y. Li, Y. Zhu, S. Pei, Y. Yin, and D. Wang, “Analytical Determination and Influence Analysis of Stiffness Matrix of Ball Bearing under Different Load Conditions,” *Machines*, vol. 10, no. 4, Apr. 2022, doi: 10.3390/machines10040238.

[144] Y. Guo and R. G. Parker, “Stiffness matrix calculation of rolling element bearings using a finite element/contact mechanics model,” *Mech Mach Theory*, vol. 51, pp. 32–45, May 2012, doi: 10.1016/j.mechmachtheory.2011.12.006.

[145] X. Sheng, B. Li, Z. Wu, and H. Li, “Calculation of ball bearing speed-varying stiffness,” *Mech Mach Theory*, vol. 81, pp. 166–180, 2014, doi: 10.1016/j.mechmachtheory.2014.07.003.

[146] E. Krämer, *Dynamics of Rotors and Foundations*. Springer Berlin Heidelberg, 1993. doi: 10.1007/978-3-662-02798-1.

[147] “Fundamental Rating Factors and Calculation Methods for Involute Spur and Helical Gear Teeth.” [Online]. Available: http://www.agma.org.]

ANEXOS

Anexo 1. Vistas de ensamblaje de banco de pruebas para generar desalineamientos.